



CMS-TOP-20-010

CERN-EP-2021-210  
2022/02/18

# Inclusive and differential cross section measurements of single top quark production in association with a Z boson in proton-proton collisions at $\sqrt{s} = 13$ TeV

The CMS Collaboration<sup>\*</sup>

## Abstract

Inclusive and differential cross sections of single top quark production in association with a Z boson are measured in proton-proton collisions at a center-of-mass energy of 13 TeV with a data sample corresponding to an integrated luminosity of  $138 \text{ fb}^{-1}$  recorded by the CMS experiment. Events are selected based on the presence of three leptons, electrons or muons, associated with leptonic Z boson and top quark decays. The measurement yields an inclusive cross section of  $87.9^{+7.5}_{-7.3} (\text{stat})^{+7.3}_{-6.0} (\text{syst}) \text{ fb}$  for a dilepton invariant mass greater than 30 GeV, in agreement with standard model (SM) calculations and represents the most precise determination to date. The ratio between the cross sections for the top quark and the top antiquark production in association with a Z boson is measured as  $2.37^{+0.56}_{-0.42} (\text{stat})^{+0.27}_{-0.13} (\text{syst})$ . Differential measurements at parton and particle levels are performed for the first time. Several kinematic observables are considered to study the modeling of the process. Results are compared to theoretical predictions with different assumptions on the source of the initial-state b quark and found to be in agreement, within the uncertainties. Additionally, the spin asymmetry, which is sensitive to the top quark polarization, is determined from the differential distribution of the polarization angle at parton level to be  $0.54 \pm 0.16 (\text{stat}) \pm 0.06 (\text{syst})$ , in agreement with SM predictions.

*Published in the Journal of High Energy Physics as doi:10.1007/JHEP02(2022)107.*



## 1 Introduction

The electroweak production of a top quark or antiquark in association with a  $Z$  boson, the  $tZq$  process, was recently observed in proton-proton (pp) collisions at a center-of-mass energy of 13 TeV at the CERN LHC by both the CMS and ATLAS experiments [1, 2]. The process has unique features that make it a suitable probe for several interactions in the standard model (SM) of particle physics. Figure 1 shows representative leading-order (LO) Feynman diagrams of  $tZq$ , where  $\ell$  stands for an electron or muon, including also off-shell photons ( $\gamma^*$ ) and the possibility of nonresonant dilepton emission to correctly account for interference effects. Throughout the text, unless stated otherwise,  $tZq$  stands collectively for the top quark and antiquark production, including nonresonant dilepton emission. Because of the pure electroweak nature of  $tZq$  production, corrections to the cross section arising from quantum chromodynamics (QCD) are typically small. As a result, the study of  $tZ$ ,  $tWb$ , and  $WWZ$  couplings in  $tZq$  production is not primarily affected by QCD uncertainties [3]. This makes an analysis of  $tZq$  production advantageous in comparison to the associated production of a top quark-antiquark pair ( $t\bar{t}$ ) and a  $Z$  boson ( $t\bar{t}Z$ ), where the  $t\bar{t}$  is produced via a QCD interaction.

The top quark is strongly polarized in this process because of its electroweak production mechanism. Measurement of the top quark polarization in the  $tZq$  process provides complementary information to the existing studies of the top quark electroweak interactions [4–8]. Furthermore, the  $tZq$  process offers the possibility of measuring the top quark and antiquark production cross sections separately, as well as their ratio. These measurements yield potential sensitivity to different parameterizations of the parton distribution functions (PDFs) of the proton.

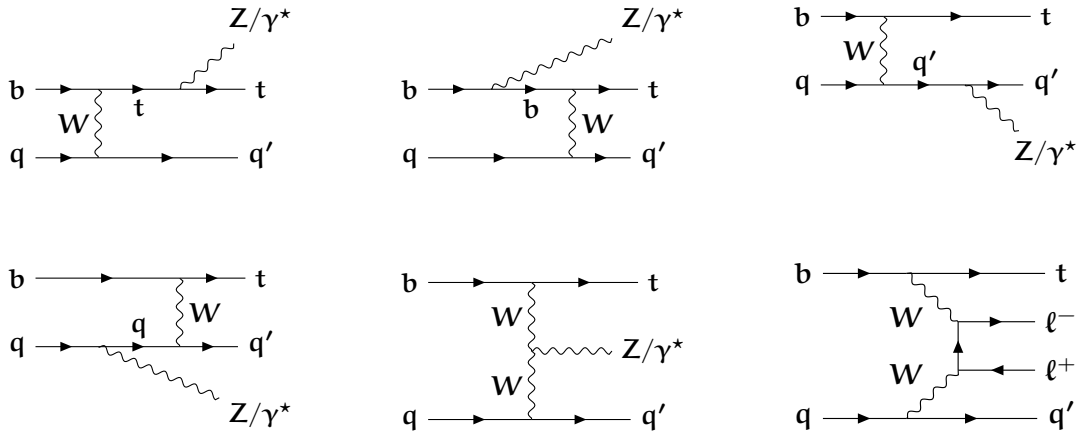


Figure 1: Representative LO Feynman diagrams for the  $tZq$  production process. The production mechanism of nonresonant lepton pairs (lower right) is included in the signal definition to correctly account for interference effects.

Previous measurements of the inclusive  $tZq$  cross section  $\sigma_{tZq}$  in leptonic final states have reached a precision of about 15% [1, 2, 9, 10] and are in agreement with the SM predictions at next-to-LO (NLO),  $\sigma_{tZq}^{\text{SM}} = 94.2^{+1.9}_{-1.8} \text{ (scale)} \pm 2.5 \text{ (PDF)} \text{ fb}$ , for a dilepton invariant mass greater than 30 GeV [10]. The systematic uncertainty associated with the energy scale used in the calculations arises from variations of the factorization and renormalization scales. The calculation is performed in the five-flavor scheme (5FS), where the  $b$  quark content of the proton is described by the appropriate PDF. No differential measurement of the  $tZq$  process has been reported so far.

This paper presents the most precise measurement of  $\sigma_{tZq}$  to date, as well as the first measurement of differential cross sections for the  $tZq$  process. Data from pp collisions at  $\sqrt{s} = 13 \text{ TeV}$

collected by the CMS experiment, corresponding to an integrated luminosity of  $138 \text{ fb}^{-1}$  [11], are used in this analysis. The improved precision on  $\sigma_{tZq}$  in this measurement compared to the previous results [1, 2, 9, 10] is due to the larger data sample, an optimized lepton identification, and the use of various control regions in data [1]. The inclusive measurement is extended to report the first separate determination of the Z boson associated production cross sections of the top quark and antiquark, as well as their ratio. The studies are performed in final states with three leptons (electrons or muons), including also a small contribution from sequential  $\tau$  lepton decays. Two selected leptons of same flavor and opposite charge are assumed to come from the Z boson decay, while the third lepton is associated with the leptonic decay of the W boson produced in the top quark decay. Both the inclusive and differential cross section measurements heavily rely on multivariate classifiers to separate the tZq signal from various background processes including  $t\bar{t}Z$ . The results are obtained by performing maximum likelihood fits on distributions that are obtained from the responses of the classifiers. Tabulated results are provided in HEPData [12].

The differential distributions are extracted at both parton and particle levels using a likelihood-based unfolding (as detailed in, e.g., Ref. [13]). Measured observables at parton level are the transverse momenta,  $p_T$ , of the top quark, the Z boson, and the lepton from the top quark decay, together with the invariant masses of the three leptons and the  $t + Z$  system. The azimuthal angular distance between the two leptons from the Z boson decay, as well as the cosine of the top quark polarization angle, are also measured. The differential measurement of the top quark polarization angle is used to determine the top quark spin asymmetry. Additionally, the  $p_T$  and absolute pseudorapidity,  $|\eta|$ , of the jet corresponding to the light-flavor quark that recoils against the virtual W boson ( $q'$  in Fig. 1), denoted as the recoiling jet or  $j'$ , are measured at the particle level. Results are compared with predictions using the four-flavor scheme (4FS), where the incoming b quark is produced in the gluon-splitting process, and the 5FS.

The paper is organized as follows: the CMS detector is briefly introduced in Section 2. Section 3 is devoted to the data and simulated samples, and the identification and selection requirements applied to the reconstructed objects. A description of the event selection and reconstruction is presented in Section 4, while the estimation of the backgrounds is discussed in Section 5. Discussion of systematic uncertainties affecting the presented measurements follows in Section 6. Sections 7 and 8 are dedicated to the description of the methodology and the obtained results relevant to the inclusive and differential measurements, respectively. Finally, the paper is summarized in Section 9.

## 2 The CMS detector, data, and simulated samples

The central feature of the CMS apparatus [14] is a superconducting solenoid of 6 m internal diameter, providing a magnetic field of 3.8 T. Silicon pixel and strip trackers, a lead tungstate crystal electromagnetic calorimeter (ECAL), and a brass and scintillator hadron calorimeter, each composed of a barrel and two endcap sections, reside within the solenoid. Forward calorimeters extend the  $\eta$  coverage provided by the barrel and endcap detectors. Muons are detected in gas-ionization detectors embedded in the steel flux-return yoke outside the solenoid.

The data events used in the analysis correspond to the pp collisions recorded by the CMS experiment in 2016–2018. Events are required to pass several selection criteria defined at trigger level including the presence of either one, two, or three leptons (electrons or muons) [15]. The combination of these triggers yields a trigger selection efficiency close to 100% in the full phase space relevant to the presented study. In order to compare the recorded and selected data with SM predictions, dedicated sets of simulated samples are employed, with consistent modeling

of the running conditions for each data-taking year.

The tZq process requires the presence of a bottom quark in the initial state. This can be described using the 5FS as shown in Fig. 1, where the b quark production depends on the proton PDF. The Monte Carlo (MC) event simulation produced in the 5FS is preferable in the calculation of the total production cross sections [16]. The modeling of the kinematic properties of the particles in the final state is, however, expected to be more precise in the 4FS, where the b quark is explicitly required to be associated with the gluon-splitting process at the matrix element (ME) level [16]. This directly leads to the presence of a second b quark that is produced with relatively small  $p_T$ . On the other hand, the additional vertex in the 4FS ME leads to an increased uncertainty related to the renormalization and factorization scales used in the calculation. Examples of LO and NLO Feynman diagrams corresponding to the tZq production in the 4FS are shown in Fig. 2. In the extraction procedure applied to the tZq events, the prediction of the signal process is based on the 4FS calculations and is normalized to the production cross section obtained in the 5FS. An alternative tZq signal sample is generated in the 5FS with the same generator as used in the simulation of the default tZq sample, and is compared to the unfolded results at the parton and particle levels.

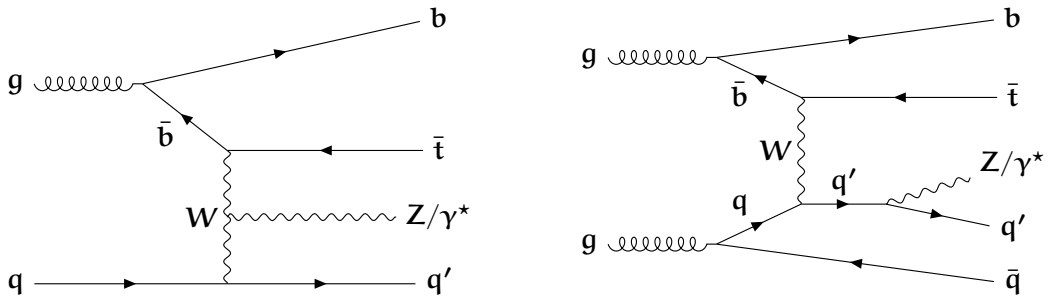


Figure 2: An example of the LO (left) and NLO (right) Feynman diagrams for the tZq production process in the 4FS. The  $Z/\gamma^*$  interference term is included in the MC event simulation. In the case of the NLO generation, the gg- and q $\bar{q}$ -initiated processes are possible, with an additional quark or gluon present in the final state.

Using MADGRAPH5\_aMC@NLO (v2.4.2) [17, 18], the tZq signal events are generated at NLO precision in perturbative QCD, such that processes initiated by gluon (gg) and quark (q $\bar{q}$ ) pairs are included and the radiation of an additional gluon is allowed. The nonresonant dilepton production and  $Z/\gamma^*$  interference is also included in the simulation. The same ME generator is used to simulate the dominant background processes: associated production of a W and Z boson (WZ), t $\bar{t}$  production in association with a Z (t $\bar{t}Z$ ) or W (t $\bar{t}W$ ) boson, production of a photon in association with a Z ( $Z\gamma$ ) or W ( $W\gamma$ ) boson or with a top quark ( $t\gamma$ ), production of three electroweak gauge bosons (VVV), and production of four top quarks (t $\bar{t}tt$ ). Other background processes, which are simulated at LO with MADGRAPH [17], include single top quark production in association with a Higgs boson (tHq), with a Higgs boson and an additional W boson (tHW), and with a W and Z boson (tWZ). Additional background processes considered include t $\bar{t}$  production in association with a photon (t $\bar{t}\gamma$ ), with two electroweak gauge bosons (t $\bar{t}VV$ ), with one electroweak gauge boson and a Higgs boson (t $\bar{t}VH$ ), and with two Higgs bosons (t $\bar{t}HH$ ). For processes with the associated production of two Z bosons (ZZ), as well as t $\bar{t}$  production in association with a Higgs boson (t $\bar{t}H$ ), the POWHEG v2 [19–22] generator is used at NLO in QCD. The MCFM [23] generator (v7.0.1) is used for the MC event simulation at LO for the gluon-initiated ZZ production (gg  $\rightarrow$  ZZ). In the measurement of the lepton misidentification rate (see Section 5), simulated samples with the Drell–Yan (DY) and t $\bar{t}$  production processes are used. The processes are simulated at NLO with MADGRAPH5\_aMC@NLO

and POWHEG v2, respectively.

Simulated events are processed with PYTHIA (v8.2) [24] to model the fragmentation and the parton shower. The FxFx [18] merging scheme is used to avoid double counting associated with the MC event simulation in the same phase space due to the ME generation of extra partons at NLO with MADGRAPH5\_aMC@NLO. A set of CP5 tuning parameters [25] is used for the parton shower, hadronization, and modeling of the underlying event in the 2017 and 2018 MC samples, as well as of the tZq,  $t\bar{t}Z$ ,  $t\bar{t}W$ ,  $t\bar{t}H$ ,  $t\bar{t}\gamma$ ,  $Z\gamma$ , and  $t\bar{t}t\bar{t}$  MC samples in all three years. The CUETP8M1 [26, 27], CUETP8M2, and CUETP8M2T4 [28] tunes are used for other 2016 MC samples. The tZq and  $t\bar{t}Z$  MC samples in all three years, as well as MC samples for 2017 and 2018 data, are generated with the NNPDF3.1 [29] PDF set (with next-to-NLO precision in perturbative QCD for tZq). Other MC samples for 2016 are generated with the NNPDF3.0 [30] PDF set. The effects of additional pp collisions attributed to the same or adjacent bunch crossings (pileup) [31], are simulated with PYTHIA. The simulated events are reweighted according to the distribution of the number of interactions in each bunch crossing corresponding to a total inelastic pp cross section of 69.2 mb [32]. The simulation of the CMS detector is performed with GEANT4 [33].

### 3 Reconstruction and identification of physics objects

To reconstruct the physics objects described below, the same algorithms are applied to simulated events and data. The particle-flow (PF) algorithm [34] is used to reconstruct and identify photons, electrons, muons, and charged and neutral hadrons in an event, with an optimized combination of information from the various elements of the CMS detector. The missing transverse momentum vector  $\vec{p}_T^{\text{miss}}$  is computed as the negative vector  $\vec{p}_T$  sum of all the PF candidates in an event [35].

The candidate vertex with the largest value of summed  $p_T^2$  of all physics objects assigned to this vertex is taken to be the primary vertex (PV) of the pp interaction.

Jets are reconstructed by clustering the PF candidates using the anti- $k_T$  algorithm [36, 37] with a distance parameter of  $R = 0.4$ . Charged particles identified as originating from pileup interactions are discarded and an offset correction is applied to correct for remaining contributions. Jet energy corrections are derived from simulation to bring the measured response of jets to that of particle-level jets on average. In situ measurements of the momentum balance in dijet, photon+jet, Z+jet, and multijet events are used to account for any residual differences in the jet energy scale between data and simulation [38]. The jet energy resolution in simulation is corrected to match the one observed in data. Additional selection criteria are applied to each jet to remove jets potentially dominated by anomalous contributions from various subdetector components, or misreconstruction. Jets are required to have  $p_T > 25 \text{ GeV}$ ,  $|\eta| < 5$ , and be separated from any identified lepton by  $\Delta R = \sqrt{(\Delta\eta)^2 + (\Delta\phi)^2} > 0.4$ , where  $\Delta\eta$  and  $\Delta\phi$  are the pseudorapidity and azimuthal angular separation between the jet and the lepton, respectively. The relatively loose selection criterion applied to the jet  $|\eta|$  is necessary for reconstructing the light quark jet in the tZq process, which is predominantly produced in the forward region of the detector (see Fig. 1). Jets that are reconstructed within the acceptance of the CMS pixel detector ( $|\eta| < 2.4$  for 2016,  $|\eta| < 2.5$  for 2017 and 2018) are denoted as central jets.

Using the DEEPJET algorithm [39–41], central jets containing b hadrons are identified as b-tagged jets. The b tagging requirement used in the analysis corresponds to a b quark jet selection efficiency of about 85% for jets with  $p_T > 30 \text{ GeV}$  as estimated in simulated  $t\bar{t}$  events. An associated misidentification rate of 1% for jets arising from u, d, or s quarks and gluons, and

---

15% for jets arising from c quarks is obtained for those events.

The electron momentum is estimated by combining the energy measurement in the ECAL with the momentum measurement in the tracker. The momentum resolution for electrons with  $p_T \approx 45\text{ GeV}$  from  $Z \rightarrow ee^-$  decays is within 1.7–4.5%. The resolution is generally better in the barrel than in the endcap region, and depends on the bremsstrahlung energy emitted by the electron as it traverses the material in front of the ECAL [42]. Electrons are selected within  $|\eta| < 2.5$ .

Muons are reconstructed within  $|\eta| < 2.4$  using drift tubes, cathode strip chambers, and resistive plate chambers. Association of muon objects to reconstructed tracks that are measured in the silicon tracker yields the relative  $p_T$  resolution of 1% in the barrel and 3% in the endcaps for muons with  $p_T$  up to 100 GeV, and of better than 7% in the barrel for muons with  $p_T$  up to 1 TeV [43].

Leptons originating from decays of electroweak bosons are referred to as “prompt”, while those originating from hadron decays, as well as misidentified leptons from jets or hadrons, are collectively referred to as “nonprompt”. A strong separation between prompt and nonprompt leptons is obtained by using a set of discriminating variables based on the reconstructed properties of leptons and jets. A relative isolation variable is defined as the scalar  $p_T$  sum of all PF objects inside a cone of  $\Delta R = 0.3$  around the direction of the lepton, excluding the lepton itself, divided by the  $p_T$  of the lepton [44, 45]. A relative isolation parameter computed with a cone size that decreases for higher lepton  $p_T$  values is also used. The isolation variables are corrected for pileup effects. The reconstructed transverse and longitudinal impact parameters, as well as the signed impact parameter significance, of the tracks associated with the leptons, computed with respect to the PV position, are used to determine the consistency of the leptons originating from the PV. A number of variables discriminating between prompt and nonprompt leptons use information about the reconstructed jet with the smallest  $\Delta R$  with respect to the identified lepton, requiring  $\Delta R < 0.4$ . This jet is used to compute the number of charged particles matched to the jet, the ratio of the jet  $p_T$  to the lepton  $p_T$ , the lepton momentum projected on the transverse plane to the reconstructed jet direction, as well as the output discriminator value of the DEEPJET b tagging algorithm. In addition, the muon segment compatibility criteria [43] are used for selected muons, while the output discriminator value of the electron identification algorithm is used for electrons [42].

The aforementioned variables are combined into a multivariate analysis (MVA) based discriminant (lepton MVA), which is trained and evaluated with the TVMA package [46]. A boosted decision tree (BDT) algorithm is trained on a large sample of simulated prompt leptons originating from the  $tZq$ ,  $t\bar{t}Z$ , and  $t\bar{t}W$  processes, as well as nonprompt leptons taken from simulated  $t\bar{t}$  events. The requirement on the lepton MVA value corresponds to a prompt lepton selection efficiency of about 95%, while rejecting 98% of the nonprompt leptons, as evaluated from MC simulation for leptons with  $p_T > 25\text{ GeV}$ . The lepton MVA and its training discussed here are an extension and reoptimization of a similar MVA used in the first observation of the  $tZq$  process by CMS [1].

Leptons that pass the requirement on the lepton MVA are labeled as “tight” leptons and are selected for further analysis. Leptons that fail this requirement are subjected to additional criteria, including requirements on the relative lepton isolation and the DEEPJET discriminator value of the jet that is closest to the lepton. Leptons that are either tight or satisfy those additional criteria are labeled as “loose” leptons and are used in the estimation of the nonprompt-lepton background from control samples in data (as discussed in Section 5).

## 4 Event reconstruction and signal selection

Selected events are required to contain exactly three tight leptons and at least two jets, of which at least one is b tagged. The three leptons, ordered according to their  $p_T$ , must have a  $p_T$  of at least 25, 15, and 10 GeV, respectively. Two of the three leptons are required to form a pair with electric charge of opposite sign and same lepton flavor (OSSF). Furthermore, the invariant mass of the OSSF pair must be compatible with the Z boson mass within 15 GeV. In case of an ambiguity, the OSSF pair with the mass closest to the Z boson mass is chosen.

Events that satisfy the aforementioned conditions define the signal region. For tZq events with three prompt leptons the selection efficiency is about 20%. For the inclusive and differential measurements the signal region is furthermore divided into subregions based on the number of jets and b-tagged jets. In order to study the background prediction, we define dedicated control regions that are complementary to the signal region. They are discussed in detail in Section 5.

A good discrimination between the tZq process and various backgrounds contributing to the signal region is achieved by using MVA techniques. In the final step of the measurement, the output score of an MVA is used in maximum likelihood fits to extract the inclusive and differential tZq cross sections. A full event reconstruction, described below, is performed to obtain a set of additional variables used as inputs for the MVA to improve the separation between signal and background events. Identified physics objects are used to compute several observables for the differential cross section measurement.

The four-momentum of the neutrino in the decay of the W boson originating from the top quark is reconstructed similarly to Ref. [47]. First, the lepton that is not associated with the OSSF lepton pair, denoted as  $\ell_t$ , is assigned to the W boson. Then, a W boson mass constraint on the system of the  $\vec{p}_T^{\text{miss}}$  and  $\vec{p}_T(\ell_t)$  is imposed. This leads to two solutions, or in some cases one solution, for the neutrino four-momentum. The top quark candidate is reconstructed by combining the four-momenta of the neutrino solution(s), the  $\ell_t$ , and a b-tagged jet. In the case of an ambiguity, the combination that gives the top quark candidate mass closest to the value of 172.5 GeV is chosen. A particular feature of the tZq process is the recoiling jet that is often radiated in the forward detector region. This jet is identified with an efficiency of about 86% by selecting the jet with the highest  $p_T$ , excluding b-tagged jets.

The most powerful discriminating variables used in the event classification are obtained from the event reconstruction and correspond to the scalar  $p_T$  sum of all jets, the maximum invariant mass and maximum  $p_T$  of any two-jet system, the maximum DEEPJET score of any jet, the number of jets in the event, and the  $|\eta|$  of the recoiling jet. Predicted distributions of these variables compared to data are shown in Fig. 3.

Other discriminating variables are the reconstructed top quark mass, the invariant mass of the OSSF lepton pair, the angle between  $j'$  and the b-tagged jet associated with the top quark decay, the number of b-tagged jets, the scalar sum of the  $p_T$  of all selected leptons and  $p_T^{\text{miss}}$ , and  $p_T^{\text{miss}}$  itself. The transverse mass of the reconstructed W boson ( $m_T^W$ ) is also included in the event classification and is defined as:

$$m_T^W = \sqrt{2p_T^{\text{miss}} p_T(\ell_t) [1 - \cos \Delta\phi]}, \quad (1)$$

where  $\Delta\phi$  is the difference in azimuthal angle between  $\vec{p}_T(\ell_t)$  and  $\vec{p}_T^{\text{miss}}$ .

The top quark polarization is linked to the polarization of the lepton from its decay and can be measured with respect to the direction of the recoiling quark. The cosine of the top quark

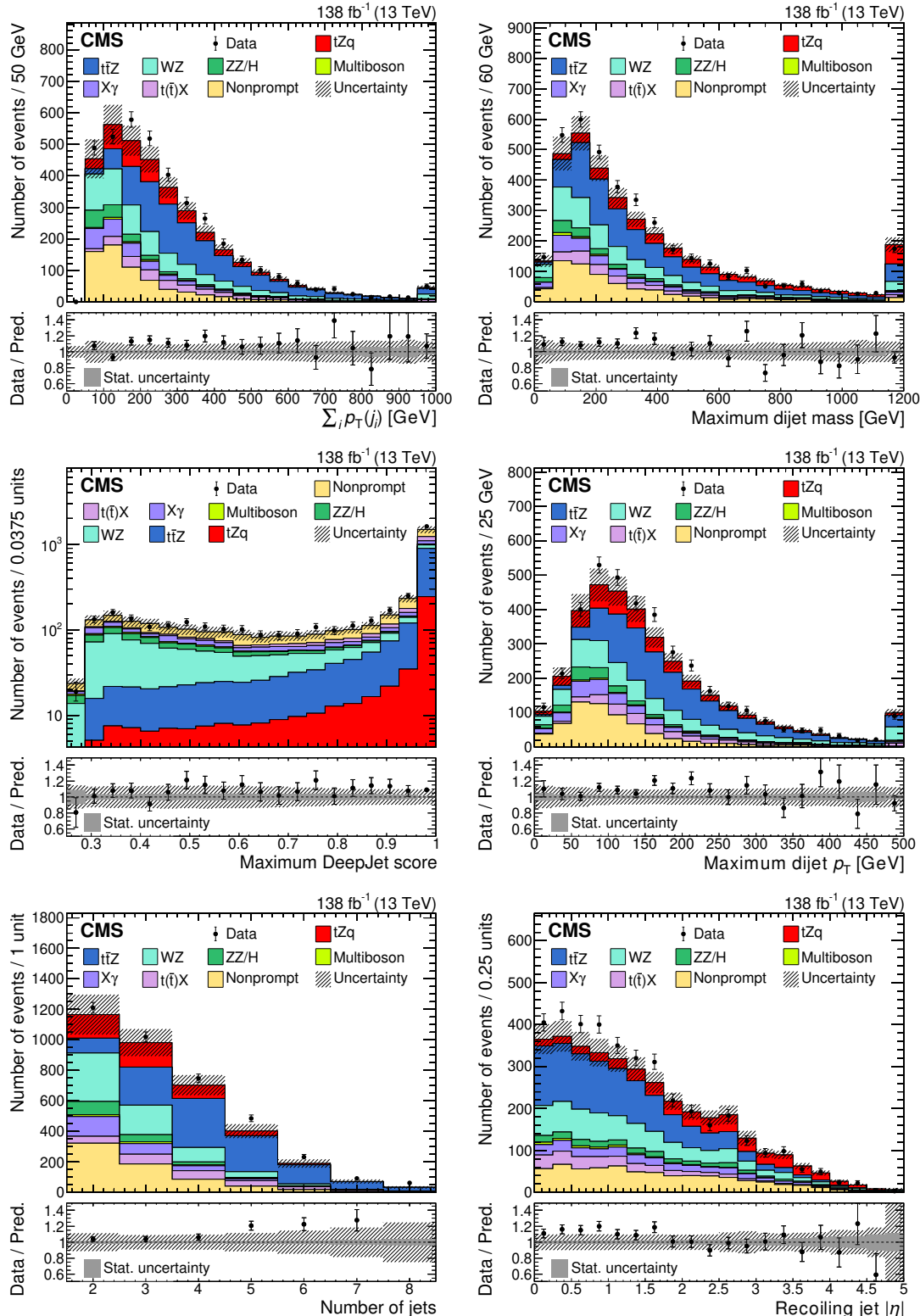


Figure 3: Distributions of the most powerful discriminating variables in the signal region for the data (points) and predictions (colored histograms), including the scalar  $p_T$  sum of all jets (upper left), the maximum invariant mass of any two-jet system (upper right), the maximum DEEPJET score of any jet (middle left), the maximum  $p_T$  value of any two-jet system (middle right), the number of jets in the event (lower left), and the  $|\eta|$  of the recoiling jet (lower right). The last bins include the overflows. The lower panels show the ratio of the data to the sum of the predictions. The vertical lines on the data points represent the statistical uncertainty in the data; the shaded area corresponds to the total uncertainty in the prediction; the gray area in the ratio indicates the uncertainty related to the limited statistical precision in the prediction.

polarization angle  $\cos(\theta_{\text{pol}}^*)$  is defined similarly to Ref. [8] as:

$$\cos(\theta_{\text{pol}}^*) = \frac{\vec{p}(\text{q}'^*) \cdot \vec{p}(\ell_t^*)}{|\vec{p}(\text{q}'^*)| |\vec{p}(\ell_t^*)|}, \quad (2)$$

where  $\vec{p}(\text{q}'^*)$  and  $\vec{p}(\ell_t^*)$  are the three-momenta of the recoiling quark and the lepton from the top quark decay, respectively. The asterisks indicate that the three-momenta are measured in the top quark candidate rest frame. The polarization  $P$  of the top quark is related to the spin asymmetry as  $A_\ell = \frac{1}{2} P a_\ell$ , where  $a_\ell$  refers to the spin-analyzing power of the lepton associated with the top quark decay and is equal to unity in LO calculations [48, 49]. The spin asymmetry  $A_\ell$  is related to the differential cross section as a function of  $\cos(\theta_{\text{pol}}^*)$  by:

$$\frac{d\sigma}{d \cos(\theta_{\text{pol}}^*)} = \sigma_{tZq} \left( \frac{1}{2} + A_\ell \cos(\theta_{\text{pol}}^*) \right). \quad (3)$$

## 5 Background determination

Several background contributions to the signal region are studied, divided into two main categories. The first contains processes that include three genuine prompt leptons. Events in the second category contain at least one nonprompt lepton, and therefore enter the signal region by virtue of imperfect nonprompt-lepton rejection. Background contributions from the first category are modeled using the MC simulations, whereas the backgrounds from the second are estimated using a technique based on control samples in data.

The production of WZ bosons is an important source of background events, especially for events with a small number of reconstructed jets or b-tagged jets. The inclusive production cross section of this process is both predicted and measured with high precision [50]. In order to validate the predictions obtained for WZ production with additional jets, a dedicated data control region is defined with similar lepton identification requirements as used in the signal region, but vetoing events containing a b-tagged jet. Additionally,  $p_T^{\text{miss}} > 50 \text{ GeV}$  is required, accounting for the reconstructed missing momentum originating due to the neutrino coming from the W boson decay. Figure 4 shows the predicted jet multiplicity and  $m_T^W$  distributions compared to data in this control region. Good agreement in the overall normalization and shape of the presented distributions is observed. In the signal region, about 30% of the simulated WZ events have a jet containing a bottom quark. The other 70% enter the signal region because of misidentification in the heavy-flavor jet tagging algorithm, with jets originating from light quarks and c quarks each contributing about half. The modeling of the WZ process with b quarks is subject to an uncertainty that is not constrained in the control region because there is a negligible fraction of events with an additional b quark. A dedicated study of this uncertainty was performed in DY events [51], resulting in an additional uncertainty of 20% assigned to the normalization of WZ selected events containing an additional b quark in the signal region.

The dominant background in the subregions with a large number of jets or b-tagged jets comes from the  $t\bar{t}Z$  process. The modeling and normalization of  $t\bar{t}Z$  is validated in two distinct ways. In the signal region, good separation of this process from  $tZq$  is achieved with the MVA technique. Hence, the signal region contains an implicit control region for  $t\bar{t}Z$  at low MVA discriminant values. Additionally, a dedicated control region is defined that requires an event to contain four leptons, with an OSSF pair compatible with the Z boson mass. If a second OSSF pair is present, it is required not to be compatible with the Z boson mass (within 15 GeV) in

order to suppress the contribution from the ZZ process. The distributions of the number of b-tagged jets in data and the prediction for this t̄tZ-enriched control region are shown in the lower-left plot of Fig. 4. The data exceed the prediction especially for the bin with two b-tagged jets where the t̄tZ contribution is large. This observed underprediction is consistent with previous measurements [51].

The background from ZZ events in the final states involving three leptons consists of events where both Z bosons decay leptonically, but one of the leptons is not reconstructed or does not satisfy the lepton selection requirements. The ZZ control region requires the presence of four leptons that are used to form two OSSF pairs, both of them compatible with the Z boson mass within 15 GeV. The distributions of the number of jets in data and the prediction for this ZZ-enriched control region are shown in the lower-right plot of Fig. 4.

The Z $\gamma$  process can represent a background to the signal region via conversion of the photon to an electron-positron pair in the detector material. In such a process, the converted photon may transfer a large part of its momentum to one of the two leptons. This leads to the production of one lepton of sufficient  $p_T$  to pass the selection criteria, with the other lepton failing those requirements. The leptonic decay of the Z boson yields the additional two leptons needed to satisfy the three-lepton selection. The selected events for the Z $\gamma$  control region must contain three tight leptons whose combined invariant mass must be compatible with the Z boson mass within 15 GeV, whereas any pair of leptons is required to fail this invariant mass constraint. With this selection, a pure Z $\gamma$  region is obtained, allowing the validation of the modeling of photon conversions in the detector material. Figure 5 displays the distributions for the number of selected muons in an event (left) and the three-lepton invariant mass (right) from the data and prediction for the Z $\gamma$  control region. The plots show the contributions from “external” photon conversions, where a real photon converts into a pair of (mostly) electrons from its interaction in the detector material, and so-called “internal” conversions, where a virtual photon decays into a pair of leptons. Also note that in all figures, Z $\gamma$  is the major contribution to the background category labeled ‘X $\gamma$ ’, with only minor contributions from other processes involving photons.

Other sources associated with the prompt-lepton backgrounds lead to much smaller contributions and are also estimated from simulation. They mainly include tWZ, t̄tH, and t̄tW events, as well as the production of three massive electroweak bosons (VVV).

The second major category of background includes those containing at least one nonprompt lepton. These arise from either t̄t dileptonic events or DY production with an additional selected lepton that is either misidentified from a jet or a genuine lepton from hadron decay. This contribution is estimated from data using the so-called “tight-to-loose ratio” method [45]. The key feature of this method is the measurement of the probability for a nonprompt lepton satisfying the loose-quality definition to pass the tight-selection criteria. This probability, the “misidentification rate”, is measured in a kinematic region enriched in QCD multijet events. In order to estimate the nonprompt-lepton background contribution to the signal region, the measured misidentification rate is used to compute a transfer factor, which is applied to events in a region with similar selection criteria as the signal region, except that at least one of the three loose leptons is not identified as a tight lepton.

In the first step of this procedure, the method is validated using simulated samples. The misidentification rate is measured in simulated QCD multijet events and applied to simulated t̄t and DY events. A good description of nonprompt leptons in simulation is obtained in terms of all kinematic variables used in the multivariate classifier for signal extraction, as well as the classifier output score itself (shown in Appendix A). This indicates that the method can be used

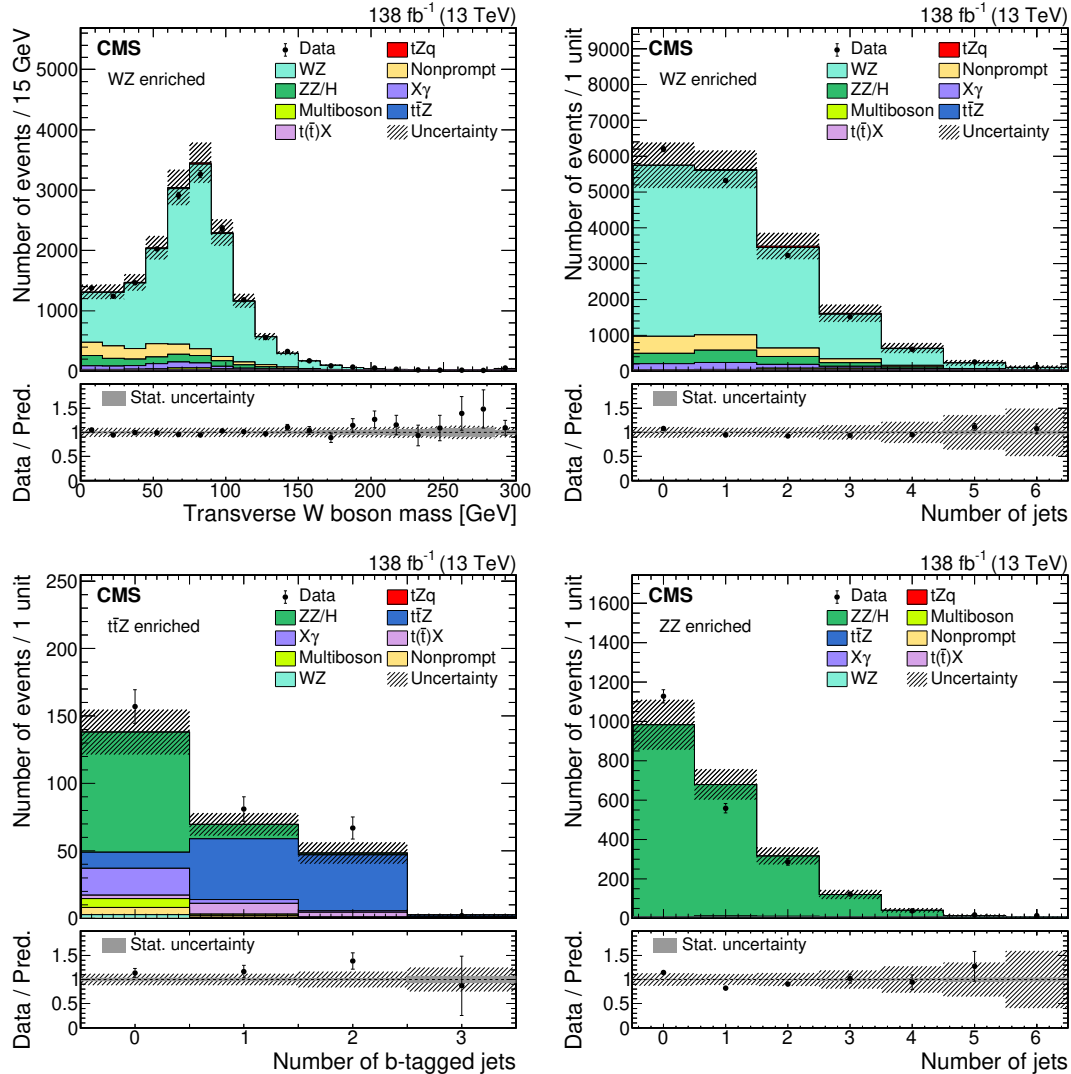


Figure 4: Distributions of the transverse W boson mass (upper left) and the number of selected jets (upper right) for the WZ-enriched control region, the number of b-tagged jets (lower left) in the  $t\bar{t}Z$ -enriched control region, and the number of jets (lower right) in the ZZ-enriched control region for the data (points) and predictions (colored histograms). The lower panels show the ratio of the data to the sum of the predictions. The vertical lines on the data points represent the statistical uncertainty in the data; the shaded area corresponds to the total uncertainty in the prediction; the gray area in the ratio indicates the uncertainty related to the limited statistical precision in the prediction.

to predict the nonprompt-lepton kinematic properties in  $t\bar{t}$  and DY events with misidentification rates measured in QCD multijet events.

Next, the misidentification rate is measured in a multijet-enriched data sample. The event selection criteria in this measurement aim at selecting events containing nonprompt or misidentified leptons. Events are required to have exactly one loose lepton, at least one jet with  $p_T > 30 \text{ GeV}$  that does not overlap with the lepton within  $\Delta R = 0.7$ , and  $p_T^{\text{miss}} < 20 \text{ GeV}$ , in order to suppress contamination from processes containing prompt leptons.

The misidentification rate is defined as the ratio of the number of events with a nonprompt lepton passing the tight selection to the number of events with a nonprompt lepton passing

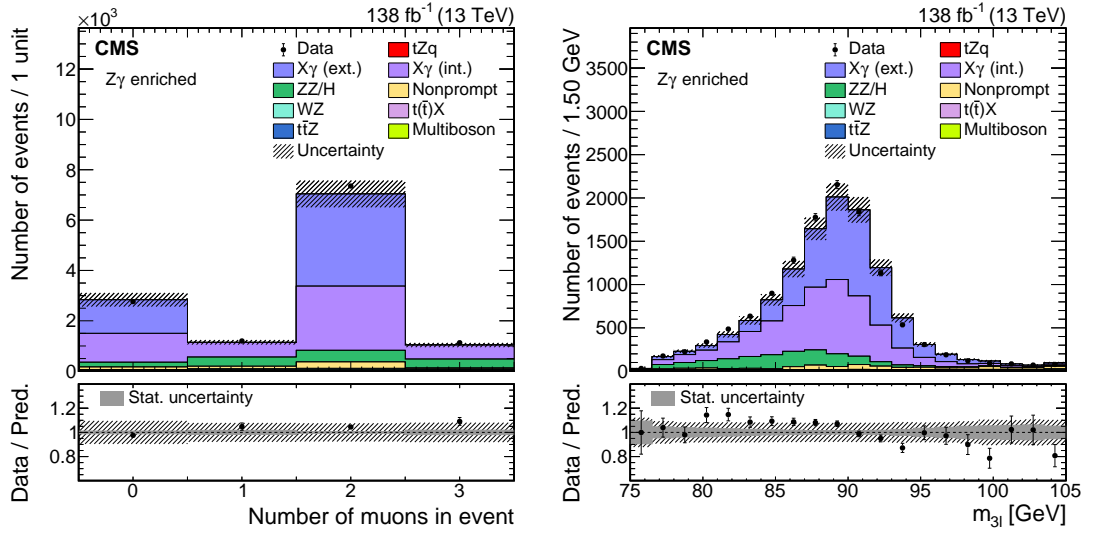


Figure 5: Distributions in the  $Z\gamma$ -enriched control region of the number of selected muons (left) and the invariant mass of the three-lepton system (right) for the data (points) and predictions (colored histograms). The contributions in the simulation from “external” photon conversions, where a real photon converts into a pair of (mostly) electrons from its interaction in the detector material, and so-called “internal” conversions, where a virtual photon decays into a pair of leptons, are shown separately. The lower panels show the ratio of the data to the sum of the predictions. The vertical lines on the data points represent the statistical uncertainty in the data; the shaded area corresponds to the total uncertainty in the prediction; the gray area in the ratio indicates the uncertainty related to the limited statistical precision in the prediction.

the loose selection. Prompt-lepton contamination from electroweak processes is subtracted using simulation. The misidentification rate is calculated separately for electrons and muons, and binned in  $p_T$  and  $|\eta|$  to take into account the kinematic properties of nonprompt leptons passing the tight-lepton definition.

Finally, the method is validated in data using a dedicated nonprompt-lepton control region. This region is defined similarly to the signal region, with the exception that either an OSSF pair is vetoed or the invariant mass of the OSSF pair is required to be incompatible with the  $Z$  boson mass. The nonprompt-lepton control region is defined for events with exactly one b-tagged jet and two or three jets, as these represent the events in the signal region for which the nonprompt-lepton background is sizable. The result of this validation is shown in Fig. 6, where the contribution labeled “nonprompt” is obtained using the approach described above. There is good agreement between the data and the nonprompt-lepton background prediction obtained from the control region in data.

## 6 Systematic uncertainties

The inclusive and differential measurements are affected by similar sources of experimental and theoretical uncertainties. The measurements follow the same approach to assessing the systematic uncertainties, modulo some small differences that are motivated by different fitting procedures.

The trigger efficiency is the probability of events that pass the analysis selection criteria to satisfy any of the trigger selection requirements. This efficiency is measured in a data sample where events are required to pass a set of reference triggers uncorrelated with any of the trigger

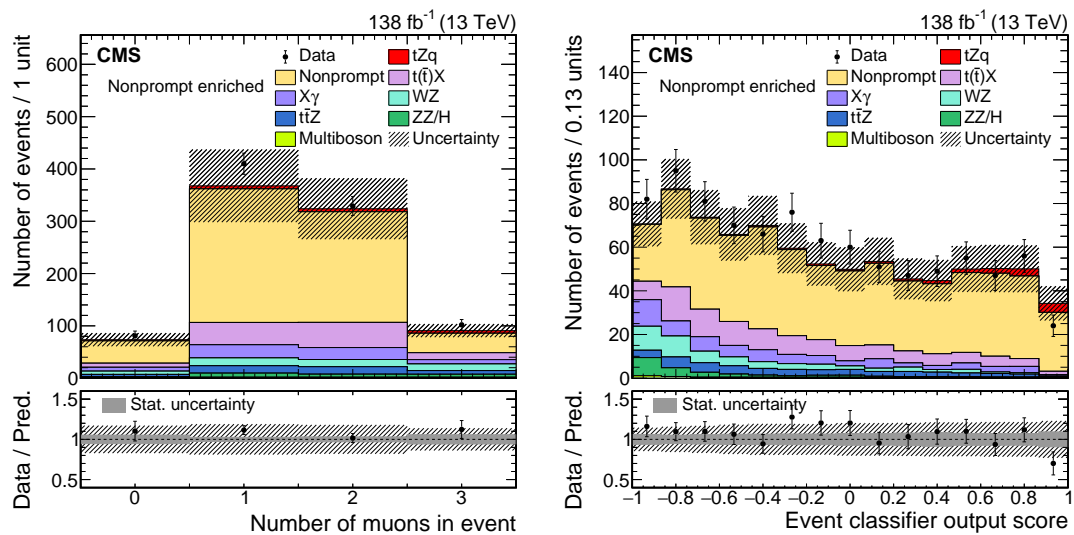


Figure 6: Distributions of the number of selected muons per event (left) and the output score of the multivariate classifier used for the signal extraction in the inclusive cross section measurement (right) in a control region enriched with nonprompt leptons for data (points) and predictions (colored histograms). The lower panels show the ratio of the data to the sum of the predictions. The vertical lines on the data points represent the statistical uncertainty in the data; the shaded area corresponds to the total uncertainty in the prediction; the gray area in the ratio indicates the uncertainty related to the limited statistical precision in the prediction.

requirements used in this analysis. An efficiency consistent with 100% is measured in both simulation and data, and therefore no correction is applied. Driven by the limited statistical precision of the trigger efficiency measurement, a systematic uncertainty of 2% is assigned to cover potential differences between data and simulation. This systematic uncertainty affects all processes equally, but because of its statistical origin, it is considered to be uncorrelated across the data-taking years.

The integrated luminosity measured in each data-taking period is used to normalize the predictions obtained from simulation with an associated systematic uncertainty of 1.2–2.5%, which is partially correlated across the data-taking years [11, 52, 53].

The pileup uncertainty alters the distribution of the number of pp collisions per bunch crossing. It is estimated by varying the total pp inelastic cross section in all simulated samples by  $\pm 4.6\%$  [32], affecting both the shape of the distributions that are fit in the signal extraction and the normalization of the predictions. This source of uncertainty is fully correlated across the data-taking years and processes.

In the 2016 and 2017 data sets, a too-early response of triggers related to the ECAL led to the mistaken selection of data events from the previous bunch crossing. In order to account for this effect, the simulated events are reweighted as a function of the  $p_T$  and  $\eta$  of selected jets and photons with the corresponding uncertainties. This source of uncertainty is fully correlated across all 2016 and 2017 simulated samples, but absent for the 2018 simulation.

Several uncertainties arise from the reconstruction and identification of various physics objects. Data-to-simulation scale factors are derived to correct the efficiencies of prompt-lepton reconstruction and identification, as well as the b tagging efficiency of reconstructed jets. The scale factors are varied within the associated uncertainties, affecting both the shape and normalization of the derived predictions in simulation. The uncertainties in the scale factors are split into

a statistical part originating from the finite statistical precision of the methods used to obtain them, and a systematic part originating from the methodology itself. The first part is considered to be uncorrelated between the data-taking years, while the latter part is treated as fully correlated.

The four-momentum of each selected jet is varied to account for the uncertainty in the jet energy resolution and the jet energy scale [38]. These variations are consistently propagated to  $\vec{p}_T^{\text{miss}}$  and the b tagging efficiency scale factors, and are considered to be partially correlated across all data-taking years and processes. An additional uncertainty, related to the unclustered energy, is taken into account by varying all unclustered contributions to  $\vec{p}_T^{\text{miss}}$  within their respective resolutions and propagating these changes to  $\vec{p}_T^{\text{miss}}$ . This uncertainty is considered to be uncorrelated among the data-taking years.

The tight-to-loose ratio method that is used for the estimation of the nonprompt-lepton background from control samples in data was verified and no bias in the shapes of various variable distributions was observed (as shown in Appendix A and Fig. 6). Therefore, no shape uncertainty is assigned to the nonprompt-lepton background estimate from data. Based on the level of agreement in the nonprompt-lepton control regions in data, a conservative normalization uncertainty of 30% is applied to this process, which covers the discrepancies (as shown in Fig. 6). It is considered correlated across the data-taking years.

Theoretical uncertainties include systematic effects associated with the renormalization and factorization scales at ME level, as well as with the PDFs used in the simulation. The former uncertainties are propagated to the final measurement by varying both scales independently up and down by a factor of two, avoiding the case where one scale is varied up while the other is varied down. The latter is propagated by reweighting the simulation using the corresponding variations in the NNPDF sets [29, 30]. Both types of systematic uncertainty are treated as fully correlated across the data-taking years, but while the PDF uncertainty is also correlated across all processes, the QCD scale uncertainties are considered uncorrelated between QCD- and electroweak-induced processes. These sources affect both the production cross section and the acceptance of all simulated processes. The systematic effect in the cross section is not taken into account for the  $t\bar{t}Z$ ,  $WZ$ ,  $ZZ$ , and  $Z\gamma$  processes, and only the acceptance effects are considered. Instead, a global normalization uncertainty is assigned to each of these processes. An uncertainty of 10% is applied to the  $WZ$ ,  $ZZ$ , and  $Z\gamma$  processes, which is larger than the typical uncertainty from dedicated measurements [50, 54]. This covers any difference in the considered phase space and is based on the study of control regions. The  $t\bar{t}Z$  cross section is measured to a precision of 8% [51]. However, there is some tension between the theoretical prediction and the measurement. In this analysis, a normalization uncertainty of 15% is assigned to the  $t\bar{t}Z$  process to cover this effect. The theoretical uncertainties associated with the renormalization scales for the initial- and final-state radiations (ISR and FSR) are estimated in a similar way, independent of the other scale uncertainties, by varying the corresponding scales up and down by a factor of two. Both sources of uncertainty are fully correlated across the data-taking years, but while the FSR uncertainty is also correlated across all processes, the ISR uncertainty is treated as uncorrelated between QCD-induced ( $t\bar{t}Z$ ) and electroweak-induced ( $tZq$ ) processes. The uncertainties related to the choice of the color-reconnection model used in the parton shower and to the underlying event tune are estimated for  $tZq$  and  $t\bar{t}Z$  with additional MC samples, produced with different color-reconnection models and varied underlying event tunes, respectively [25, 55]. Both are considered correlated across the data-taking years and processes.

In the differential measurement, choices used in estimating the background uncertainties are

slightly different with respect to the inclusive measurement to give more freedom to the differential fit. The theoretical uncertainties in PDFs, ISR, FSR, and the renormalization and factorization scales, are considered for the tZq and t̄Z processes. No a priori normalization uncertainty is applied to WZ, ZZ, and Z $\gamma$  events since the normalizations are kept freely floating in the fit. In addition, a normalization uncertainty of 25% is applied to the triboson processes [56]. For other rare processes involving top quarks, such as tWZ and t̄t in association with two additional bosons, a normalization uncertainty of 50% is assigned.

The impact of the dominant sources of systematic uncertainties in the inclusive tZq cross section measurement is discussed in more detail in Section 7.2

## 7 Inclusive cross section measurement

### 7.1 Signal extraction

The measurement of the inclusive tZq cross section is performed by fitting the distribution of the BDT discriminant used to separate the tZq signal from the various backgrounds. A binary BDT classifier is trained using the TVMA [46] package. The discriminating input variables are similar to those used in an earlier CMS measurement of the tZq process [1]. The most powerful ones were discussed in Section 4 and shown in Fig. 3.

The measurement uses a maximum likelihood fit of the predicted signal and background contributions to the data, binned in the distribution of the BDT discriminant. The likelihood  $\mathcal{L}$  to be maximized consists of the product of bin-by-bin Poisson probabilities  $\mathcal{P}$  for observing a given number of data events in each bin [57]:

$$\mathcal{L} = \prod_i \mathcal{P}(y_i^{\text{obs}} | y_i^{\text{exp}}) \prod_k p(\hat{\theta}_k | \theta_k), \quad (4)$$

where  $y_i^{\text{obs}}$  and  $y_i^{\text{exp}}$  are the observed and expected numbers of events in the  $i$ th bin, respectively. The number of expected events in bin  $i$  depends on the signal and background predictions as:

$$y_i^{\text{exp}} (\sigma_{\text{tZq}}, \vec{w}, \vec{\theta}) = s_i (\sigma_{\text{tZq}}, \vec{\theta}) + \sum_j b_{i,j} (w_j, \vec{\theta}), \quad (5)$$

where  $s_i$  is the expected number of tZq events in the  $i$ th bin, which depends on the targeted cross section  $\sigma_{\text{tZq}}$  and nuisance parameters  $\vec{\theta}$  to describe the uncertainties in the prediction. The variable  $b_{i,j}$  denotes the number of expected events from the  $j$ th background process in the  $i$ th bin, which depends on its normalization  $w_j$  and nuisance parameters  $\vec{\theta}$ . The factors  $p(\hat{\theta}_k | \theta_k)$  in Eq. (4) represent the probability of obtaining a best fit value  $\hat{\theta}_k$  for the  $k$ th nuisance parameter, given its a priori value  $\theta_k$ . This probability is log-normally distributed for normalization uncertainties and has a Gaussian density for shape uncertainties.

For the inclusive measurement, the signal region is subdivided into three subregions based on the number of jets and b-tagged jets: exactly 1 b-tagged jet and 2 or 3 jets (dominated by the WZ and nonprompt backgrounds), 1 b-tagged jet and  $\geq 4$  jets (dominated by the t̄Z and WZ backgrounds), and  $\geq 2$  b-tagged jets (dominated by the t̄Z background).

The fit is performed simultaneously for all considered data-taking years and event categories. The corresponding BDT discriminant distributions are shown in Fig. 7 for both the prefit (left) and postfit (right) normalizations. The control regions discussed in Section 5 are included in the fit, which allows a better constraint on the relevant systematic uncertainties in the background processes, especially their normalizations. The distributions used in the fit are the transverse

$W$  boson mass for the  $WZ$  control region, the number of jets for the  $ZZ$  and  $Z\gamma$  control region, the number of b-tagged jets for the  $t\bar{t}Z$  control region, and finally the total event yield for the nonprompt control region.

All sources of systematic uncertainties discussed in Section 6 are treated as nuisance parameters in the fit, with a consistent treatment of all correlations between various uncertainties.

## 7.2 Results

The predicted cross section for the  $tZq$  process, where the  $Z$  boson decays to a pair of electrons, muons, or  $\tau$  leptons, is  $\sigma_{tZq}^{\text{SM}} = 94.2^{+1.9}_{-1.8}$  (scale)  $\pm 2.5$  (PDF) fb [10]. The calculation is performed at NLO in the 5FS and also includes nonresonant lepton-pair production with  $m_{\ell\ell'} > 30$  GeV.

The signal strength is defined as the ratio of the observed to the predicted  $tZq$  cross sections and is measured in the signal region defined in Sections 4 and 7.1. The result is:

$$\mu = \frac{\sigma_{tZq}}{\sigma_{tZq}^{\text{SM}}} = 0.933^{+0.080}_{-0.077} \text{ (stat)}^{+0.078}_{-0.064} \text{ (syst)},$$

Using the predicted cross section mentioned above, this signal strength corresponds to the measured cross section of

$$\sigma_{tZq} = 87.9^{+7.5}_{-7.3} \text{ (stat)}^{+7.3}_{-6.0} \text{ (syst)} \text{ fb}.$$

Combining the statistical and systematic uncertainties in quadrature, the measured  $tZq$  cross section has a precision of 11%, which is an improvement over the previous measurements of this process [1, 2]. This is partly due to the smaller integrated luminosity of  $77 \text{ fb}^{-1}$  in earlier measurements. Another improvement comes from a broader definition of the signal by including events with two or more b-tagged jets, and events with at least four selected jets. The latter subregion, whose distributions are shown in the middle plots of Fig. 7, provides an important contribution to the improved sensitivity of this measurement. Additional gain comes from the improved performance of the lepton MVA and the looser selection criteria applied to this discriminant. The working point used in this analysis has a signal efficiency and background rejection of about 95% and 98%, respectively (as discussed in Section 3), whereas for the typical tighter working point, these numbers are 90% and 99%, respectively. The loosening of the lepton MVA selection criteria allowed better constraints on the relevant systematic uncertainties in the nonprompt-lepton background prediction using the dedicated control regions.

The dominant systematic uncertainties affecting the inclusive cross section measurement are shown in Fig. 8. These uncertainties include the effects on acceptance from varying the renormalization and factorization scales associated with the  $tZq$  and  $t\bar{t}Z$  processes, the normalization uncertainties in all the considered processes discussed in Section 6, and several other sources related to the b tagging efficiency correction, color reconnection, and parton showering. The impact of the color-reconnection model choice on the  $tZq$  signal strength is one-sided since it results from using an alternative model as opposed to a model parameter varied up and down. All sources of systematic uncertainty not shown in Fig. 8 have smaller impacts than the dominant ones discussed here. The best fit values of the nuisance parameters are all within one standard deviation of their expected values, and the measured impacts on the signal strength are generally in agreement with the corresponding expected values. The measured normalization of  $t\bar{t}Z$  events is shifted by about one standard deviation with respect to the theoretical prediction, and indicates an underprediction of this background. This is expected and is consistent with the previously published results [51]. The increased contribution from  $t\bar{t}Z$  events

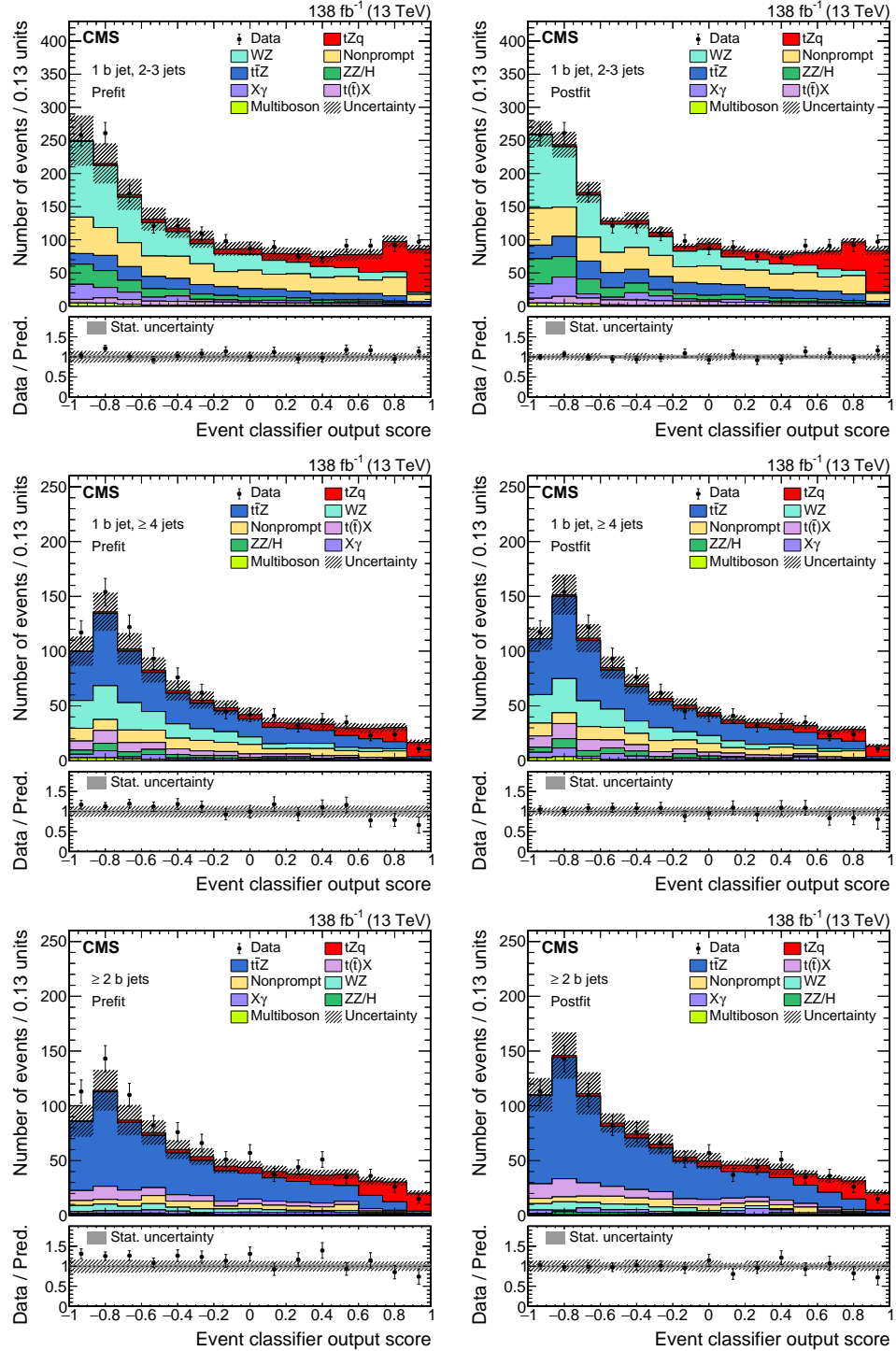


Figure 7: Distributions of the event BDT discriminant in the signal region for data (points) and predictions (colored histograms). The results are shown for prefit (left) and postfit (right) distributions in mutually exclusive signal subregions: exactly one b-tagged jet, 2–3 jets (upper); exactly one b-tagged jet,  $\geq 4$  jets (middle); and  $\geq 2$  b-tagged jets (lower). The lower panels show the ratio of the data to the sum of the predictions. The vertical lines on the data points represent the statistical uncertainty in the data; the shaded area corresponds to the total uncertainty in the prediction; the gray area in the ratio indicates the uncertainty related to the limited statistical precision.

after the fit results in a good agreement of prediction to data in both the  $t\bar{t}Z$ -dominated signal subregion (lower plots in Fig. 7) and the  $t\bar{t}Z$  control region with four leptons.

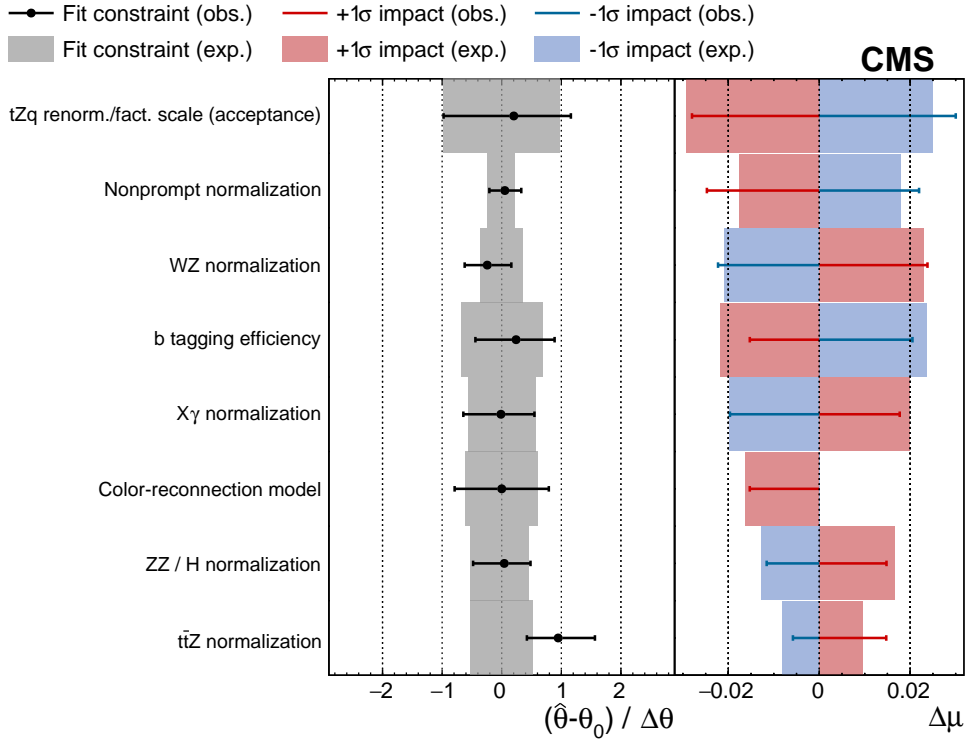


Figure 8: Summary of the dominant systematic uncertainties affecting the inclusive  $tZq$  cross section measurement. The left column lists the sources of systematic uncertainty, treated as nuisance parameters in the fit, in order of importance. In the middle column, the black points with the horizontal bars show for each source the difference between the observed best fit value ( $\hat{\theta}$ ) and the nominal value ( $\theta_0$ ), divided by the expected standard deviation ( $\Delta\theta$ ). The right column plots the change in the  $tZq$  signal strength  $\mu$  if a nuisance parameter is varied one standard deviation up (red), or down (blue). The gray, red, and blue bands display the same quantity as their corresponding markers, but using a simulated data set where all nuisance parameters are set to their expected values.

Figure 9 displays some noteworthy kinematic prefit distributions in the  $tZq$ -enriched region, where in addition to the signal selection detailed in Section 4, the BDT score is required to be greater than 0.5. The number of  $tZq$  signal and background events passing this selection are estimated to be 252 and 264, respectively, implying that the contribution of the signal in this  $tZq$ -enriched region is about 49%. Furthermore, these plots show a good sensitivity to the kinematic properties of the  $tZq$  signal and a good agreement between the data and simulation, with the exception of the  $m(3\ell)$  variable, as discussed further in Section 8. The imperfect simulation of reconstruction inefficiencies and detector acceptance effects (combined and labeled as “detector level” effects) could result in discrepancies between the shape and normalization of the measured distributions and the simulated ones. The good agreement between the measured and simulated distributions in the figure shows that these possible effects are relatively small in this phase space. Furthermore, the number of events in the data associated with the  $tZq$  process means that a differential cross section measurement is possible, once the detector-level effects are corrected for, as described in Section 8.

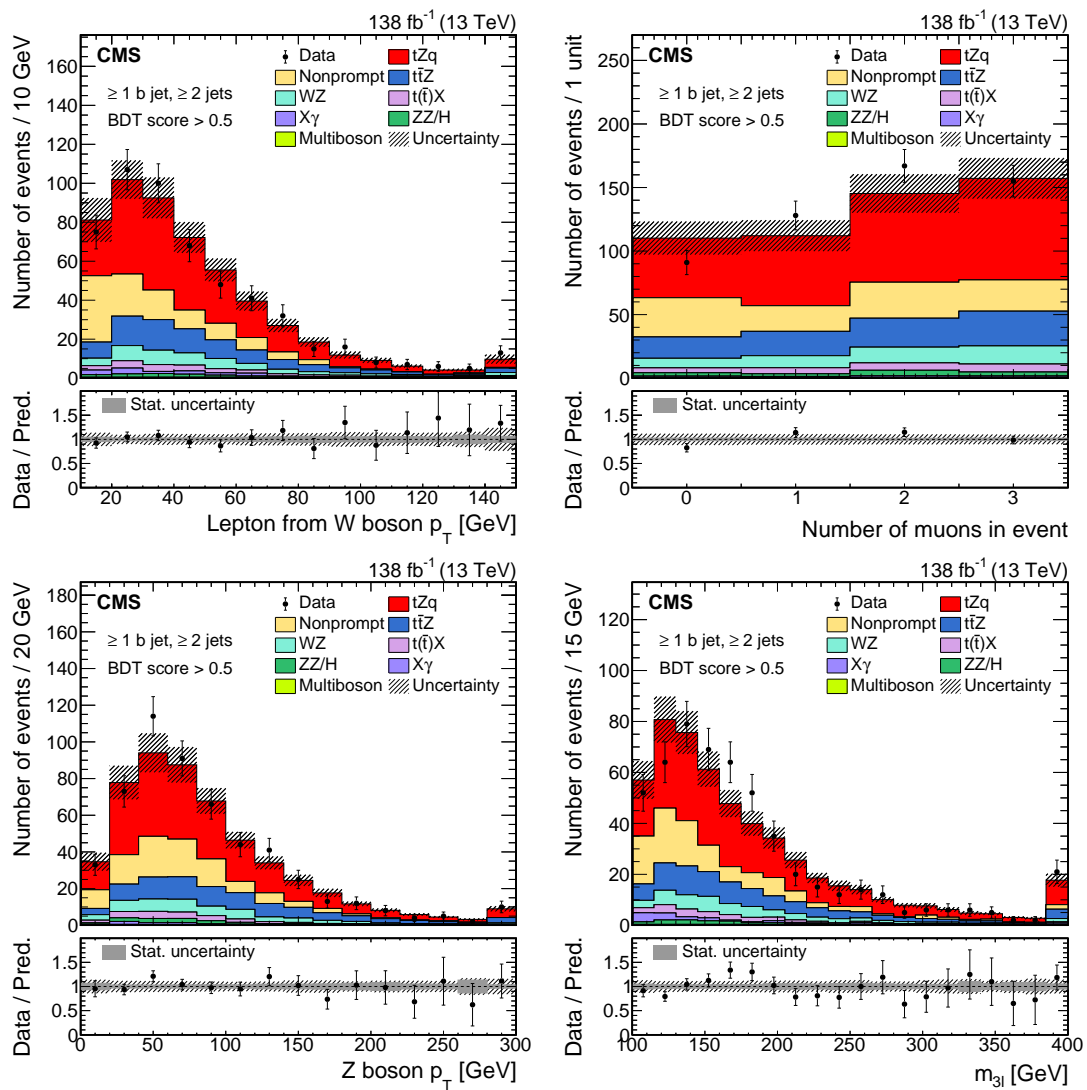


Figure 9: Prefit distributions at the detector level of some of the important variables used in the tZq analysis from a tZq-enriched region for the data (points) and predictions (colored histograms). The selection criteria discussed in Section 4 have been used, along with the requirement that the event BDT discriminant be greater than 0.5. The variables shown are as follows: transverse momentum of the lepton associated with the decay of the top quark (upper left), number of muons in the event (upper right), reconstructed transverse momentum of the Z boson (lower left) and transverse mass of the W boson (lower right). The lower panels show the ratio of the data to the sum of the predictions. The vertical lines on the data points represent the statistical uncertainty in the data; the shaded area corresponds to the total uncertainty in the prediction; the gray area in the ratio indicates the uncertainty related to the limited statistical precision in the prediction.

In addition to the inclusive tZq cross section, the production cross sections of a top quark ( $tZq(\ell_t^+)$ ), top antiquark ( $\bar{t}Zq(\ell_t^-)$ ), and their ratio  $R$  are determined. To this end, the signal regions are split further based on the charge of the lepton associated with the top quark (or antiquark) decay, and the fit procedure is modified to simultaneously extract the signal strengths for the top quark and antiquark processes. For the measurement of the ratio  $R$ , the fit procedure is modified further to directly obtain the best fit result for the ratio. The measured signal

strengths for the separate top quark and antiquark cross sections are:

$$\begin{aligned}\mu_{tZq(\ell_t^+)} &= 1.02^{+0.10}_{-0.09} \text{ (stat)}^{+0.07}_{-0.06} \text{ (syst)}, \\ \mu_{\bar{t}Zq(\ell_t^-)} &= 0.79^{+0.15}_{-0.14} \text{ (stat)}^{+0.09}_{-0.08} \text{ (syst)}.\end{aligned}$$

Using the MADGRAPH5\_aMC@NLO 5FS predictions for the cross sections, these signal strengths translate into:

$$\begin{aligned}\sigma_{tZq(\ell_t^+)} &= 62.2^{+5.9}_{-5.7} \text{ (stat)}^{+4.4}_{-3.7} \text{ (syst)} \text{ fb}, \\ \sigma_{\bar{t}Zq(\ell_t^-)} &= 26.1^{+4.8}_{-4.6} \text{ (stat)}^{+3.0}_{-2.8} \text{ (syst)} \text{ fb}, \\ R &= 2.37^{+0.56}_{-0.42} \text{ (stat)}^{+0.27}_{-0.13} \text{ (syst)}.\end{aligned}$$

The relative systematic uncertainty is reduced in the ratio measurement due to partial correlations. Although currently dominated by the statistical uncertainties, these results show promise for a future precise determination (at the high-luminosity LHC) of the top quark to antiquark production cross section ratio in the rare process  $tZq$ , similarly to what has already been obtained for  $t$ -channel single top quark production [58].

## 8 Measurements of the differential cross sections and the spin asymmetry

Differential  $tZq$  cross section measurements are performed as functions of several observables at the parton and particle levels, as defined in Section 8.1. The selected observables are potentially sensitive to beyond-SM effects and can provide information on the modeling of the  $tZq$  process. Observables based only on lepton kinematic properties are the transverse momenta of the  $Z$  boson,  $p_T(Z)$ , and the lepton from the top quark,  $p_T(\ell_t)$ , the invariant mass of the three leptons,  $m(3\ell)$ , and the difference in azimuthal angle between the two leptons from the  $Z$  boson decay,  $\Delta\phi(\ell, \ell')$ . Other selected variables rely on the top quark reconstruction and include the cosine of the top quark polarization angle,  $\cos(\theta_{\text{pol}}^*)$ , and the invariant mass of the  $t + Z$  system,  $m(t, Z)$ . The last two observables are the  $p_T(j')$  and  $|\eta(j')|$  at the particle level of the recoiling jet.

A likelihood-based unfolding procedure is performed to separately measure the cross section  $\sigma_{tZq, k}$ , in each kinematic region defined by each generator-level bin  $k \in \{1, 2, \dots\}$ , where the generator level here corresponds to truth information at either the parton or particle levels, defined in the next section. The unfolding procedure accounts for the finite resolution and limited acceptance of the detector and, at the parton level, for hadronization effects. Compared to the inclusive measurement, not one but multiple signal parameters associated with the different generator-level bins are extracted in a multidimensional maximum likelihood fit. The first term in Eq. (5) is therefore replaced by a sum over signal contributions from the generator-level bins,

$$s_i \left( \sigma_{tZq}, \vec{\theta} \right) \rightarrow \sum_k s_{i, k} \left( \sigma_{tZq, k}, \vec{\theta} \right). \quad (6)$$

To extract the signal in multiple kinematic regions requires not only the separation between the  $tZq$  and background processes, but also the mutual separation of the  $tZq$  contributions coming from different generator-level bins corresponding to the different kinematic regions. For this reason, an alternative categorization of events in the signal region with respect to the inclusive measurement and a more elaborate classifier have been developed.

## 8.1 Parton- and particle-level definitions

The binning of the various observables at the generator level is optimized based on a trade-off between the expected number of tZq events in each bin at the detector level, the bin width, and the stability and purity of the response matrix that relates the generator-level distributions to the detector-level distributions in the simulated tZq signal. The stability is based on all reconstructed events and defined as the fraction of events from a generator-level bin that are observed in the corresponding detector-level bin. The purity is based on all reconstructed events and defined as the fraction of events from a detector-level bin that belong to the corresponding generator-level bin.

Observables associated only with leptons generally have good measurement resolution, and a total of four bins is chosen. This is also motivated by the number of events in the data set and the purity and stability values above 95%. For observables involving jets, a total of three bins is chosen to account for the poorer resolution compared to the lepton observables, and to lessen the effects from statistical fluctuations. The corresponding purity and stability values are above 55%. With this choice of binning, the application of a regularization procedure was found to be unnecessary. Examples of two response matrices, for the  $p_T(Z)$  at the parton level and  $p_T(t)$  at the particle level, are shown in Fig. 10.

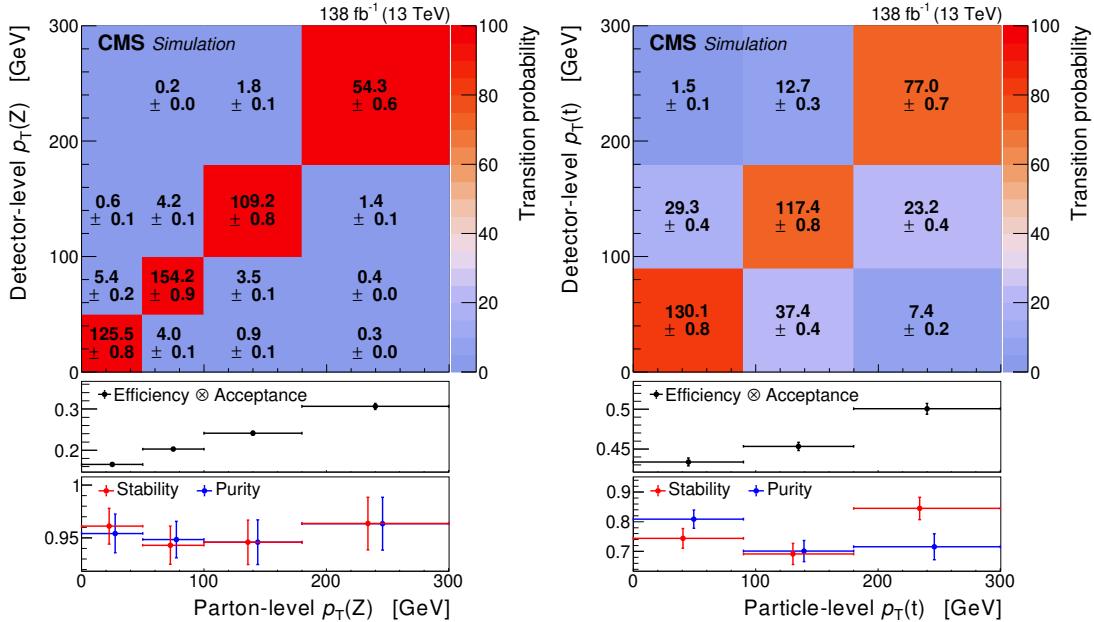


Figure 10: Response matrices for  $p_T(Z)$  at the parton level (left) and  $p_T(t)$  at the particle level (right) for tZq events in the full and visible phase space, respectively. The expected number of reconstructed events is given for each bin. The color indicates the transition probability for an event in a generator-level bin to have a reconstructed value corresponding to a given detector-level bin. The efficiency times acceptance values of reconstructing events are plotted in the middle panels. The lower panels show the stability and purity values as defined in the text. The vertical bars on the points give the statistical uncertainty and the horizontal bars show the bin width.

Generator-level definitions at the parton and particle levels are used. At the parton level, the measurement is performed in the full phase space of events with three prompt leptons. Parton-level objects are defined based on event generator particles after ISR and FSR and before hadronization. The generated on-shell top quark is selected and the lepton from its decay is identi-

fied. The leptons that are not associated with the decay products of the top quark are assigned to the OSSF lepton pair. The quark that recoils against the virtual W boson is identified as the quark with flavor u, d, s, or c. In the case of an ambiguity, the one with the highest  $p_T$  is chosen.

The particle-level definition aims at minimizing the dependency on the choice of the generator and reducing the uncertainty associated with the extrapolation to the detector level. A collection of so-called “dressed” leptons is defined through a clustering process involving prompt electrons or muons and photons that do not arise from hadronic decays using the anti- $k_T$  algorithm with  $R = 0.1$  [36, 37]. Jets are clustered from all stable (lifetime  $>30\text{ ps}$ ) particles, excluding prompt leptons but including neutrinos from hadronic decays, with the anti- $k_T$  algorithm and  $R = 0.4$ . Using the ghost-clustering method [59], b hadrons are scaled to have an infinitely small momentum and included in the clustering process. A jet is labeled as a b-tagged jet if such a ghost b hadron is clustered inside it. The  $\vec{p}_T^{\text{miss}}$  is defined as the vector  $\vec{p}_T$  sum of all neutrinos from W, Z, or prompt  $\tau$  decays. Further selection criteria on  $p_T$ ,  $\eta$ , and  $\Delta R(j, \ell)$  are applied to these objects, and the events are selected and reconstructed using the same requirements and algorithms as in the signal region at the detector level. The measurement at the particle level is hence performed in a fiducial phase space, leading to the fact that the absolute differential cross sections are reduced by a factor of about two with respect to the parton-level measurements. Reconstructed tZq events outside the fiducial phase space make up about 7% of all reconstructed tZq events. They are included in the signal extraction and scaled in the fit with the integrated differential cross section.

## 8.2 Signal extraction and fit strategy

In the measurement of the differential tZq cross sections, a multiclass neural network, implemented via the TENSORFLOW [60] package, is used. The neural network contains 22 input and five output nodes to distinguish tZq events from  $t\bar{t}Z$ , WZ,  $t(\bar{t})X$ , and all other backgrounds. The most important input variables are shown in Fig. 3. The separation into multiple output nodes is based on the distinct nature of the different backgrounds and provides an improved isolation of tZq events compared to a binary classifier.

For the signal extraction, events in the signal region (defined in Section 4) are additionally required to have fewer than four central jets. Events with four or more central jets are dominated by  $t\bar{t}Z$  events and used as a control region ( $t\bar{t}Z \rightarrow 3\ell$ ). The remaining events in the signal region are split into three subregions (four for observables only involving leptons) based on the value of the observable at the detector level, using the bin ranges from the definition of the parton- and particle-level bins. As a result, the tZq contribution from each parton- and particle-level bin of the considered observable is enriched in the corresponding subregion at the detector level. To isolate the tZq events from various background events, each subregion is binned in the neural network score of the tZq output node. As an example, the prefit and post-fit  $p_T(j')$  and  $m(3\ell)$  distributions in the signal region are shown in Figs. 11 and 12, respectively.

To further constrain the normalization of various backgrounds, additional complementary control regions with three or four leptons are defined, as described in Section 5, and included in the signal extraction. Events in these control regions are additionally required to have at least two jets to minimize the uncertainty associated with the extrapolation of the various backgrounds to the signal region. Events in the  $t\bar{t}Z \rightarrow 3\ell$  control region are fit as a function of the neural network score of the  $t\bar{t}Z$  output node to separate the  $t\bar{t}Z$  process, while events in the WZ control regions are fit as a function of  $m_T^W$ . The  $Z\gamma$  control region consists of two bins that are included in the fit, which are determined from the number of selected electrons. Events in the  $t\bar{t}Z \rightarrow 4\ell$  control region are separated into three bins in the fit, as a function of the number of b-tagged

jets in the event. Events in the ZZ and nonprompt-lepton control regions are fit in one bin.

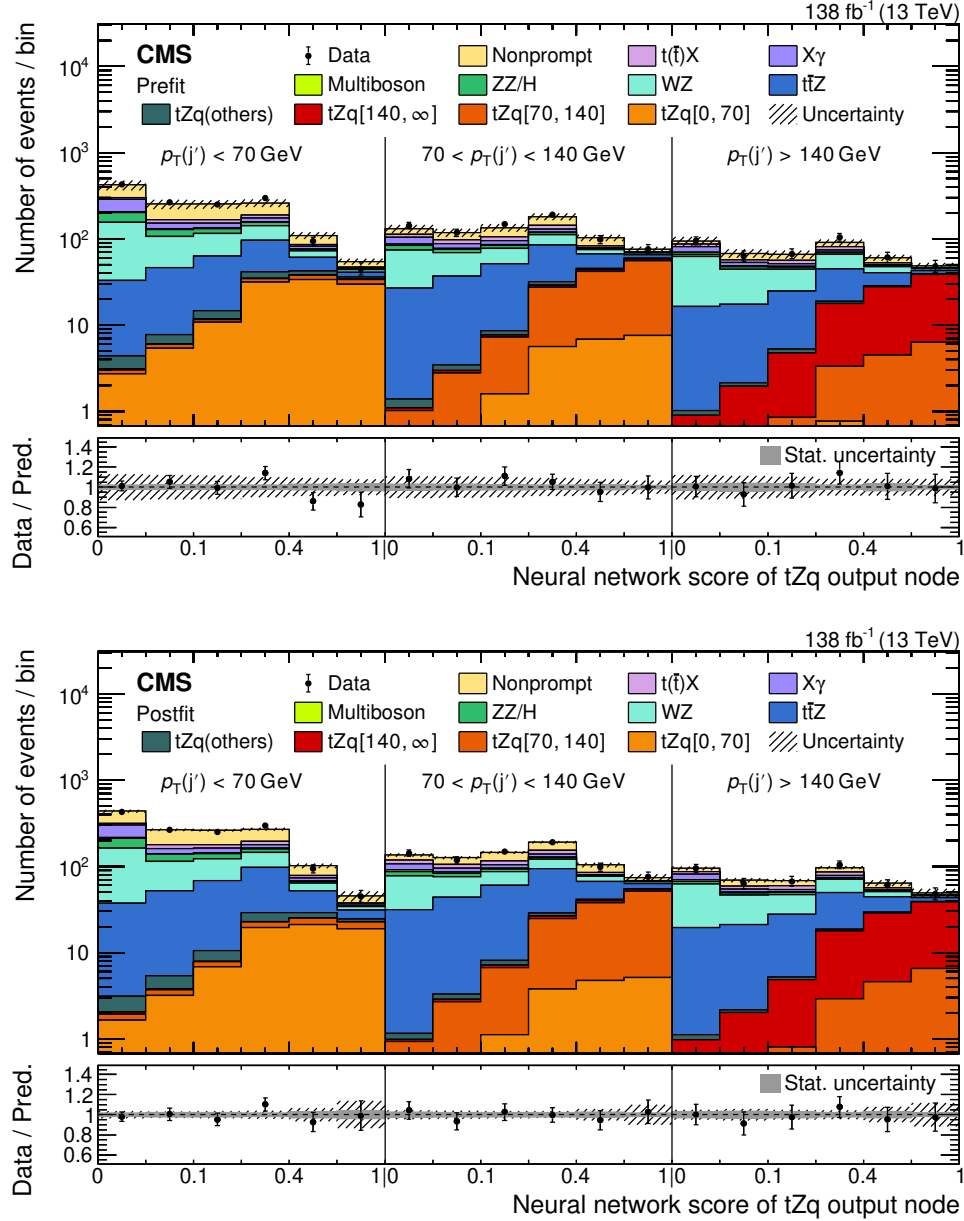


Figure 11: Prefit (upper) and postfit (lower) distributions of the neural network score from the tZq output node for events in the signal region with fewer than four jets, used for the  $p_T(j')$  differential cross section measurement at the particle level. The data are shown by the points and the predictions by the colored histograms. The vertical lines on the points represent the statistical uncertainty in the data, and the hatched region the total uncertainty in the prediction. The events are split into three subregions based on the value of  $p_T(j')$  measured at the detector level. Three different tZq templates, defined by the same intervals of  $p_T(j')$  at the particle level and shown in different shades of orange and red, are used to model the contribution of each particle-level bin. Reconstructed tZq events that are outside the fiducial phase space are labeled as “tZq (others)” and represent a minor contribution. The lower panels show the ratio of the data to the sum of the predictions, with the gray band indicating the uncertainty from the finite number of MC events.

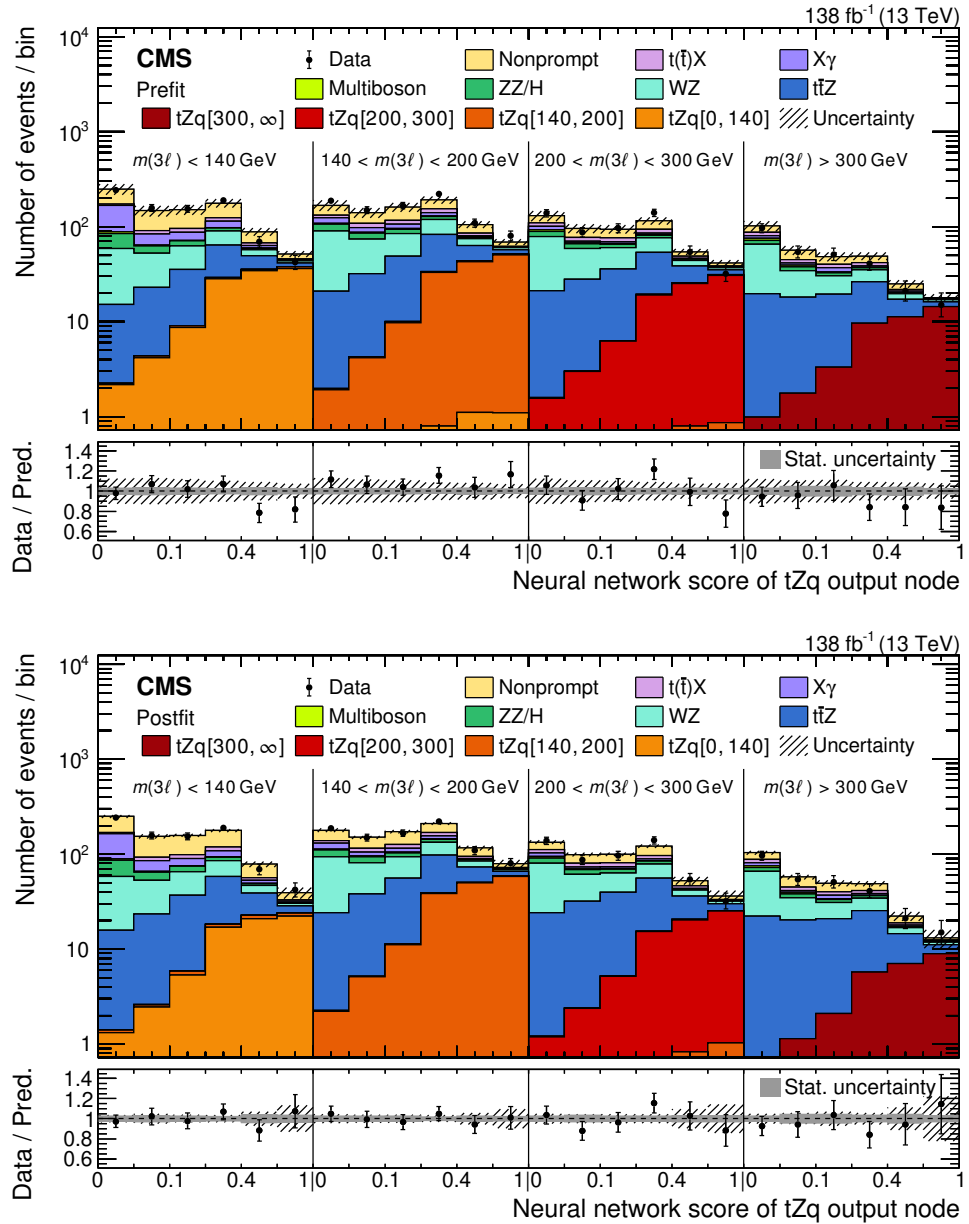


Figure 12: Prefit (upper) and postfit (lower) distributions of the neural network score from the tZq output node for events in the signal region with fewer than four jets, used for the  $m(3\ell)$  differential cross section measurement at the parton level. The data are shown by the points and the predictions by the colored histograms. The vertical lines on the points represent the statistical uncertainty in the data, and the hatched region the total uncertainty in the prediction. The events are split into four subregions based on the value of  $m(3\ell)$  measured at the detector level. Four different tZq templates, defined by the same intervals of  $m(3\ell)$  at the parton level and shown in different shades of orange and red, are used to model the contribution of each parton-level bin. The lower panels show the ratio of the data to the sum of the predictions, with the gray band indicating the uncertainty from the finite number of MC events.

### 8.3 Results

The measured absolute differential cross sections are shown in Figs. 13–15. The last bin of each distribution also includes the overflow contributions.

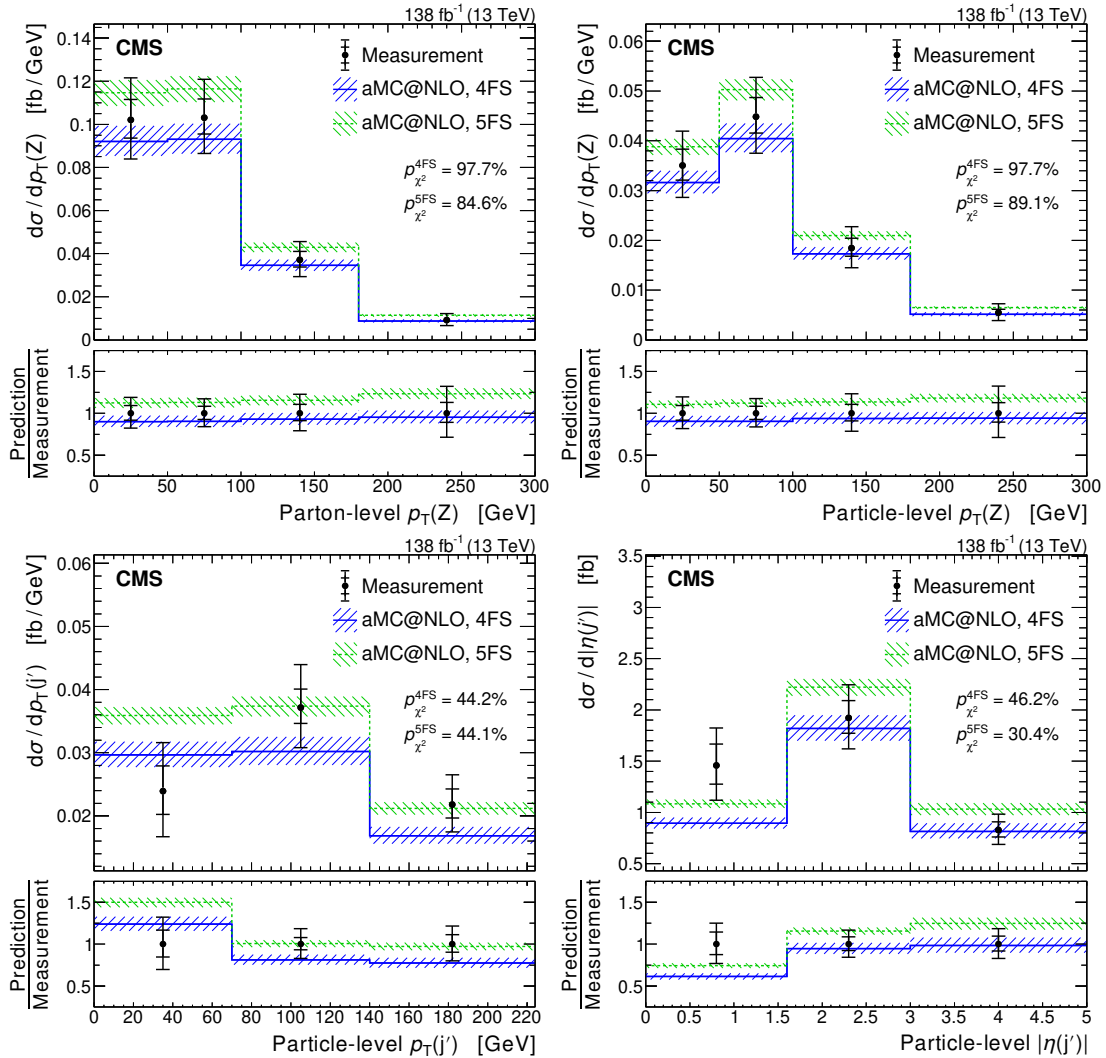


Figure 13: Absolute differential cross sections as a function of  $p_T(Z)$  measured at the parton (upper left) and particle levels (upper right), as well as a function of  $p_T(j')$  (lower left) and  $|\eta(j')|$  (lower right) at the particle level. The observed values are shown as black points, with the inner and outer vertical bars giving the systematic and total uncertainties, respectively. The SM predictions for the tZq process are based on events simulated in the 5FS (green) and 4FS (blue). The  $p$ -values of the  $\chi^2$  tests are given to quantify their compatibility with the measurement. The lower panels show the ratio of the simulation to the measurement.

The full covariance matrix is obtained from the fit and the normalized differential cross sections, shown in Figs. 16–18, are calculated by dividing each absolute differential cross section value by the sum of the values from all the bins. In general, observables that include quarks in their definition are measured to a precision of around 20–30% in each bin. For observables that are associated with leptons only the uncertainty goes down to 15% in some bins. As a cross-check, the differential cross section of each distribution is integrated, extrapolated, and compared to the result of the inclusive measurement. In all cases, the results are in good agreement within the associated uncertainties.

The measured distributions are compared with theoretical predictions of tZq at NLO in QCD for the 4FS and 5FS. Uncertainties in these predictions include the effects from the ME factorization and renormalization scales, PDF, ISR, and FSR, as discussed before. For the normalization

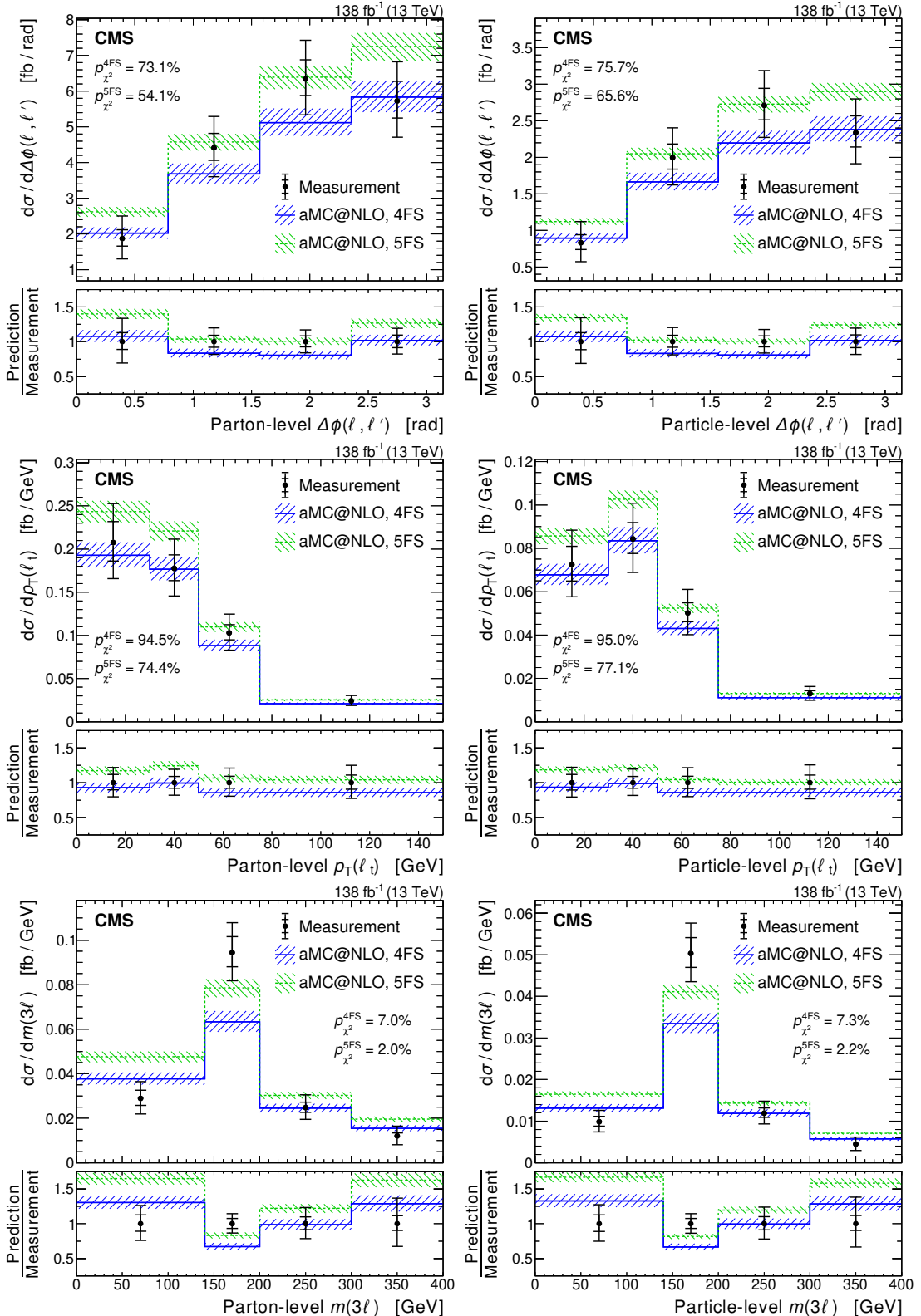


Figure 14: Absolute differential cross sections at the parton (left) and particle level (right) measured as a function of  $\Delta\phi(\ell, \ell')$  (upper),  $p_T(\ell_t)$  (middle) and  $m(3\ell)$  (lower). The observed values are shown as black points, with the inner and outer vertical bars giving the systematic and total uncertainties, respectively. The SM predictions for the  $tZq$  process are based on events simulated in the 5FS (green) and 4FS (blue). The  $p$ -values of the  $\chi^2$  tests are given to quantify their compatibility with the measurement. The lower panels show the ratio of the simulation to the measurement.

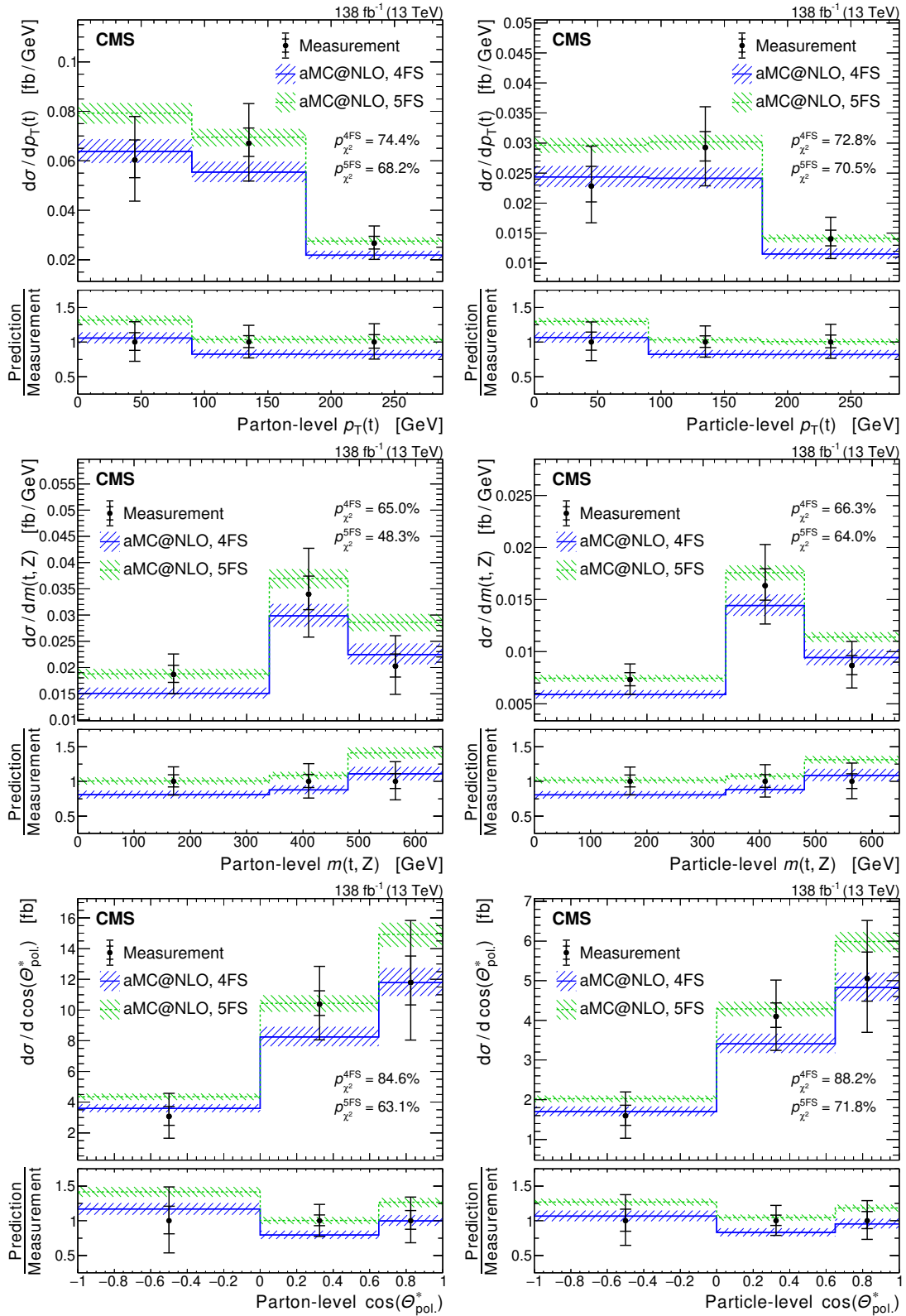


Figure 15: Absolute differential cross sections at the parton (left) and particle level (right) measured as a function of  $p_T(t)$  (upper),  $m(t, Z)$  (middle) and  $\cos(\theta_{\text{pol}}^*)$  (lower). The observed values are shown as black points, with the inner and outer vertical bars giving the systematic and total uncertainties, respectively. The SM predictions for the  $tZq$  process are based on events simulated in the 5FS (green) and 4FS (blue). The  $p$ -values of the  $\chi^2$  tests are given to quantify their compatibility with the measurement. The lower panels show the ratio of the simulation to the measurement.

of the 4FS a cross section of  $73.6 \pm 6.2$  (scale)  $\pm 0.4$  (PDF) fb is used, as obtained from the MADGRAPH5\_aMC@NLO generator.

Although the 5FS predicts larger cross sections [61, 62] as compared with the 4FS, the absolute differential cross sections measurements are compatible with both calculations within the uncertainties. The two methods yield similar results for the normalized differential cross sections, both of which are compatible with the measurement. The only exception is the normalized  $m(3\ell)$  differential cross section, shown in the lower plots of Fig. 17, where neither scheme is able to describe the measurement around 175 GeV. The level of agreement between the unfolded measurements and the theoretical predictions is quantified using  $p$ -values from a  $\chi^2$  test, summarized in Table B.1, where the full covariance matrix for the measurement and each prediction is considered.

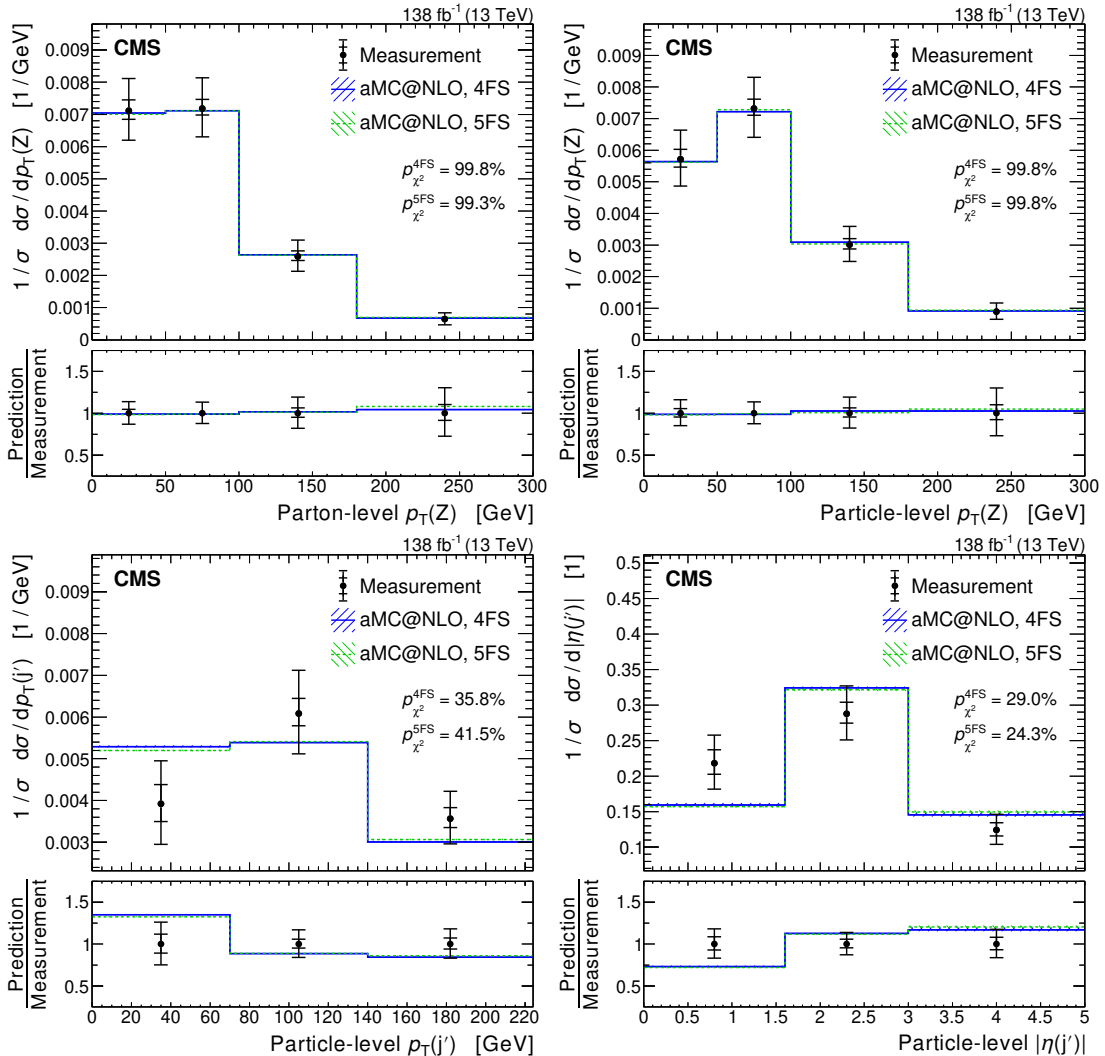


Figure 16: Normalized differential cross sections measured as a function of  $p_T(Z)$  at the parton (upper left) and particle level (upper right), as well as a function of  $p_T(j')$  (lower left) and  $|\eta(j')|$  (lower right) at the particle level. The observed values are shown as black points, with the inner and outer vertical bars giving the systematic and total uncertainties, respectively. The SM predictions for the  $tZq$  process are based on events simulated in the 5FS (green) and 4FS (blue). The  $p$ -values of the  $\chi^2$  tests are given to quantify their compatibility with the measurement. The lower panels show the ratio of the simulation to the measurement.

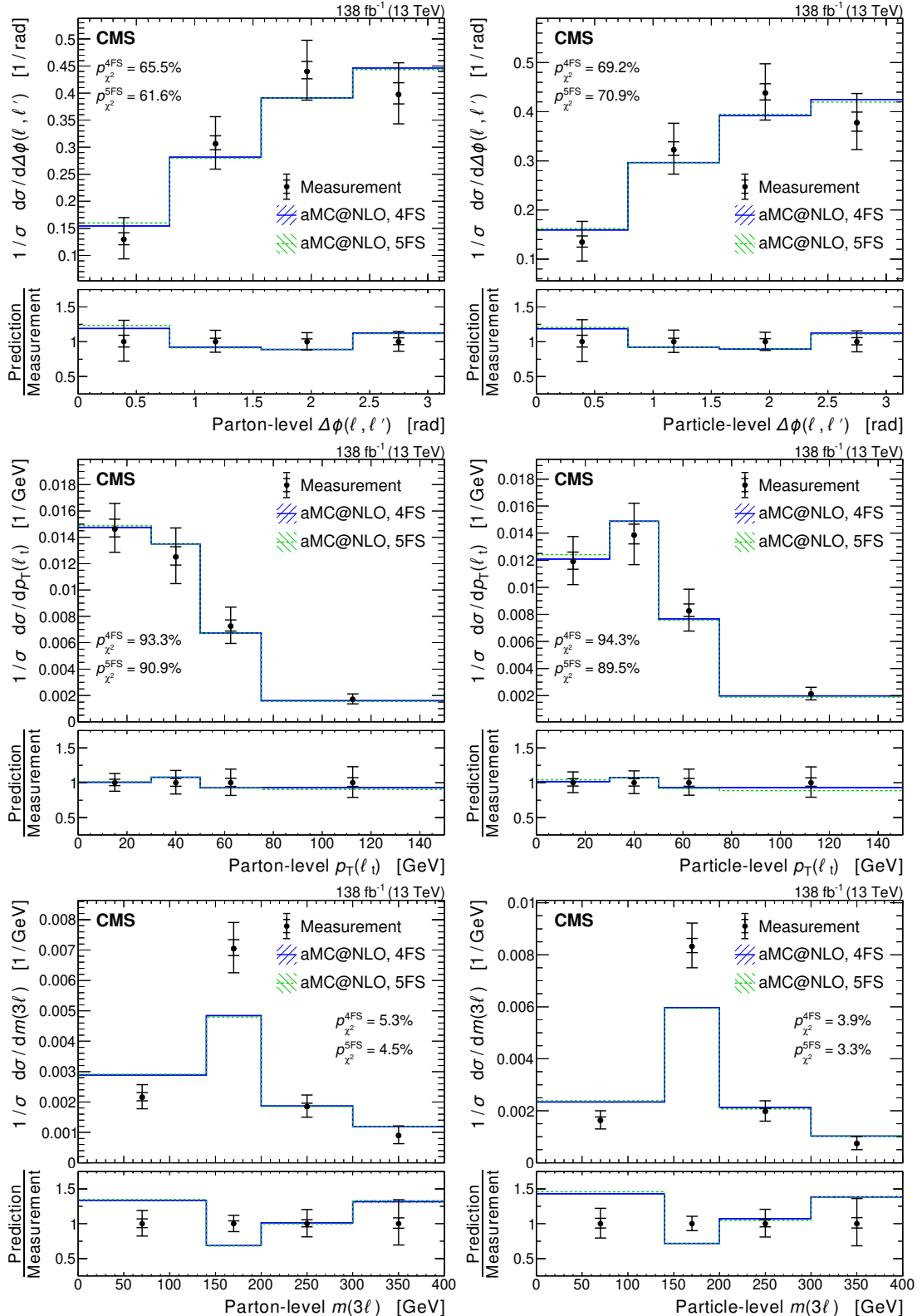


Figure 17: Normalized differential cross sections measured at the parton (left) and particle level (right) as a function of  $\Delta\phi(\ell, \ell')$  (upper),  $p_T(\ell_t)$  (middle) and  $m(3\ell)$  (lower). The observed values are shown as black points, with the inner and outer vertical bars giving the systematic and total uncertainties, respectively. The SM predictions for the tZq process are based on events simulated in the 5FS (green) and 4FS (blue). The  $p$ -values of the  $\chi^2$  tests are given to quantify their compatibility with the measurement. The lower panels show the ratio of the simulation to the measurement.

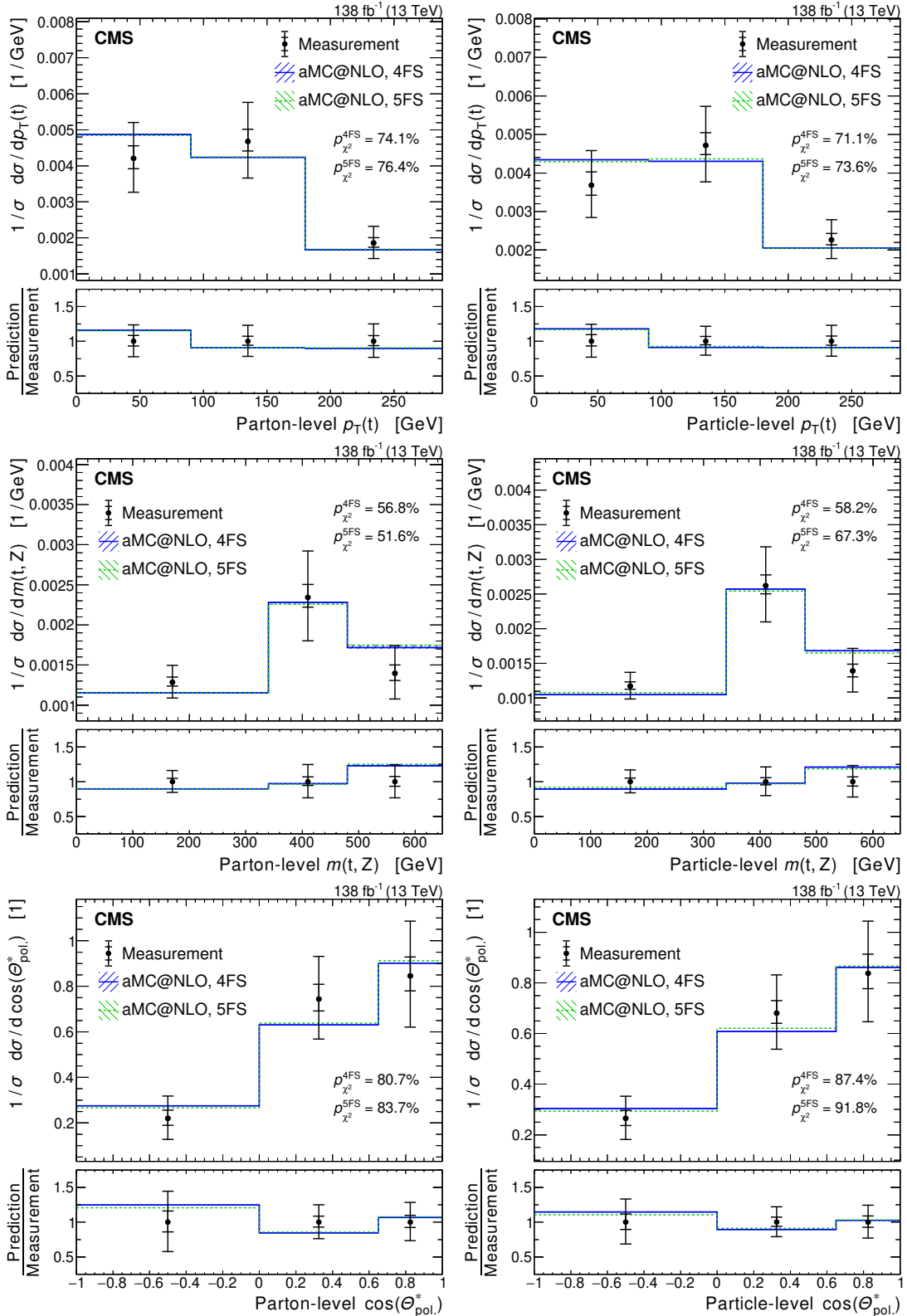


Figure 18: Normalized differential cross sections measured at the parton (left) and particle level (right) as a function of  $p_T(t)$  (upper),  $m(t,Z)$  (middle) and  $\cos(\theta_{\text{pol}}^*)$  (lower). The observed values are shown as black points, with the inner and outer vertical bars giving the systematic and total uncertainties, respectively. The SM predictions for the  $tZq$  process are based on events simulated in the 5FS (green) and 4FS (blue). The  $p$ -values of the  $\chi^2$  tests are given to quantify their compatibility with the measurement. The lower panels show the ratio of the simulation to the measurement.

In the measurement of the spin asymmetry, the fit of  $\cos(\theta_{\text{pol}}^*)$  at the parton level is reparameterized according to Eq. (3) such that the spin asymmetry is directly used as a free parameter in the fit. Apart from the spin asymmetry, the total cross section is left freely floating in the fit as well, to account for the overall normalization. The spin asymmetry is measured as

$$A_\ell = 0.54 \pm 0.16 \text{ (stat)} \pm 0.06 \text{ (syst)},$$

compatible with SM predictions of  $A_\ell^{4\text{FS}} = 0.44$  (in the 4FS) and  $A_\ell^{5\text{FS}} = 0.45$  (in the 5FS) from MADGRAPH5\_aMC@NLO simulations at NLO. Uncertainties in the SM predictions from ISR, FSR, PDFs, and renormalization and factorization scales at ME level were found to be negligible with respect to those of the measured value. Additional prefit and postfit results, the extracted distribution, and the likelihood as a function of the spin asymmetry are given in Appendix C.

The uncertainties in both the differential cross section and spin asymmetry measurements are dominated by the statistical component. The leading systematic uncertainties come from the experimental uncertainties, including the background modeling, b tagging efficiency, and lepton identification. For measurements using observables that include quarks in their definition, the jet energy scale also represents an important source of systematic uncertainty. The leading theoretical uncertainties are associated with the renormalization and factorization scales at ME level, and FSR effects.

## 9 Summary

Inclusive and differential cross section measurements of single top quark production in association with a Z boson (tZq) are presented using events with three leptons (electrons or muons). The data sample for this measurement was collected by the CMS experiment at the LHC in proton-proton collisions at a center-of-mass energy of 13 TeV and corresponds to an integrated luminosity of  $138 \text{ fb}^{-1}$ . Including nonresonant lepton pairs, an inclusive cross section of  $\sigma_{\text{tZq}} = 87.9^{+7.5}_{-7.3} \text{ (stat)}^{+7.3}_{-6.0} \text{ (syst)} \text{ fb}$  is obtained for dilepton invariant masses greater than 30 GeV. This result is the most precise inclusive tZq cross section measurement to date, with a relative precision about 25% better than previously published results. For the first time, the inclusive tZq cross sections are also measured separately for top quark and antiquark production, obtaining  $\sigma_{\text{tZq}(\ell_t^+)} = 62.2^{+5.9}_{-5.7} \text{ (stat)}^{+4.4}_{-3.7} \text{ (syst)} \text{ fb}$  and  $\sigma_{\bar{\text{t}}\text{Zq}(\ell_t^-)} = 26.1^{+4.8}_{-4.6} \text{ (stat)}^{+3.0}_{-2.8} \text{ (syst)} \text{ fb}$ , respectively, with the ratio of  $2.37^{+0.56}_{-0.42} \text{ (stat)}^{+0.27}_{-0.13} \text{ (syst)}$ . The measured values compared to the theoretical predictions are summarized in Fig. 19.

The differential tZq cross sections are measured for the first time at the parton and particle levels using a binned maximum-likelihood-based unfolding. The studied observables are the transverse momenta of the top quark, the Z boson, and the lepton associated with the top quark decay, as well as the invariant masses of the three leptons and the t + Z system. Also used as observables are the difference in azimuthal angle between the two leptons from the Z boson decay, the cosine of the top quark polarization angle, and, at the particle level, the transverse momentum and absolute pseudorapidity of the recoiling jet. The results are mostly compatible with the standard model predictions using both the four- and five-flavor schemes, while the sensitivity is not sufficient to show a preference for one or the other. From the differential distribution of the top quark polarization angle, the top quark spin asymmetry is measured to be  $A_\ell = 0.54 \pm 0.16 \text{ (stat)} \pm 0.06 \text{ (syst)}$ , in agreement with the standard model prediction.

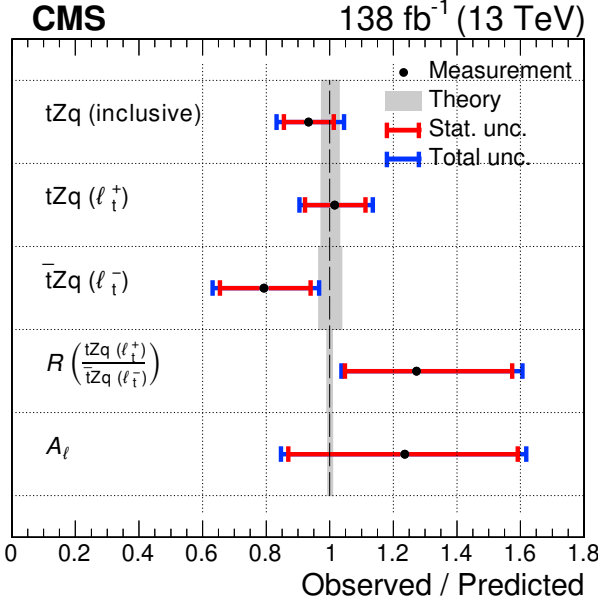


Figure 19: Measured values of the inclusive tZq cross section (first row), top quark and anti-quark cross sections (second and third rows) and their ratio (fourth row), together with the top quark spin asymmetry in the tZq process (last row). Each row shows the ratio between the observed and the SM predicted values. The black points show the central values, while the red and blue bars refer to the statistical and total uncertainties in the measurements, respectively. Uncertainties in the predictions are indicated by the gray bands.

## Acknowledgments

We congratulate our colleagues in the CERN accelerator departments for the excellent performance of the LHC and thank the technical and administrative staffs at CERN and at other CMS institutes for their contributions to the success of the CMS effort. In addition, we gratefully acknowledge the computing centers and personnel of the Worldwide LHC Computing Grid and other centers for delivering so effectively the computing infrastructure essential to our analyses. Finally, we acknowledge the enduring support for the construction and operation of the LHC, the CMS detector, and the supporting computing infrastructure provided by the following funding agencies: BMBWF and FWF (Austria); FNRS and FWO (Belgium); CNPq, CAPES, FAPERJ, FAPERGS, and FAPESP (Brazil); MES and BNSF (Bulgaria); CERN; CAS, MoST, and NSFC (China); MINCIENCIAS (Colombia); MSES and CSF (Croatia); RIF (Cyprus); SENESCYT (Ecuador); MoER, ERC PUT and ERDF (Estonia); Academy of Finland, MEC, and HIP (Finland); CEA and CNRS/IN2P3 (France); BMBF, DFG, and HGF (Germany); GSRI (Greece); NKFIH (Hungary); DAE and DST (India); IPM (Iran); SFI (Ireland); INFN (Italy); MSIP and NRF (Republic of Korea); MES (Latvia); LAS (Lithuania); MOE and UM (Malaysia); BUAP, CINVESTAV, CONACYT, LNS, SEP, and UASLP-FAI (Mexico); MOS (Montenegro); MBIE (New Zealand); PAEC (Pakistan); MSHE and NSC (Poland); FCT (Portugal); JINR (Dubna); MON, RosAtom, RAS, RFBR, and NRC KI (Russia); MESTD (Serbia); SEIDI, CPAN, PCTI, and FEDER (Spain); MOSTR (Sri Lanka); Swiss Funding Agencies (Switzerland); MST (Taipei); ThEPCenter, IPST, STAR, and NSTDA (Thailand); TUBITAK and TAEK (Turkey); NASU (Ukraine); STFC (United Kingdom); DOE and NSF (USA).

Individuals have received support from the Marie-Curie program and the European Research Council and Horizon 2020 Grant, contract Nos. 675440, 724704, 752730, 758316, 765710,

824093, 884104, and COST Action CA16108 (European Union); the Leventis Foundation; the Alfred P. Sloan Foundation; the Alexander von Humboldt Foundation; the Belgian Federal Science Policy Office; the Fonds pour la Formation à la Recherche dans l’Industrie et dans l’Agriculture (FRIA-Belgium); the Agentschap voor Innovatie door Wetenschap en Technologie (IWT-Belgium); the F.R.S.-FNRS and FWO (Belgium) under the “Excellence of Science – EOS” – be.h project n. 30820817; the Beijing Municipal Science & Technology Commission, No. Z191100007219010; the Ministry of Education, Youth and Sports (MEYS) of the Czech Republic; the Deutsche Forschungsgemeinschaft (DFG), under Germany’s Excellence Strategy – EXC 2121 “Quantum Universe” – 390833306, and under project number 400140256 - GRK2497; the Lendület (“Momentum”) Program and the János Bolyai Research Scholarship of the Hungarian Academy of Sciences, the New National Excellence Program ÚNKP, the NKFIA research grants 123842, 123959, 124845, 124850, 125105, 128713, 128786, and 129058 (Hungary); the Council of Science and Industrial Research, India; the Latvian Council of Science; the Ministry of Science and Higher Education and the National Science Center, contracts Opus 2014/15/B/ST2/03998 and 2015/19/B/ST2/02861 (Poland); the Fundação para a Ciência e a Tecnologia, grant CEECIND/01334/2018 (Portugal); the National Priorities Research Program by Qatar National Research Fund; the Ministry of Science and Higher Education, projects no. 14.W03.31.0026 and no. FSWW-2020-0008, and the Russian Foundation for Basic Research, project No.19-42-703014 (Russia); the Programa Estatal de Fomento de la Investigación Científica y Técnica de Excelencia María de Maeztu, grant MDM-2015-0509 and the Programa Severo Ochoa del Principado de Asturias; the Stavros Niarchos Foundation (Greece); the Rachadapisek Sompot Fund for Postdoctoral Fellowship, Chulalongkorn University and the Chulalongkorn Academic into Its 2nd Century Project Advancement Project (Thailand); the Kavli Foundation; the Nvidia Corporation; the SuperMicro Corporation; the Welch Foundation, contract C-1845; and the Weston Havens Foundation (USA).

## References

- [1] CMS Collaboration, “Observation of single top quark production in association with a Z boson in proton-proton collisions at  $\sqrt{s} = 13$  TeV”, *Phys. Rev. Lett.* **122** (2019) 132003, doi:10.1103/PhysRevLett.122.132003, arXiv:1812.05900.
- [2] ATLAS Collaboration, “Observation of the associated production of a top quark and a Z boson in pp collisions at  $\sqrt{s} = 13$  TeV with the ATLAS detector”, *JHEP* **07** (2020) 124, doi:10.1007/JHEP07(2020)124, arXiv:2002.07546.
- [3] C. Degrande et al., “Single-top associated production with a Z or H boson at the LHC: the SMEFT interpretation”, *JHEP* **10** (2018) 005, doi:10.1007/JHEP10(2018)005, arXiv:1804.07773.
- [4] ATLAS Collaboration, “Search for anomalous couplings in the Wtb vertex from the measurement of double differential angular decay rates of single top quarks produced in the t channel with the ATLAS detector”, *JHEP* **04** (2016) 023, doi:10.1007/jhep04(2016)023, arXiv:1510.03764.
- [5] CMS Collaboration, “Measurement of top quark polarisation in t-channel single top quark production”, *JHEP* **04** (2016) 073, doi:10.1007/jhep04(2016)073, arXiv:1511.02138.

- [6] ATLAS Collaboration, “Probing the Wtb vertex structure in  $t$ -channel single top quark production and decay in pp collisions at  $\sqrt{s} = 8$  TeV with the ATLAS detector”, *JHEP* **04** (2017) 124, doi:10.1007/jhep04(2017)124, arXiv:1702.08309.
- [7] ATLAS Collaboration, “Analysis of the Wtb vertex from the measurement of triple-differential angular decay rates of single top quarks produced in the  $t$  channel at  $\sqrt{s} = 8$  TeV with the ATLAS detector”, *JHEP* **12** (2017) 017, doi:10.1007/jhep12(2017)017, arXiv:1707.05393.
- [8] CMS Collaboration, “Measurement of differential cross sections and charge ratios for  $t$ -channel single top quark production in proton-proton collisions at  $\sqrt{s} = 13$  TeV”, *Eur. Phys. J. C* **80** (2020) 370, doi:10.1140/epjc/s10052-020-7858-1, arXiv:1907.08330.
- [9] ATLAS Collaboration, “Measurement of the production cross section of a single top quark in association with a Z boson in proton-proton collisions at 13 TeV with the ATLAS detector”, *Phys. Lett. B* **780** (2018) 557, doi:10.1016/j.physletb.2018.03.023, arXiv:1710.03659.
- [10] CMS Collaboration, “Measurement of the associated production of a single top quark and a Z boson in pp collisions at  $\sqrt{s} = 13$  TeV”, *Phys. Lett. B* **779** (2018) 358, doi:10.1016/j.physletb.2018.02.025, arXiv:1712.02825.
- [11] CMS Collaboration, “Precision luminosity measurement in proton-proton collisions at  $\sqrt{s} = 13$  TeV in 2015 and 2016 at CMS”, *Eur. Phys. J. C* **81** (2021) 800, doi:10.1140/epjc/s10052-021-09538-2, arXiv:2104.01927.
- [12] HEPData record for this analysis, 2021. doi:10.17182/hepdata.105865.
- [13] CMS Collaboration, “Measurement of inclusive and differential Higgs boson production cross sections in the diphoton decay channel in proton-proton collisions at  $\sqrt{s} = 13$  TeV”, *JHEP* **01** (2019) 183, doi:10.1007/jhep01(2019)183, arXiv:1807.03825.
- [14] CMS Collaboration, “The CMS experiment at the CERN LHC”, *JINST* **3** (2008) S08004, doi:10.1088/1748-0221/3/08/s08004.
- [15] CMS Collaboration, “The CMS trigger system”, *JINST* **12** (2017) P01020, doi:10.1088/1748-0221/12/01/P01020, arXiv:1609.02366.
- [16] D. Pagani, I. Tsinikos, and E. Vryonidou, “NLO QCD+EW predictions for tHj and tZj production at the LHC”, *JHEP* **08** (2020) 082, doi:10.1007/JHEP08(2020)082, arXiv:2006.10086.
- [17] J. Alwall et al., “The automated computation of tree-level and next-to-leading order differential cross sections, and their matching to parton shower simulations”, *JHEP* **07** (2014) 079, doi:10.1007/JHEP07(2014)079, arXiv:1405.0301.
- [18] R. Frederix and S. Frixione, “Merging meets matching in MC@NLO”, *JHEP* **12** (2012) 061, doi:10.1007/JHEP12(2012)061, arXiv:1209.6215.
- [19] P. Nason, “A new method for combining NLO QCD with shower Monte Carlo algorithms”, *JHEP* **11** (2004) 040, doi:10.1088/1126-6708/2004/11/040, arXiv:hep-ph/0409146.

- [20] S. Frixione, P. Nason, and C. Oleari, “Matching NLO QCD computations with parton shower simulations: the POWHEG method”, *JHEP* **11** (2007) 070, doi:10.1088/1126-6708/2007/11/070, arXiv:0709.2092.
- [21] S. Alioli, P. Nason, C. Oleari, and E. Re, “A general framework for implementing NLO calculations in shower Monte Carlo programs: the POWHEG BOX”, *JHEP* **06** (2010) 043, doi:10.1007/JHEP06(2010)043, arXiv:1002.2581.
- [22] H. B. Hartanto, B. Jäger, L. Reina and D. Wackerlo, “Higgs boson production in association with top quarks in the POWHEG BOX”, *Phys. Rev. D* **91** (2015) 094003, doi:10.1103/physrevd.91.094003, arXiv:1501.04498.
- [23] J. M. Campbell and R. K. Ellis, “MCFM for the Tevatron and the LHC”, *Nucl. Phys. B (Proc. Suppl.)* **205** (2010) 10, doi:10.1016/j.nuclphysbps.2010.08.011, arXiv:1007.3492.
- [24] T. Sjöstrand et al., “An introduction to PYTHIA 8.2”, *Comput. Phys. Commun.* **191** (2015) 159, doi:10.1016/j.cpc.2015.01.024, arXiv:1410.3012.
- [25] CMS Collaboration, “Extraction and validation of a new set of CMS PYTHIA 8 tunes from underlying-event measurements”, *Eur. Phys. J. C* **80** (2020) doi:10.1140/epjc/s10052-019-7499-4, arXiv:1903.12179.
- [26] P. Skands, S. Carrazza, and J. Rojo, “Tuning PYTHIA 8.1: the Monash 2013 tune”, *Eur. Phys. J. C* **74** (2014) doi:10.1140/epjc/s10052-014-3024-y, arXiv:1404.5630.
- [27] CMS Collaboration, “Event generator tunes obtained from underlying event and multiparton scattering measurements”, *Eur. Phys. J. C* **76** (2016) doi:10.1140/epjc/s10052-016-3988-x, arXiv:1512.00815.
- [28] CMS Collaboration, “Investigations of the impact of the parton shower tuning in PYTHIA 8 in the modelling of  $t\bar{t}$  at  $\sqrt{s} = 8$  and 13 TeV”, CMS Physics Analysis Summary CMS-PAS-TOP-16-021, 2016.
- [29] NNPDF Collaboration, “Parton distributions from high-precision collider data”, *Eur. Phys. J. C* **77** (2017) 663, doi:10.1140/epjc/s10052-017-5199-5, arXiv:1706.00428.
- [30] NNPDF Collaboration, “Parton distributions for the LHC Run II”, *JHEP* **04** (2015) 040, doi:10.1007/jhep04(2015)040, arXiv:1410.8849.
- [31] CMS Collaboration, “Pileup mitigation at CMS in 13 TeV data”, *JINST* **15** (2020) P09018, doi:10.1088/1748-0221/15/09/p09018, arXiv:2003.00503.
- [32] CMS Collaboration, “Measurement of the inelastic proton-proton cross section at  $\sqrt{s} = 13$  TeV”, *JHEP* **07** (2018) 161, doi:10.1007/jhep07(2018)161, arXiv:1802.02613.
- [33] GEANT4 Collaboration, “GEANT4—a simulation toolkit”, *Nucl. Instrum. Meth. A* **506** (2003) 250, doi:10.1016/S0168-9002(03)01368-8.
- [34] CMS Collaboration, “Particle-flow reconstruction and global event description with the CMS detector”, *JINST* **12** (2017) P10003, doi:10.1088/1748-0221/12/10/P10003, arXiv:1706.04965.

- [35] CMS Collaboration, “Performance of missing transverse momentum reconstruction in proton-proton collisions at  $\sqrt{s} = 13$  TeV using the CMS detector”, *JINST* **14** (2019) P07004, doi:10.1088/1748-0221/14/07/P07004, arXiv:1903.06078.
- [36] M. Cacciari, G. P. Salam, and G. Soyez, “The anti- $k_T$  jet clustering algorithm”, *JHEP* **04** (2008) 063, doi:10.1088/1126-6708/2008/04/063, arXiv:0802.1189.
- [37] M. Cacciari, G. P. Salam, and G. Soyez, “FASTJET user manual”, *Eur. Phys. J. C* **72** (2012) 1896, doi:10.1140/epjc/s10052-012-1896-2, arXiv:1111.6097.
- [38] CMS Collaboration, “Jet energy scale and resolution in the CMS experiment in pp collisions at 8 TeV”, *JINST* **12** (2017) P02014, doi:10.1088/1748-0221/12/02/P02014, arXiv:1607.03663.
- [39] CMS Collaboration, “Identification of heavy-flavour jets with the CMS detector in pp collisions at 13 TeV”, *JINST* **13** (2018) P05011, doi:10.1088/1748-0221/13/05/P05011, arXiv:1712.07158.
- [40] E. Bols et al., “Jet flavour classification using DEEPJET”, *JINST* **15** (2020) P12012, doi:10.1088/1748-0221/15/12/p12012, arXiv:2008.10519.
- [41] CMS Collaboration, “Performance of the DEEPJET b tagging algorithm using  $41.9 \text{ fb}^{-1}$  of data from proton-proton collisions at 13 TeV with Phase 1 CMS detector”, CMS Detector Performance Note CMS-DP-2018-058, 2018.
- [42] CMS Collaboration, “Performance of electron reconstruction and selection with the CMS detector in proton-proton collisions at  $\sqrt{s} = 8$  TeV”, *JINST* **10** (2015) P06005, doi:10.1088/1748-0221/10/06/P06005, arXiv:1502.02701.
- [43] CMS Collaboration, “Performance of the CMS muon detector and muon reconstruction with proton-proton collisions at  $\sqrt{s} = 13$  TeV”, *JINST* **13** (2018) P06015, doi:10.1088/1748-0221/13/06/P06015, arXiv:1804.04528.
- [44] K. Rehermann and B. Tweedie, “Efficient identification of boosted semileptonic top quarks at the LHC”, *JHEP* **03** (2011) 059, doi:10.1007/jhep03(2011)059, arXiv:1007.2221.
- [45] CMS Collaboration, “Search for new physics in same-sign dilepton events in proton-proton collisions at  $\sqrt{s} = 13$  TeV”, *Eur. Phys. J. C* **76** (2016) 8, doi:10.1140/epjc/s10052-016-4261-z, arXiv:1605.03171.
- [46] H. Voss, A. Höcker, J. Stelzer, and F. Tegenfeldt, “TVMA, the toolkit for multivariate data analysis with ROOT”, in *XIth International Workshop on Advanced Computing and Analysis Techniques in Physics Research (ACAT)*, p. 40. 2007. arXiv:physics/0703039. [PoS(ACAT)040]. doi:10.22323/1.050.0040.
- [47] CMS Collaboration, “Measurement of the  $t$ -channel single top quark production cross section in pp collisions at  $\sqrt{s} = 7$  TeV”, *Phys. Rev. Lett.* **107** (2011) 091802, doi:10.1103/physrevlett.107.091802, arXiv:1106.3052.
- [48] M. Ježabek and J. H. Kühn, “V-A tests through leptons from polarised top quarks”, *Phys. Lett. B* **329** (1994) 317, doi:10.1016/0370-2693(94)90779-x, arXiv:hep-ph/9403366.

- [49] J. A. Aguilar-Saavedra and J. Bernabéu, “W polarisation beyond helicity fractions in top quark decays”, *Nucl. Phys. B* **840** (2010) 349,  
*doi*:10.1016/j.nuclphysb.2010.07.012, *arXiv*:1005.5382.
- [50] CMS Collaboration, “Measurements of the  $\text{pp} \rightarrow \text{WZ}$  inclusive and differential production cross section and constraints on charged anomalous triple gauge couplings at  $\sqrt{s} = 13 \text{ TeV}$ ”, *JHEP* **04** (2019) 122, *doi*:10.1007/JHEP04(2019)122,  
*arXiv*:1901.03428.
- [51] CMS Collaboration, “Measurement of top quark pair production in association with a Z boson in proton-proton collisions at  $\sqrt{s} = 13 \text{ TeV}$ ”, *JHEP* **03** (2020) 056,  
*doi*:10.1007/JHEP03(2020)056, *arXiv*:1907.11270.
- [52] CMS Collaboration, “CMS luminosity measurement for the 2017 data-taking period at  $\sqrt{s} = 13 \text{ TeV}$ ”, CMS Physics Analysis Summary CMS-PAS-LUM-17-004, 2018.
- [53] CMS Collaboration, “CMS luminosity measurement for the 2018 data-taking period at  $\sqrt{s} = 13 \text{ TeV}$ ”, CMS Physics Analysis Summary CMS-PAS-LUM-18-002, 2019.
- [54] CMS Collaboration, “Measurements of the  $\text{pp} \rightarrow \text{ZZ}$  production cross section and the  $Z \rightarrow 4\ell$  branching fraction, and constraints on anomalous triple gauge couplings at  $\sqrt{s} = 13 \text{ TeV}$ ”, *Eur. Phys. J. C* **78** (2018) 165,  
*doi*:10.1140/epjc/s10052-018-5567-9, *arXiv*:1709.08601.
- [55] S. Argyropoulos and T. Sjöstrand, “Effects of color reconnection on  $t\bar{t}$  final states at the LHC”, *JHEP* **11** (2014) 043, *doi*:10.1007/jhep11(2014)043, *arXiv*:1407.6653.
- [56] CMS Collaboration, “Observation of the production of three massive gauge bosons at  $\sqrt{s} = 13 \text{ TeV}$ ”, *Phys. Rev. Lett.* **125** (2020) 151802,  
*doi*:10.1103/physrevlett.125.151802, *arXiv*:2006.11191.
- [57] J. S. Conway, “Incorporating nuisance parameters in likelihoods for multisource spectra”, 2011. <https://arxiv.org/abs/1103.0354v1>.
- [58] CMS Collaboration, “Measurement of the single top quark and antiquark production cross sections in the  $t$  channel and their ratio in proton-proton collisions at  $\sqrt{s} = 13 \text{ TeV}$ ”, *Phys. Lett. B* **800** (2020) 135042, *doi*:10.1016/j.physletb.2019.135042,  
*arXiv*:1812.10514.
- [59] M. Cacciari, G. P. Salam, and G. Soyez, “The catchment area of jets”, *JHEP* **04** (2008) 005,  
*doi*:10.1088/1126-6708/2008/04/005, *arXiv*:0802.1188.
- [60] M. Abadi et al., “TENSORFLOW: large-scale machine learning on heterogeneous systems”, 2015. Software available from tensorflow.org. <https://www.tensorflow.org/>.
- [61] F. Maltoni, G. Ridolfi, and M. Ubiali, “b-initiated processes at the LHC: a reappraisal”, *JHEP* **07** (2012) 022, *doi*:10.1007/jhep07(2012)022, *arXiv*:1203.6393.
- [62] M. Lim, F. Maltoni, G. Ridolfi, and M. Ubiali, “Anatomy of double heavy-quark initiated processes”, *JHEP* **09** (2016) 132, *doi*:10.1007/jhep09(2016)132,  
*arXiv*:1605.09411.

## A Validation of the misidentification-rate method in simulation

Figure A.1 shows the results of the misidentification-rate optimization and validation using the tight-to-loose ratio method, as described in Section 5. This cross-check is fully simulation-based: the misidentification rate is measured in simulated QCD multijet samples and evaluated separately in simulated DY and  $t\bar{t}$  samples. The event BDT discriminant distributions are shown for (left) simulated trilepton events from the DY process, and (right) simulated  $t\bar{t}$  events. The black points are the nonprompt-lepton predictions from the simulation, and the colored histograms the predictions using the tight-to-loose ratio method applied to the same simulated events. The lower panels give the ratio of the two predictions. The good agreement between the two predictions for the two different types of simulated events validates the method for determining the nonprompt-lepton background.

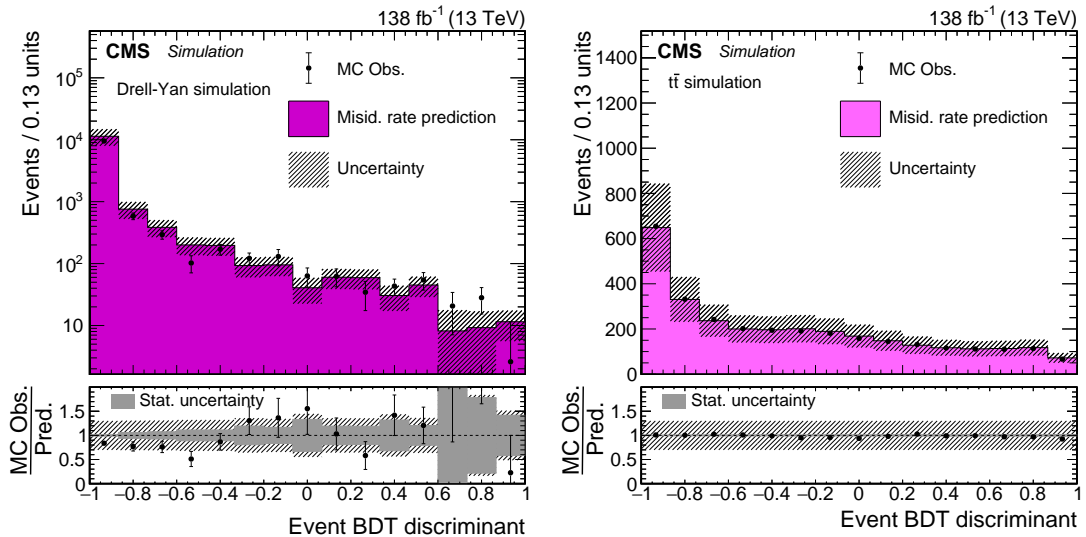


Figure A.1: The event BDT discriminant distributions for simulated (left) trilepton DY events and (right)  $t\bar{t}$  events. The black points give the nonprompt-lepton predictions from the simulation, while the colored histograms represent a similar prediction estimated with the misidentification rate method applied to the same events. The lower panels plot the ratio of the observed MC prediction to the prediction from the misidentification rate method. The vertical bars on the points show the statistical uncertainty in the observed MC distribution. The hatched bands represent the total uncertainty in the misidentification rate predictions and the shaded band its statistical component in the ratio.

## B Hypothesis tests of differential cross sections

The level of agreement of the measured differential cross sections with the theory predictions is quantified with  $p$ -values of  $\chi^2$  tests as summarized in Table B.1. The full covariance matrix for the measurement and each prediction is considered.

## C Extraction of the top quark spin asymmetry

Additional material on the likelihood fit used for the extraction of the spin asymmetry is given. The prefit and postfit distributions are shown in Fig. C.1 where a good agreement with the data is visible. The extracted parton-level bins and the likelihood as a function of the spin asymmetry are shown in Fig. C.2.

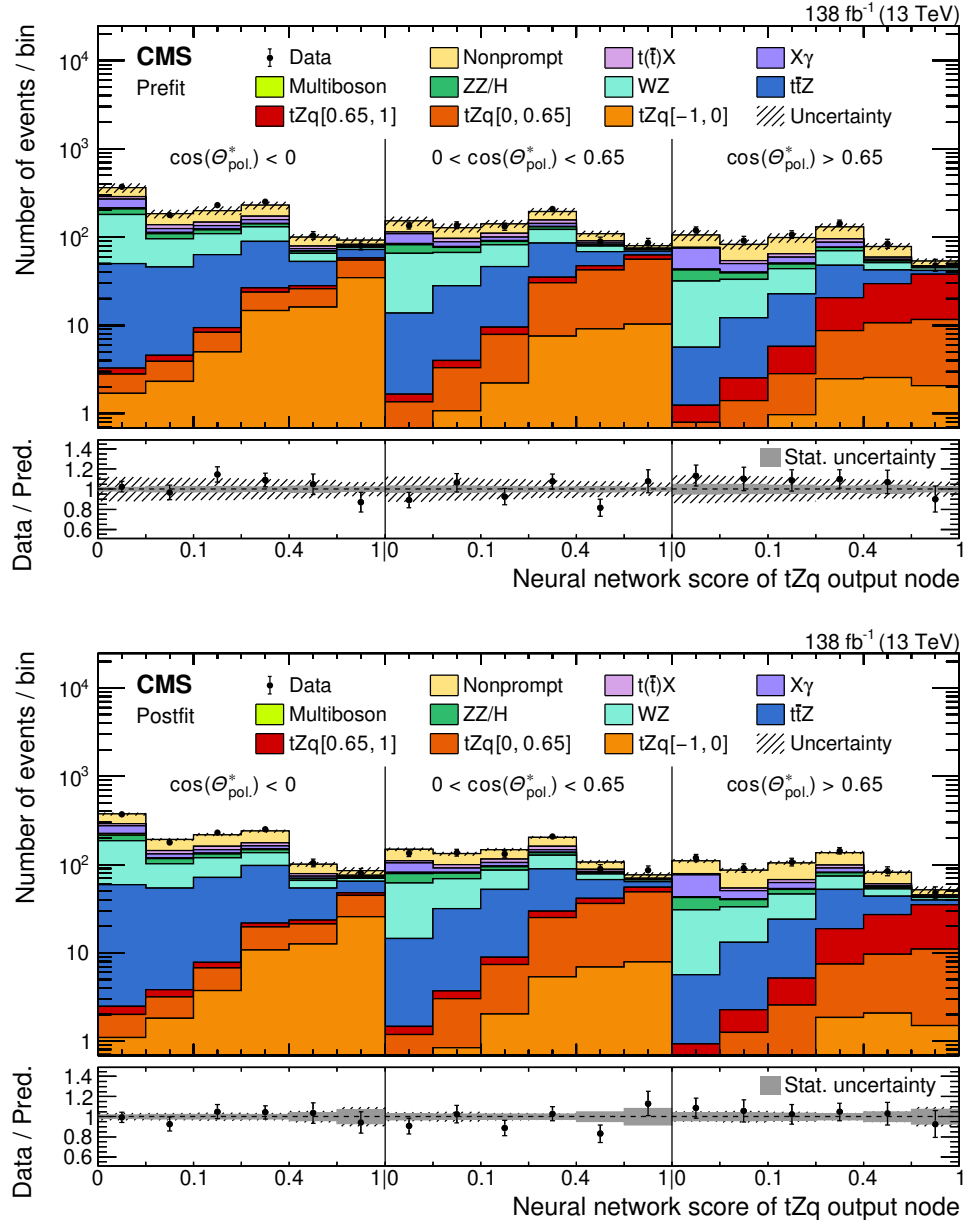


Figure C.1: Prefit (upper) and postfit (lower) distributions of the neural network score from the tZq output node for events in the signal region with fewer than four jets, used for the measurement of the spin asymmetry from the  $\cos(\theta_{\text{pol}}^*)$  distribution at the parton level. The data are shown by the points and the predictions by the colored histograms. The vertical lines on the points represent the statistical uncertainty in the data, and the hatched region the total uncertainty in the prediction. The events are split into three subregions based on the value of  $\cos(\theta_{\text{pol}}^*)$  measured at the detector level. Three different tZq templates, defined by the same intervals of  $\cos(\theta_{\text{pol}}^*)$  at parton level and shown in different shades of orange and red, are used to model the contribution of each parton-level bin. The lower panels show the ratio of the data to the sum of the predictions, with the gray band indicating the uncertainty from the finite number of MC events.

Table B.1: Summary of the  $p$ -values from the  $\chi^2$  test between the unfolded measurements and theoretical predictions from the 4FS and 5FS. The test is performed on the measurements of the absolute and normalized differential cross sections at the parton and particle levels for the observables given in the first column. All numbers are given in percent.

Observable	Parton level				Particle level			
	Absolute		Normalized		Absolute		Normalized	
	4FS	5FS	4FS	5FS	4FS	5FS	4FS	5FS
$p_T(Z)$	97.7	84.6	99.8	99.3	97.7	89.1	99.8	99.8
$\Delta\phi(\ell, \ell')$	73.1	54.1	65.5	61.6	75.7	65.6	69.2	70.9
$p_T(\ell_t)$	94.5	74.4	93.3	90.9	95.0	77.1	94.3	89.5
$m(3\ell)$	7.0	2.0	5.4	4.5	7.3	2.2	3.9	3.3
$p_T(t)$	74.4	68.2	74.1	76.4	72.8	70.5	71.1	73.6
$m(t, Z)$	65.0	48.3	56.8	51.6	66.3	64.0	58.2	67.3
$\cos(\theta_{\text{pol}}^*)$	84.6	63.1	80.7	83.7	88.2	71.8	87.4	91.8
$p_T(j')$	—	—	—	—	44.2	44.1	35.8	41.5
$ \eta(j') $	—	—	—	—	46.2	30.4	29.0	24.3

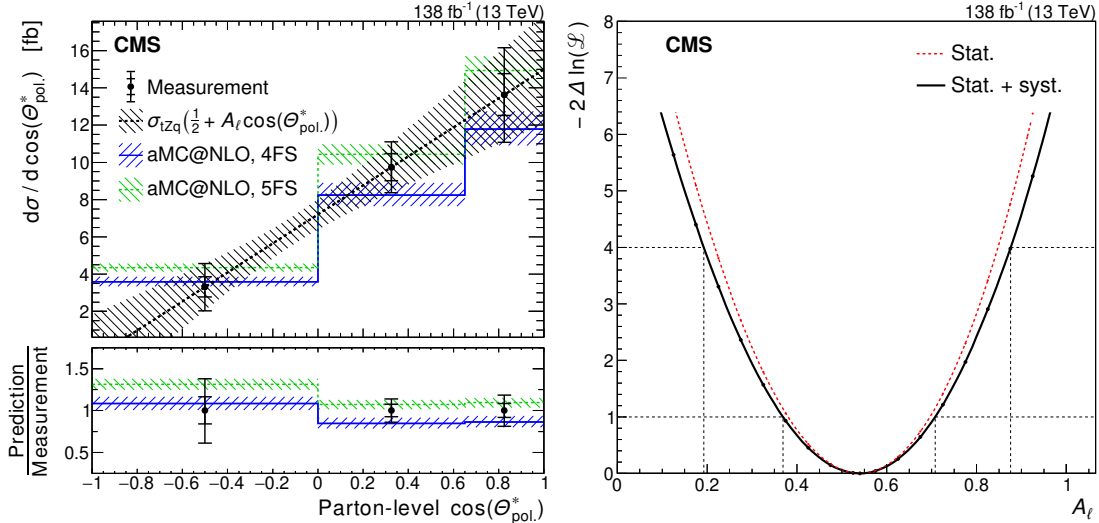


Figure C.2: The left plot shows the measured absolute  $\cos(\theta_{\text{pol}}^*)$  differential cross section at the parton level used in the extraction of the top quark spin asymmetry. The generator-level bins are parameterized according to Eq. (3), shown as a dashed black line in the plot, such that the spin asymmetry is directly used as a free parameter in the fit. The observed values of the generator-level bins are shown as black points with the inner and outer vertical bars giving the systematic and total uncertainties, respectively. The SM predictions for events simulated in the 5FS (dashed green line) and 4FS (solid blue line) are plotted as well. The hatched regions indicate the corresponding uncertainties, respectively. The lower panel displays the ratio of the MC prediction to the measurement. On the right, the negative log likelihood in the fit for the spin asymmetry  $A_\ell$  is shown when considering only the statistical uncertainties (dashed red line) or the combined statistical and systematic uncertainties (solid black line). The dotted black lines indicate the one (inner) and two (outer) standard deviation confidence intervals, respectively.



## D The CMS Collaboration

**Yerevan Physics Institute, Yerevan, Armenia**

A. Tumasyan

**Institut für Hochenergiephysik, Vienna, Austria**

W. Adam , J.W. Andrejkovic, T. Bergauer , S. Chatterjee , K. Damanakis, M. Dragicevic , A. Escalante Del Valle , R. Frühwirth<sup>1</sup>, M. Jeitler<sup>1</sup> , N. Krammer, L. Lechner , D. Liko, I. Mikulec, P. Paulitsch, F.M. Pitters, J. Schieck<sup>1</sup> , R. Schöfbeck , D. Schwarz, S. Templ , W. Waltenberger , C.-E. Wulz<sup>1</sup> 

**Institute for Nuclear Problems, Minsk, Belarus**

V. Chekhovsky, A. Litomin, V. Makarenko 

**Universiteit Antwerpen, Antwerpen, Belgium**

M.R. Darwish<sup>2</sup>, E.A. De Wolf, T. Janssen , T. Kello<sup>3</sup>, A. Lelek , H. Rejeb Sfar, P. Van Mechelen , S. Van Putte, N. Van Remortel 

**Vrije Universiteit Brussel, Brussel, Belgium**

F. Blekman , E.S. Bols , J. D'Hondt , M. Delcourt, H. El Faham , S. Lowette , S. Moortgat , A. Morton , D. Müller , A.R. Sahasransu , S. Tavernier , W. Van Doninck

**Université Libre de Bruxelles, Bruxelles, Belgium**

D. Beghin, B. Bilin , B. Clerbaux , G. De Lentdecker, L. Favart , A. Grebenyuk, A.K. Kalsi , K. Lee, M. Mahdavikhorrami, I. Makarenko , L. Moureaux , L. Pétré, A. Popov , N. Postiau, E. Starling , L. Thomas , M. Vanden Bemden, C. Vander Velde , P. Vanlaer 

**Ghent University, Ghent, Belgium**

T. Cornelis , D. Dobur, J. Knolle , L. Lambrecht, G. Mestdach, M. Niedziela , C. Roskas, A. Samalan, K. Skovpen , M. Tytgat , B. Vermassen, L. Wezenbeek

**Université Catholique de Louvain, Louvain-la-Neuve, Belgium**

A. Benecke, A. Bethani , G. Bruno, F. Bury , C. Caputo , P. David , C. Delaere , I.S. Donertas , A. Giannanco , K. Jaffel, Sa. Jain , V. Lemaitre, K. Mondal , J. Prisciandaro, A. Taliercio, M. Teklishyn , T.T. Tran, P. Vischia , S. Wertz 

**Centro Brasileiro de Pesquisas Fisicas, Rio de Janeiro, Brazil**

G.A. Alves , C. Hensel, A. Moraes , P. Rebello Teles 

**Universidade do Estado do Rio de Janeiro, Rio de Janeiro, Brazil**

W.L. Aldá Júnior , M. Alves Gallo Pereira , M. Barroso Ferreira Filho, H. Brandao Malbouisson, W. Carvalho , J. Chinellato<sup>4</sup>, E.M. Da Costa , G.G. Da Silveira<sup>5</sup> , D. De Jesus Damiao , S. Fonseca De Souza , C. Mora Herrera , K. Mota Amarilo, L. Mundim , H. Nogima, A. Santoro, S.M. Silva Do Amaral , A. Sznajder , M. Thiel, F. Torres Da Silva De Araujo<sup>6</sup> , A. Vilela Pereira 

**Universidade Estadual Paulista (a), Universidade Federal do ABC (b), São Paulo, Brazil**

C.A. Bernardes<sup>5</sup> , L. Calligaris , T.R. Fernandez Perez Tomei , E.M. Gregores , D.S. Lemos , P.G. Mercadante , S.F. Novaes , Sandra S. Padula 

**Institute for Nuclear Research and Nuclear Energy, Bulgarian Academy of Sciences, Sofia, Bulgaria**

A. Aleksandrov, G. Antchev , R. Hadjiiska, P. Iaydjiev, M. Misheva, M. Rodozov, M. Shopova, G. Sultanov

**University of Sofia, Sofia, Bulgaria**

A. Dimitrov, T. Ivanov, L. Litov , B. Pavlov, P. Petkov, A. Petrov

**Beihang University, Beijing, China**

T. Cheng , T. Javaid<sup>7</sup>, M. Mittal, L. Yuan

**Department of Physics, Tsinghua University, Beijing, China**

M. Ahmad , G. Bauer, C. Dozen<sup>8</sup> , Z. Hu , J. Martins<sup>9</sup> , Y. Wang, K. Yi<sup>10,11</sup>

**Institute of High Energy Physics, Beijing, China**

E. Chapon , G.M. Chen<sup>7</sup> , H.S. Chen<sup>7</sup> , M. Chen , F. Iemmi, A. Kapoor , D. Leggat, H. Liao, Z.-A. Liu<sup>7</sup> , V. Milosevic , F. Monti , R. Sharma , J. Tao , J. Thomas-Wilsker, J. Wang , H. Zhang , J. Zhao 

**State Key Laboratory of Nuclear Physics and Technology, Peking University, Beijing, China**

A. Agapitos, Y. An, Y. Ban, C. Chen, A. Levin , Q. Li , X. Lyu, Y. Mao, S.J. Qian, D. Wang , J. Xiao

**Sun Yat-Sen University, Guangzhou, China**

M. Lu, Z. You 

**Institute of Modern Physics and Key Laboratory of Nuclear Physics and Ion-beam Application (MOE) - Fudan University, Shanghai, China**

X. Gao<sup>3</sup>, H. Okawa , Y. Zhang 

**Zhejiang University, Hangzhou, China, Zhejiang, China**

Z. Lin , M. Xiao 

**Universidad de Los Andes, Bogota, Colombia**

C. Avila , A. Cabrera , C. Florez , J. Fraga

**Universidad de Antioquia, Medellin, Colombia**

J. Mejia Guisao, F. Ramirez, J.D. Ruiz Alvarez , C.A. Salazar Gonzalez 

**University of Split, Faculty of Electrical Engineering, Mechanical Engineering and Naval Architecture, Split, Croatia**

D. Giljanovic, N. Godinovic , D. Lelas , I. Puljak 

**University of Split, Faculty of Science, Split, Croatia**

Z. Antunovic, M. Kovac, T. Sculac 

**Institute Rudjer Boskovic, Zagreb, Croatia**

V. Brigljevic , D. Ferencek , D. Majumder , M. Roguljic, A. Starodumov<sup>12</sup> , T. Susa 

**University of Cyprus, Nicosia, Cyprus**

A. Attikis , K. Christoforou, E. Erodotou, A. Ioannou, G. Kole , M. Kolosova, S. Konstantinou, J. Mousa , C. Nicolaou, F. Ptochos , P.A. Razis, H. Rykaczewski, H. Saka 

**Charles University, Prague, Czech Republic**

M. Finger<sup>13</sup>, M. Finger Jr.<sup>13</sup> , A. Kveton

**Escuela Politecnica Nacional, Quito, Ecuador**

E. Ayala

**Universidad San Francisco de Quito, Quito, Ecuador**

E. Carrera Jarrin 

**Academy of Scientific Research and Technology of the Arab Republic of Egypt, Egyp-**

**tian Network of High Energy Physics, Cairo, Egypt**  
H. Abdalla<sup>14</sup> , Y. Assran<sup>15,16</sup> 

**Center for High Energy Physics (CHEP-FU), Fayoum University, El-Fayoum, Egypt**  
A. Lotfy , M.A. Mahmoud 

**National Institute of Chemical Physics and Biophysics, Tallinn, Estonia**  
S. Bhowmik , R.K. Dewanjee , K. Ehataht, M. Kadastik, S. Nandan, C. Nielsen, J. Pata, M. Raidal , L. Tani, C. Veelken

**Department of Physics, University of Helsinki, Helsinki, Finland**

P. Eerola , L. Forthomme , H. Kirschenmann , K. Osterberg , M. Voutilainen 

**Helsinki Institute of Physics, Helsinki, Finland**

S. Barthuar, E. Brücken , F. Garcia , J. Havukainen , M.S. Kim , R. Kinnunen, T. Lampén, K. Lassila-Perini , S. Lehti , T. Lindén, M. Lotti, L. Martikainen, M. Myllymäki, J. Ott , H. Siikonen, E. Tuominen , J. Tuominiemi

**Lappeenranta University of Technology, Lappeenranta, Finland**

P. Luukka , H. Petrow, T. Tuuva

**IRFU, CEA, Université Paris-Saclay, Gif-sur-Yvette, France**

C. Amendola , M. Besancon, F. Couderc , M. Dejardin, D. Denegri, J.L. Faure, F. Ferri , S. Ganjour, P. Gras, G. Hamel de Monchenault , P. Jarry, B. Lenzi , E. Locci, J. Malcles, J. Rander, A. Rosowsky , M.Ö. Sahin , A. Savoy-Navarro<sup>17</sup>, M. Titov , G.B. Yu 

**Laboratoire Leprince-Ringuet, CNRS/IN2P3, Ecole Polytechnique, Institut Polytechnique de Paris, Palaiseau, France**

S. Ahuja , F. Beaudette , M. Bonanomi , A. Buchot Perraguin, P. Busson, A. Cappati, C. Charlot, O. Davignon, B. Diab, G. Falmagne , S. Ghosh, R. Granier de Cassagnac , A. Hakimi, I. Kucher , J. Motta, M. Nguyen , C. Ochando , P. Paganini , J. Rembser, R. Salerno , U. Sarkar , J.B. Sauvan , Y. Sirois , A. Tarabini, A. Zabi, A. Zghiche 

**Université de Strasbourg, CNRS, IPHC UMR 7178, Strasbourg, France**

J.-L. Agram<sup>18</sup> , J. Andrea, D. Apparu, D. Bloch , G. Bourgatte, J.-M. Brom, E.C. Chabert, C. Collard , D. Darej, J.-C. Fontaine<sup>18</sup>, U. Goerlach, C. Grimault, A.-C. Le Bihan, E. Nibigira , P. Van Hove 

**Institut de Physique des 2 Infinis de Lyon (IP2I ), Villeurbanne, France**

E. Asilar , S. Beauceron , C. Bernet , G. Boudoul, C. Camen, A. Carle, N. Chanon , D. Contardo, P. Depasse , H. El Mamouni, J. Fay, S. Gascon , M. Gouzevitch , B. Ille, I.B. Laktineh, H. Lattaud , A. Lesauvage , M. Lethuillier , L. Mirabito, S. Perries, K. Shchablo, V. Sordini , L. Torterotot , G. Touquet, M. Vander Donckt, S. Viret

**Georgian Technical University, Tbilisi, Georgia**

I. Lomidze, T. Toriashvili<sup>19</sup>, Z. Tsamalaidze<sup>13</sup>

**RWTH Aachen University, I. Physikalisches Institut, Aachen, Germany**

V. Botta, L. Feld , K. Klein, M. Lipinski, D. Meuser, A. Pauls, N. Röwert, J. Schulz, M. Teroerde 

**RWTH Aachen University, III. Physikalisches Institut A, Aachen, Germany**

A. Dodonova, D. Eliseev, M. Erdmann , P. Fackeldey , B. Fischer, S. Ghosh , T. Hebbeker , K. Hoepfner, F. Ivone, L. Mastrolorenzo, M. Merschmeyer , A. Meyer , G. Mocellin, S. Mondal, S. Mukherjee , D. Noll , A. Novak, T. Pook , A. Pozdnyakov 

Y. Rath, H. Reithler, J. Roemer, A. Schmidt , S.C. Schuler, A. Sharma , L. Vigilante, S. Wiedenbeck, S. Zaleski

**RWTH Aachen University, III. Physikalisches Institut B, Aachen, Germany**

C. Dziwok, G. Flügge, W. Haj Ahmad<sup>20</sup> , O. Hlushchenko, T. Kress, A. Nowack , C. Pistone, O. Pooth, D. Roy , A. Stahl<sup>21</sup> , T. Ziemons , A. Zotz

**Deutsches Elektronen-Synchrotron, Hamburg, Germany**

H. Aarup Petersen, M. Aldaya Martin, P. Asmuss, S. Baxter, M. Bayatmakou, O. Behnke, A. Bermúdez Martínez, S. Bhattacharya, A.A. Bin Anuar , K. Borras<sup>22</sup>, D. Brunner, A. Campbell , A. Cardini , C. Cheng, F. Colombina, S. Consuegra Rodríguez , G. Correia Silva, V. Danilov, M. De Silva, L. Didukh, G. Eckerlin, D. Eckstein, L.I. Estevez Banos , O. Filatov , E. Gallo<sup>23</sup>, A. Geiser, A. Giraldi, A. Grohsjean , M. Guthoff, A. Jafari<sup>24</sup> , N.Z. Jomhari , H. Jung , A. Kasem<sup>22</sup> , M. Kasemann , H. Kaveh , C. Kleinwort , R. Kogler , D. Krücker , W. Lange, J. Lidrych , K. Lipka, W. Lohmann<sup>25</sup>, R. Mankel, I.-A. Melzer-Pellmann , M. Mendizabal Morentin, J. Metwally, A.B. Meyer , M. Meyer , J. Mnich , A. Mussgiller, Y. Otarid, D. Pérez Adán , D. Pitzl, A. Raspereza, B. Ribeiro Lopes, J. Rübenach, A. Saggio , A. Saibel , M. Savitskyi , M. Scham<sup>26</sup>, V. Scheurer, S. Schnake, P. Schütze, C. Schwanenberger<sup>23</sup> , M. Shchedrolosiev, R.E. Sosa Ricardo , D. Stafford, N. Tonon , M. Van De Klundert , R. Walsh , D. Walter, Q. Wang , Y. Wen , K. Wichmann, L. Wiens, C. Wissing, S. Wuchterl 

**University of Hamburg, Hamburg, Germany**

R. Aggleton, S. Albrecht , S. Bein , L. Benato , P. Connor , K. De Leo , M. Eich, F. Feindt, A. Fröhlich, C. Garbers , E. Garutti , P. Gunnellini, M. Hajheidari, J. Haller , A. Hinzmann , G. Kasieczka, R. Klanner , T. Kramer, V. Kutzner, J. Lange , T. Lange , A. Lobanov , A. Malara , A. Nigamova, K.J. Pena Rodriguez, M. Rieger , O. Rieger, P. Schleper, M. Schröder , J. Schwandt , J. Sonneveld , H. Stadie, G. Steinbrück, A. Tews, I. Zoi 

**Karlsruher Institut fuer Technologie, Karlsruhe, Germany**

J. Bechtel , S. Brommer, M. Burkart, E. Butz , R. Caspart , T. Chwalek, W. De Boer<sup>†</sup>, A. Dierlamm, A. Droll, K. El Morabit, N. Faltermann , M. Giffels, J.o. Gosewisch, A. Gottmann, F. Hartmann<sup>21</sup> , C. Heidecker, U. Husemann , P. Keicher, R. Koppenhöfer, S. Maier, M. Metzler, S. Mitra , Th. Müller, M. Neukum, A. Nürnberg, G. Quast , K. Rabbertz , J. Rauser, D. Savoiu , M. Schnepf, D. Seith, I. Shvetsov, H.J. Simonis, R. Ulrich , J. Van Der Linden, R.F. Von Cube, M. Wassmer, M. Weber , S. Wieland, R. Wolf , S. Wozniewski, S. Wunsch

**Institute of Nuclear and Particle Physics (INPP), NCSR Demokritos, Aghia Paraskevi, Greece**

G. Anagnostou, G. Daskalakis, T. Geralis , A. Kyriakis, D. Loukas, A. Stakia 

**National and Kapodistrian University of Athens, Athens, Greece**

M. Diamantopoulou, D. Karasavvas, G. Karathanasis, P. Kontaxakis , C.K. Koraka, A. Manousakis-Katsikakis, A. Panagiotou, I. Papavergou, N. Saoulidou , K. Theofilatos , E. Tziaferi , K. Vellidis, E. Vourliotis

**National Technical University of Athens, Athens, Greece**

G. Bakas, K. Kousouris , I. Papakrivopoulos, G. Tsipolitis, A. Zacharopoulou

**University of Ioánnina, Ioánnina, Greece**

K. Adamidis, I. Bestintzanos, I. Evangelou , C. Foudas, P. Gianneios, P. Katsoulis, P. Kokkas,

N. Manthos, I. Papadopoulos , J. Strologas 

**MTA-ELTE Lendület CMS Particle and Nuclear Physics Group, Eötvös Loránd University, Budapest, Hungary**

M. Csanad , K. Farkas, M.M.A. Gadallah<sup>27</sup> , S. Lököс<sup>28</sup> , P. Major, K. Mandal , A. Mehta , G. Pasztor , A.J. Rádl, O. Surányi, G.I. Veres 

**Wigner Research Centre for Physics, Budapest, Hungary**

M. Bartók<sup>29</sup> , G. Bencze, C. Hajdu , D. Horvath<sup>30</sup> , F. Sikler , V. Veszpremi 

**Institute of Nuclear Research ATOMKI, Debrecen, Hungary**

S. Czellar, D. Fasanella , J. Karancsi<sup>29</sup> , J. Molnar, Z. Szillasi, D. Teyssier

**Institute of Physics, University of Debrecen, Debrecen, Hungary**

P. Raics, Z.L. Trocsanyi<sup>31</sup> , B. Ujvari

**Karoly Robert Campus, MATE Institute of Technology, Gyongyos, Hungary**

T. Csorgo<sup>32</sup> , F. Nemes<sup>32</sup>, T. Novak

**Indian Institute of Science (IISc), Bangalore, India**

S. Choudhury, J.R. Komaragiri , D. Kumar, L. Panwar , P.C. Tiwari 

**National Institute of Science Education and Research, HBNI, Bhubaneswar, India**

S. Bahinipati<sup>33</sup> , C. Kar , P. Mal, T. Mishra , V.K. Muraleedharan Nair Bindhu<sup>34</sup>, A. Nayak<sup>34</sup> , P. Saha, N. Sur , S.K. Swain, D. Vats<sup>34</sup>

**Panjab University, Chandigarh, India**

S. Bansal , S.B. Beri, V. Bhatnagar , G. Chaudhary , S. Chauhan , N. Dhingra<sup>35</sup> , R. Gupta, A. Kaur, M. Kaur , S. Kaur, P. Kumari , M. Meena, K. Sandeep , J.B. Singh , A.K. Virdi 

**University of Delhi, Delhi, India**

A. Ahmed, A. Bhardwaj , B.C. Choudhary , M. Gola, S. Keshri , A. Kumar , M. Naimuddin , P. Priyanka , K. Ranjan, A. Shah 

**Saha Institute of Nuclear Physics, HBNI, Kolkata, India**

M. Bharti<sup>36</sup>, R. Bhattacharya, S. Bhattacharya , D. Bhowmik, S. Dutta, S. Dutta, B. Gomber<sup>37</sup> , M. Maity<sup>38</sup>, P. Palit , P.K. Rout , G. Saha, B. Sahu , S. Sarkar, M. Sharan, B. Singh<sup>36</sup>, S. Thakur<sup>36</sup>

**Indian Institute of Technology Madras, Madras, India**

P.K. Behera , S.C. Behera, P. Kalbhor , A. Muhammad, R. Pradhan, P.R. Pujahari, A. Sharma , A.K. Sikdar

**Bhabha Atomic Research Centre, Mumbai, India**

D. Dutta , V. Jha, V. Kumar , D.K. Mishra, K. Naskar<sup>39</sup>, P.K. Netrakanti, L.M. Pant, P. Shukla 

**Tata Institute of Fundamental Research-A, Mumbai, India**

T. Aziz, S. Dugad, M. Kumar

**Tata Institute of Fundamental Research-B, Mumbai, India**

S. Banerjee , R. Chudasama, M. Guchait, S. Karmakar, S. Kumar, G. Majumder, K. Mazumdar, S. Mukherjee 

**Indian Institute of Science Education and Research (IISER), Pune, India**

K. Alpana, S. Dube , B. Kansal, A. Laha, S. Pandey , A. Rane , A. Rastogi , S. Sharma 

**Isfahan University of Technology, Isfahan, Iran**H. Bakhshiansohi<sup>40</sup> , E. Khazaie, M. Zeinali<sup>41</sup>**Institute for Research in Fundamental Sciences (IPM), Tehran, Iran**S. Chenarani<sup>42</sup>, S.M. Etesami , M. Khakzad , M. Mohammadi Najafabadi **University College Dublin, Dublin, Ireland**M. Grunewald **INFN Sezione di Bari <sup>a</sup>, Bari, Italy, Università di Bari <sup>b</sup>, Bari, Italy, Politecnico di Bari <sup>c</sup>, Bari, Italy**M. Abbrescia<sup>a,b</sup> , R. Aly<sup>a,b,43</sup> , C. Aruta<sup>a,b</sup>, A. Colaleo<sup>a</sup> , D. Creanza<sup>a,c</sup> , N. De Filippis<sup>a,c</sup> , M. De Palma<sup>a,b</sup> , A. Di Florio<sup>a,b</sup>, A. Di Pilato<sup>a,b</sup> , W. Elmetenawee<sup>a,b</sup> , L. Fiore<sup>a</sup> , A. Gelmi<sup>a,b</sup> , M. Gul<sup>a</sup> , G. Iaselli<sup>a,c</sup> , M. Ince<sup>a,b</sup> , S. Lezki<sup>a,b</sup> , G. Maggi<sup>a,c</sup> , M. Maggi<sup>a</sup> , I. Margjeka<sup>a,b</sup>, V. Mastrapasqua<sup>a,b</sup> , S. My<sup>a,b</sup> , S. Nuzzo<sup>a,b</sup> , A. Pellecchia<sup>a,b</sup>, A. Pompili<sup>a,b</sup> , G. Pugliese<sup>a,c</sup> , D. Ramos<sup>a</sup>, A. Ranieri<sup>a</sup> , G. Selvaggi<sup>a,b</sup> , L. Silvestris<sup>a</sup> , F.M. Simone<sup>a,b</sup> , Ü. Sözbilir<sup>a</sup>, R. Venditti<sup>a</sup> , P. Verwilligen<sup>a</sup> **INFN Sezione di Bologna <sup>a</sup>, Bologna, Italy, Università di Bologna <sup>b</sup>, Bologna, Italy**G. Abbiendi<sup>a</sup> , C. Battilana<sup>a,b</sup> , D. Bonacorsi<sup>a,b</sup> , L. Borgonovi<sup>a</sup>, L. Brigliadori<sup>a</sup>, R. Campanini<sup>a,b</sup> , P. Capiluppi<sup>a,b</sup> , A. Castro<sup>a,b</sup> , F.R. Cavallo<sup>a</sup> , M. Cuffiani<sup>a,b</sup> , G.M. Dallavalle<sup>a</sup> , T. Diotalevi<sup>a,b</sup> , F. Fabbri<sup>a</sup> , A. Fanfani<sup>a,b</sup> , P. Giacomelli<sup>a</sup> , L. Giommi<sup>a,b</sup> , C. Grandi<sup>a</sup> , L. Guiducci<sup>a,b</sup>, S. Lo Meo<sup>a,44</sup> , L. Lunerti<sup>a,b</sup>, S. Marcellini<sup>a</sup> , G. Masetti<sup>a</sup> , F.L. Navarreria<sup>a,b</sup> , A. Perrotta<sup>a</sup> , F. Primavera<sup>a,b</sup> , A.M. Rossi<sup>a,b</sup> , T. Rovelli<sup>a,b</sup> , G.P. Siroli<sup>a,b</sup> **INFN Sezione di Catania <sup>a</sup>, Catania, Italy, Università di Catania <sup>b</sup>, Catania, Italy**S. Albergo<sup>a,b,45</sup> , S. Costa<sup>a,b,45</sup> , A. Di Mattia<sup>a</sup> , R. Potenza<sup>a,b</sup>, A. Tricomi<sup>a,b,45</sup> , C. Tuve<sup>a,b</sup> **INFN Sezione di Firenze <sup>a</sup>, Firenze, Italy, Università di Firenze <sup>b</sup>, Firenze, Italy**G. Barbagli<sup>a</sup> , A. Cassese<sup>a</sup> , R. Ceccarelli<sup>a,b</sup>, V. Ciulli<sup>a,b</sup> , C. Civinini<sup>a</sup> , R. D'Alessandro<sup>a,b</sup> , E. Focardia<sup>a,b</sup> , G. Latino<sup>a,b</sup> , P. Lenzi<sup>a,b</sup> , M. Lizzo<sup>a,b</sup>, M. Meschini<sup>a</sup> , S. Paoletti<sup>a</sup> , R. Seidita<sup>a,b</sup>, G. Sguazzoni<sup>a</sup> , L. Viliani<sup>a</sup> **INFN Laboratori Nazionali di Frascati, Frascati, Italy**L. Benussi , S. Bianco , D. Piccolo **INFN Sezione di Genova <sup>a</sup>, Genova, Italy, Università di Genova <sup>b</sup>, Genova, Italy**M. Bozzo<sup>a,b</sup> , F. Ferro<sup>a</sup> , R. Mulargia<sup>a,b</sup>, E. Robutti<sup>a</sup> , S. Tosi<sup>a,b</sup> **INFN Sezione di Milano-Bicocca <sup>a</sup>, Milano, Italy, Università di Milano-Bicocca <sup>b</sup>, Milano, Italy**A. Benaglia<sup>a</sup> , G. Boldrini , F. Brivio<sup>a,b</sup>, F. Cetorelli<sup>a,b</sup>, F. De Guio<sup>a,b</sup> , M.E. Dinardo<sup>a,b</sup> , P. Dini<sup>a</sup> , S. Gennai<sup>a</sup> , A. Ghezzi<sup>a,b</sup> , P. Govoni<sup>a,b</sup> , L. Guzzi<sup>a,b</sup> , M.T. Lucchini<sup>a,b</sup> , M. Malberti<sup>a</sup>, S. Malvezzi , A. Massironi<sup>a</sup> , D. Menasce<sup>a</sup> , L. Moroni<sup>a</sup> , M. Paganoni<sup>a,b</sup> , D. Pedrini<sup>a</sup> , B.S. Pinolini, S. Ragazzi<sup>a,b</sup> , N. Redaelli<sup>a</sup> , T. Tabarelli de Fatis<sup>a,b</sup> , D. Valsecchi<sup>a,b,21</sup> , D. Zuolo<sup>a,b</sup> **INFN Sezione di Napoli <sup>a</sup>, Napoli, Italy, Università di Napoli 'Federico II' <sup>b</sup>, Napoli, Italy, Università della Basilicata <sup>c</sup>, Potenza, Italy, Università G. Marconi <sup>d</sup>, Roma, Italy**S. Buontempo<sup>a</sup> , F. Carnevali<sup>a,b</sup>, N. Cavallo<sup>a,c</sup> , A. De Iorio<sup>a,b</sup> , F. Fabozzi<sup>a,c</sup> , A.O.M. Iorio<sup>a,b</sup> , L. Lista<sup>a,b,46</sup> , S. Meola<sup>a,d,21</sup> , P. Paolucci<sup>a,21</sup> , B. Rossi<sup>a</sup> , C. Sciacca<sup>a,b</sup> 

**INFN Sezione di Padova <sup>a</sup>, Padova, Italy, Università di Padova <sup>b</sup>, Padova, Italy, Università di Trento <sup>c</sup>, Trento, Italy**

P. Azzi<sup>a</sup> , N. Bacchetta<sup>a</sup> , D. Bisello<sup>a,b</sup> , P. Bortignon<sup>a</sup> , A. Bragagnolo<sup>a,b</sup> , R. Carlin<sup>a,b</sup> , P. Checchia<sup>a</sup> , T. Dorigo<sup>a</sup> , U. Dosselli<sup>a</sup> , F. Gasparini<sup>a,b</sup> , U. Gasparini<sup>a,b</sup> , G. Grosso, S.Y. Hoh<sup>a,b</sup> , L. Layer<sup>a,47</sup>, E. Lusiani , M. Margoni<sup>a,b</sup> , A.T. Meneguzzo<sup>a,b</sup> , J. Pazzini<sup>a,b</sup> , P. Ronchese<sup>a,b</sup> , R. Rossin<sup>a,b</sup>, F. Simonetto<sup>a,b</sup> , G. Strong<sup>a</sup> , M. Tosi<sup>a,b</sup> , H. Yarar<sup>a,b</sup>, M. Zanetti<sup>a,b</sup> , P. Zotto<sup>a,b</sup> , A. Zucchetta<sup>a,b</sup> , G. Zumerle<sup>a,b</sup> 

**INFN Sezione di Pavia <sup>a</sup>, Pavia, Italy, Università di Pavia <sup>b</sup>, Pavia, Italy**

C. Aime<sup>a,b</sup>, A. Braghieri<sup>a</sup> , S. Calzaferri<sup>a,b</sup> , D. Fiorina<sup>a,b</sup> , P. Montagna<sup>a,b</sup>, S.P. Ratti<sup>a,b</sup>, V. Re<sup>a</sup> , C. Riccardi<sup>a,b</sup> , P. Salvini<sup>a</sup> , I. Vai<sup>a</sup> , P. Vitulo<sup>a,b</sup> 

**INFN Sezione di Perugia <sup>a</sup>, Perugia, Italy, Università di Perugia <sup>b</sup>, Perugia, Italy**

P. Asenova<sup>a,48</sup> , G.M. Bilei<sup>a</sup> , D. Ciangottini<sup>a,b</sup> , L. Fanò<sup>a,b</sup> , M. Magherini<sup>b</sup>, G. Mantovani<sup>a,b</sup>, V. Mariani<sup>a,b</sup>, M. Menichelli<sup>a</sup> , F. Moscatelli<sup>a,48</sup> , A. Piccinelli<sup>a,b</sup> , M. Presilla<sup>a,b</sup> , A. Rossi<sup>a,b</sup> , A. Santocchia<sup>a,b</sup> , D. Spiga<sup>a</sup> , T. Tedeschi<sup>a,b</sup> 

**INFN Sezione di Pisa <sup>a</sup>, Pisa, Italy, Università di Pisa <sup>b</sup>, Pisa, Italy, Scuola Normale Superiore di Pisa <sup>c</sup>, Pisa, Italy, Università di Siena <sup>d</sup>, Siena, Italy**

P. Azzurri<sup>a</sup> , G. Bagliesi<sup>a</sup> , V. Bertacchi<sup>a,c</sup> , L. Bianchini<sup>a</sup> , T. Boccali<sup>a</sup> , E. Bossini<sup>a,b</sup> , R. Castaldi<sup>a</sup> , M.A. Ciocci<sup>a,b</sup> , V. D'Amante<sup>a,d</sup> , R. Dell'Orso<sup>a</sup> , M.R. Di Domenico<sup>a,d</sup> , S. Donato<sup>a</sup> , A. Giassi<sup>a</sup> , F. Ligabue<sup>a,c</sup> , E. Manca<sup>a,c</sup> , G. Mandorli<sup>a,c</sup> , D. Matos Figueiredo, A. Messineo<sup>a,b</sup> , F. Palla<sup>a</sup> , S. Parolia<sup>a,b</sup>, G. Ramirez-Sanchez<sup>a,c</sup>, A. Rizzi<sup>a,b</sup> , G. Rolandi<sup>a,c</sup> , S. Roy Chowdhury<sup>a,c</sup>, A. Scribano<sup>a</sup>, N. Shafiei<sup>a,b</sup> , P. Spagnolo<sup>a</sup> , R. Tenchini<sup>a</sup> , G. Tonelli<sup>a,b</sup> , N. Turini<sup>a,d</sup> , A. Venturi<sup>a</sup> , P.G. Verdini<sup>a</sup> 

**INFN Sezione di Roma <sup>a</sup>, Rome, Italy, Sapienza Università di Roma <sup>b</sup>, Rome, Italy**

P. Barria<sup>a</sup> , M. Campana<sup>a,b</sup>, F. Cavallari<sup>a</sup> , D. Del Re<sup>a,b</sup> , E. Di Marco<sup>a</sup> , M. Diemoz<sup>a</sup> , E. Longo<sup>a,b</sup> , P. Meridiani<sup>a</sup> , G. Organtini<sup>a,b</sup> , F. Pandolfi<sup>a</sup>, R. Paramatti<sup>a,b</sup> , C. Quaranta<sup>a,b</sup>, S. Rahatlou<sup>a,b</sup> , C. Rovelli<sup>a</sup> , F. Santanastasio<sup>a,b</sup> , L. Soffi<sup>a</sup> , R. Tramontano<sup>a,b</sup>

**INFN Sezione di Torino <sup>a</sup>, Torino, Italy, Università di Torino <sup>b</sup>, Torino, Italy, Università del Piemonte Orientale <sup>c</sup>, Novara, Italy**

N. Amapane<sup>a,b</sup> , R. Arcidiacono<sup>a,c</sup> , S. Argiro<sup>a,b</sup> , M. Arneodo<sup>a,c</sup> , N. Bartosik<sup>a</sup> , R. Bellan<sup>a,b</sup> , A. Bellora<sup>a,b</sup> , J. Berenguer Antequera<sup>a,b</sup> , C. Biino<sup>a</sup> , N. Cartiglia<sup>a</sup> , S. Cometti<sup>a</sup> , M. Costa<sup>a,b</sup> , R. Covarelli<sup>a,b</sup> , N. Demaria<sup>a</sup> , B. Kiani<sup>a,b</sup> , F. Legger<sup>a</sup> , C. Mariotti<sup>a</sup> , S. Maselli<sup>a</sup> , E. Migliore<sup>a,b</sup> , E. Monteil<sup>a,b</sup> , M. Monteno<sup>a</sup> , M.M. Obertino<sup>a,b</sup> , G. Ortona<sup>a</sup> , L. Pacher<sup>a,b</sup> , N. Pastrone<sup>a</sup> , M. Pelliccioni<sup>a</sup> , G.L. Pinna Angioni<sup>a,b</sup>, M. Ruspa<sup>a,c</sup> , K. Shchelina<sup>a</sup> , F. Siviero<sup>a,b</sup> , V. Sola<sup>a</sup> , A. Solano<sup>a,b</sup> , D. Soldi<sup>a,b</sup> , A. Staiano<sup>a</sup> , M. Tornago<sup>a,b</sup> , D. Trocino<sup>a</sup> , A. Vagnerini<sup>a,b</sup>

**INFN Sezione di Trieste <sup>a</sup>, Trieste, Italy, Università di Trieste <sup>b</sup>, Trieste, Italy**

S. Belforte<sup>a</sup> , V. Candelise<sup>a,b</sup> , M. Casarsa<sup>a</sup> , F. Cossutti<sup>a</sup> , A. Da Rold<sup>a,b</sup> , G. Della Ricca<sup>a,b</sup> , G. Sorrentino<sup>a,b</sup>, F. Vazzoler<sup>a,b</sup> 

**Kyungpook National University, Daegu, Korea**

S. Dogra , C. Huh , B. Kim, D.H. Kim , G.N. Kim , J. Kim, J. Lee, S.W. Lee , C.S. Moon , Y.D. Oh , S.I. Pak, B.C. Radburn-Smith, S. Sekmen , Y.C. Yang

**Chonnam National University, Institute for Universe and Elementary Particles, Kwangju, Korea**

H. Kim , D.H. Moon 

**Hanyang University, Seoul, Korea**

B. Francois , T.J. Kim , J. Park 

**Korea University, Seoul, Korea**

S. Cho, S. Choi , Y. Go, B. Hong , K. Lee, K.S. Lee , J. Lim, J. Park, S.K. Park, J. Yoo

**Kyung Hee University, Department of Physics, Seoul, Republic of Korea, Seoul, Korea**

J. Goh , A. Gurtu

**Sejong University, Seoul, Korea**

H.S. Kim , Y. Kim

**Seoul National University, Seoul, Korea**

J. Almond, J.H. Bhyun, J. Choi, S. Jeon, J. Kim, J.S. Kim, S. Ko, H. Kwon, H. Lee , S. Lee, B.H. Oh, M. Oh , S.B. Oh, H. Seo , U.K. Yang, I. Yoon 

**University of Seoul, Seoul, Korea**

W. Jang, D.Y. Kang, Y. Kang, S. Kim, B. Ko, J.S.H. Lee , Y. Lee, J.A. Merlin, I.C. Park, Y. Roh, M.S. Ryu, D. Song, I.J. Watson , S. Yang

**Yonsei University, Department of Physics, Seoul, Korea**

S. Ha, H.D. Yoo

**Sungkyunkwan University, Suwon, Korea**

M. Choi, H. Lee, Y. Lee, I. Yu 

**College of Engineering and Technology, American University of the Middle East (AUM), Egaila, Kuwait, Dasman, Kuwait**

T. Beyrouthy, Y. Maghrbi

**Riga Technical University, Riga, Latvia**

K. Dreimanis , V. Veckalns<sup>49</sup> 

**Vilnius University, Vilnius, Lithuania**

M. Ambrozas, A. Carvalho Antunes De Oliveira , A. Juodagalvis , A. Rinkevicius , G. Tamulaitis 

**National Centre for Particle Physics, Universiti Malaya, Kuala Lumpur, Malaysia**

N. Bin Norjoharuddeen , W.A.T. Wan Abdullah, M.N. Yusli, Z. Zolkapli

**Universidad de Sonora (UNISON), Hermosillo, Mexico**

J.F. Benitez , A. Castaneda Hernandez , M. León Coello, J.A. Murillo Quijada , A. Sehrawat, L. Valencia Palomo 

**Centro de Investigacion y de Estudios Avanzados del IPN, Mexico City, Mexico**

G. Ayala, H. Castilla-Valdez, E. De La Cruz-Burelo , I. Heredia-De La Cruz<sup>50</sup> , R. Lopez-Fernandez, C.A. Mondragon Herrera, D.A. Perez Navarro, A. Sánchez Hernández 

**Universidad Iberoamericana, Mexico City, Mexico**

S. Carrillo Moreno, C. Oropeza Barrera , F. Vazquez Valencia

**Benemerita Universidad Autonoma de Puebla, Puebla, Mexico**

I. Pedraza, H.A. Salazar Ibarguen, C. Uribe Estrada

**University of Montenegro, Podgorica, Montenegro**

J. Mijuskovic<sup>51</sup>, N. Raicevic

**University of Auckland, Auckland, New Zealand**D. Kofcheck **University of Canterbury, Christchurch, New Zealand**P.H. Butler **National Centre for Physics, Quaid-I-Azam University, Islamabad, Pakistan**A. Ahmad, M.I. Asghar, A. Awais, M.I.M. Awan, H.R. Hoorani, W.A. Khan, M.A. Shah, M. Shoaib , M. Waqas **AGH University of Science and Technology Faculty of Computer Science, Electronics and Telecommunications, Krakow, Poland**

V. Avati, L. Grzanka, M. Malawski

**National Centre for Nuclear Research, Swierk, Poland**H. Bialkowska, M. Bluj , B. Boimska , M. Górski, M. Kazana, M. Szleper , P. Zalewski**Institute of Experimental Physics, Faculty of Physics, University of Warsaw, Warsaw, Poland**K. Bunkowski, K. Doroba, A. Kalinowski , M. Konecki , J. Krolikowski **Laboratório de Instrumentação e Física Experimental de Partículas, Lisboa, Portugal**M. Araujo, P. Bargassa , D. Bastos, A. Boletti , P. Faccioli , M. Gallinaro , J. Hollar , N. Leonardo , T. Niknejad, M. Pisano, J. Seixas , O. Toldaiev , J. Varela **Joint Institute for Nuclear Research, Dubna, Russia**S. Afanasiev, D. Budkouski, I. Golutvin, I. Gorbunov , V. Karjavine, V. Korenkov , A. Lanev, A. Malakhov, V. Matveev<sup>52,53</sup>, V. Palichik, V. Perelygin, M. Savina, D. Seitova, V. Shalaev, S. Shmatov, S. Shulha, V. Smirnov, O. Teryaev, N. Voitishin, B.S. Yuldashev<sup>54</sup>, A. Zarubin, I. Zhizhin**Petersburg Nuclear Physics Institute, Gatchina (St. Petersburg), Russia**G. Gavrilov , V. Golovtcov, Y. Ivanov, V. Kim<sup>55</sup> , E. Kuznetsova<sup>56</sup>, V. Murzin, V. Oreshkin, I. Smirnov, D. Sosnov , V. Sulimov, L. Uvarov, S. Volkov, A. Vorobyev**Institute for Nuclear Research, Moscow, Russia**Yu. Andreev , A. Dermenev, S. Gninenko , N. Golubev, A. Karneyeu , D. Kirpichnikov , M. Kirsanov, N. Krasnikov, A. Pashenkov, G. Pivovarov , A. Toropin**Institute for Theoretical and Experimental Physics named by A.I. Alikhanov of NRC 'Kurchatov Institute', Moscow, Russia**V. Epshteyn, V. Gavrilov, N. Lychkovskaya, A. Nikitenko<sup>57</sup>, V. Popov, A. Stepennov, M. Toms, E. Vlasov , A. Zhokin**Moscow Institute of Physics and Technology, Moscow, Russia**

T. Aushev

**National Research Nuclear University 'Moscow Engineering Physics Institute' (MEPhI), Moscow, Russia**O. Bychkova, M. Chadeeva<sup>58</sup> , M. Danilov<sup>59</sup> , A. Oskin, P. Parygin, E. Popova**P.N. Lebedev Physical Institute, Moscow, Russia**V. Andreev, M. Azarkin, I. Dremin , M. Kirakosyan, A. Terkulov**Skobeltsyn Institute of Nuclear Physics, Lomonosov Moscow State University, Moscow, Russia**A. Belyaev, E. Boos , V. Bunichev, M. Dubinin<sup>60</sup> , L. Dudko , A. Ershov, V. Klyukhin 

N. Korneeva , I. Lokhtin , S. Obraztsov, M. Perfilov, V. Savrin, P. Volkov

**Novosibirsk State University (NSU), Novosibirsk, Russia**

V. Blinov<sup>61</sup>, T. Dimova<sup>61</sup>, L. Kardapoltsev<sup>61</sup>, A. Kozyrev<sup>61</sup>, I. Ovtin<sup>61</sup>, O. Radchenko<sup>61</sup>, Y. Skovpen<sup>61</sup> 

**Institute for High Energy Physics of National Research Centre 'Kurchatov Institute', Protvino, Russia**

I. Azhgirey , I. Bayshev, D. Elumakhov, V. Kachanov, D. Konstantinov , P. Mandrik , V. Petrov, R. Ryutin, S. Slabospitskii , A. Sobol, S. Troshin , N. Tyurin, A. Uzunian, A. Volkov

**National Research Tomsk Polytechnic University, Tomsk, Russia**

A. Babaev, V. Okhotnikov

**Tomsk State University, Tomsk, Russia**

V. Borshch, V. Ivanchenko , E. Tcherniaev 

**University of Belgrade: Faculty of Physics and VINCA Institute of Nuclear Sciences, Belgrade, Serbia**

P. Adzic<sup>62</sup> , M. Dordevic , P. Milenovic , J. Milosevic 

**Centro de Investigaciones Energéticas Medioambientales y Tecnológicas (CIEMAT), Madrid, Spain**

M. Aguilar-Benitez, J. Alcaraz Maestre , A. Álvarez Fernández, I. Bachiller, M. Barrio Luna, Cristina F. Bedoya , C.A. Carrillo Montoya , M. Cepeda , M. Cerrada, N. Colino , B. De La Cruz, A. Delgado Peris , J.P. Fernández Ramos , J. Flix , M.C. Fouz , O. Gonzalez Lopez , S. Goy Lopez , J.M. Hernandez , M.I. Josa , J. León Holgado , D. Moran, Á. Navarro Tobar , C. Perez Dengra, A. Pérez-Calero Yzquierdo , J. Puerta Pelayo , I. Redondo , L. Romero, S. Sánchez Navas, L. Urda Gómez , C. Willmott

**Universidad Autónoma de Madrid, Madrid, Spain**

J.F. de Trocóniz, R. Reyes-Almanza 

**Universidad de Oviedo, Instituto Universitario de Ciencias y Tecnologías Espaciales de Asturias (ICTEA), Oviedo, Spain**

B. Alvarez Gonzalez , J. Cuevas , C. Erice , J. Fernandez Menendez , S. Folgueras , I. Gonzalez Caballero , J.R. González Fernández, E. Palencia Cortezon , C. Ramón Álvarez, V. Rodríguez Bouza , A. Soto Rodríguez, A. Trapote, N. Trevisani , C. Vico Villalba

**Instituto de Física de Cantabria (IFCA), CSIC-Universidad de Cantabria, Santander, Spain**

J.A. Brochero Cifuentes , I.J. Cabrillo, A. Calderon , J. Duarte Campderros , M. Fernandez , C. Fernandez Madrazo , P.J. Fernández Manteca , A. García Alonso, G. Gomez, C. Martinez Rivero, P. Martinez Ruiz del Arbol , F. Matorras , P. Matorras Cuevas , J. Piedra Gomez , C. Prieels, T. Rodrigo , A. Ruiz-Jimeno , L. Scodellaro , I. Vila, J.M. Vizan Garcia 

**University of Colombo, Colombo, Sri Lanka**

M.K. Jayananda, B. Kailasapathy<sup>63</sup>, D.U.J. Sonnadara, D.D.C. Wickramarathna

**University of Ruhuna, Department of Physics, Matara, Sri Lanka**

W.G.D. Dharmaratna , K. Liyanage, N. Perera, N. Wickramage

**CERN, European Organization for Nuclear Research, Geneva, Switzerland**

T.K. Arrestad , D. Abbaneo, J. Alimena , E. Auffray, G. Auzinger, J. Baechler, P. Baillon<sup>†</sup>, D. Barney , J. Bendavid, M. Bianco , A. Bocci , T. Camporesi, M. Capeans Garrido 

G. Cerminara, N. Chernyavskaya , S.S. Chhibra , M. Cipriani , L. Cristella , D. d'Enterria , A. Dabrowski , A. David , A. De Roeck , M.M. Defranchis , M. Deile , M. Dobson, M. Dünser , N. Dupont, A. Elliott-Peisert, N. Emriskova, F. Fallavollita<sup>64</sup>, A. Florent , G. Franzoni , W. Funk, S. Giani, D. Gigi, K. Gill, F. Glege, L. Gouskos , M. Haranko , J. Hegeman , V. Innocente , T. James, P. Janot , J. Kaspar , J. Kieseler , M. Komm , N. Kratochwil, C. Lange , S. Laurila, P. Lecoq , A. Lintuluoto, K. Long , C. Lourenço , B. Maier, L. Malgeri , S. Mallios, M. Mannelli, A.C. Marini , F. Meijers, S. Mersi , E. Meschi , F. Moortgat , M. Mulders , S. Orfanelli, L. Orsini, F. Pantaleo , E. Perez, M. Peruzzi , A. Petrilli, G. Petrucciani , A. Pfeiffer , M. Pierini , D. Piparo, M. Pitt , H. Qu , T. Quast, D. Rabady , A. Racz, G. Reales Gutiérrez, M. Rovere, H. Sakulin, J. Salfeld-Nebgen , S. Scarfi, C. Schäfer, C. Schwick, M. Selvaggi , A. Sharma, P. Silva , W. Snoeys , P. Sphicas<sup>65</sup> , S. Summers , K. Tatar , V.R. Tavolaro , D. Treille, P. Tropea, A. Tsirou, G.P. Van Onsem , J. Wanczyk<sup>66</sup>, K.A. Wozniak, W.D. Zeuner

#### **Paul Scherrer Institut, Villigen, Switzerland**

L. Caminada<sup>67</sup> , A. Ebrahimi , W. Erdmann, R. Horisberger, Q. Ingram, H.C. Kaestli, D. Kotlinski, U. Langenegger, M. Missiroli<sup>67</sup> , L. Noehte<sup>67</sup>, T. Rohe

#### **ETH Zurich - Institute for Particle Physics and Astrophysics (IPA), Zurich, Switzerland**

K. Androsov<sup>66</sup> , M. Backhaus , P. Berger, A. Calandri , A. De Cosa, G. Dissertori , M. Dittmar, M. Donegà, C. Dorfer , F. Eble, K. Gedia, F. Glessgen, T.A. Gómez Espinosa , C. Grab , D. Hits, W. Lustermann, A.-M. Lyon, R.A. Manzoni , L. Marchese , C. Martin Perez, M.T. Meinhard, F. Nessi-Tedaldi, J. Niedziela , F. Pauss, V. Perovic, S. Pigazzini , M.G. Ratti , M. Reichmann, C. Reissel, T. Reitenspiess, B. Ristic , D. Ruini, D.A. Sanz Becerra , V. Stampf, J. Steggemann<sup>66</sup> , R. Wallny , D.H. Zhu

#### **Universität Zürich, Zurich, Switzerland**

C. Amsler<sup>68</sup> , P. Bärtschi, C. Botta , D. Brzhechko, M.F. Canelli , K. Cormier, A. De Wit , R. Del Burgo, J.K. Heikkilä , M. Huwiler, W. Jin, A. Jofrehei , B. Kilminster , S. Leontsinis , S.P. Liechti, A. Macchiolo , P. Meiring, V.M. Mikuni , U. Molinatti, I. Neutelings, A. Reimers, P. Robmann, S. Sanchez Cruz , K. Schweiger , M. Senger, Y. Takahashi 

#### **National Central University, Chung-Li, Taiwan**

C. Adloff<sup>69</sup>, C.M. Kuo, W. Lin, A. Roy , T. Sarkar<sup>38</sup> , S.S. Yu

#### **National Taiwan University (NTU), Taipei, Taiwan**

L. Ceard, Y. Chao, K.F. Chen , P.H. Chen , W.-S. Hou , Y.y. Li, R.-S. Lu, E. Paganis , A. Psallidas, A. Steen, H.y. Wu, E. Yazgan , P.r. Yu

#### **Chulalongkorn University, Faculty of Science, Department of Physics, Bangkok, Thailand**

B. Asavapibhop , C. Asawatangtrakuldee , N. Srimanobhas 

#### **Çukurova University, Physics Department, Science and Art Faculty, Adana, Turkey**

F. Boran , S. Damarseckin<sup>70</sup>, Z.S. Demiroglu , F. Dolek , I. Dumanoglu<sup>71</sup> , E. Eskut, Y. Guler<sup>72</sup> , E. Gurpinar Guler<sup>72</sup> , C. Isik, O. Kara, A. Kayis Topaksu, U. Kiminsu , G. Onengut, K. Ozdemir<sup>73</sup>, A. Polatoz, A.E. Simsek , B. Tali<sup>74</sup>, U.G. Tok , S. Turkcapar, I.S. Zorbakir 

#### **Middle East Technical University, Physics Department, Ankara, Turkey**

B. Isildak<sup>75</sup>, G. Karapinar, K. Ocalan<sup>76</sup> , M. Yalvac<sup>77</sup> 

#### **Bogazici University, Istanbul, Turkey**

B. Akgun, I.O. Atakisi , E. Gülmez , M. Kaya<sup>78</sup> , O. Kaya<sup>79</sup>, Ö. Özçelik, S. Tekten<sup>80</sup>,

E.A. Yetkin<sup>81</sup> 

**Istanbul Technical University, Istanbul, Turkey**

A. Cakir , K. Cankocak<sup>71</sup> , Y. Komurcu, S. Sen<sup>82</sup> 

**Istanbul University, Istanbul, Turkey**

S. Cerci<sup>74</sup>, I. Hos<sup>83</sup>, B. Kaynak, S. Ozkorucuklu, H. Sert , D. Sunar Cerci<sup>74</sup> , C. Zorbilmez

**Institute for Scintillation Materials of National Academy of Science of Ukraine, Kharkov, Ukraine**

B. Grynyov

**National Scientific Center, Kharkov Institute of Physics and Technology, Kharkov, Ukraine**

L. Levchuk 

**University of Bristol, Bristol, United Kingdom**

D. Anthony, E. Bhal , S. Bologna, J.J. Brooke , A. Bundock , E. Clement , D. Cussans , H. Flacher , J. Goldstein , G.P. Heath, H.F. Heath , L. Kreczko , B. Krikler , S. Paramesvaran, S. Seif El Nasr-Storey, V.J. Smith, N. Stylianou<sup>84</sup> , K. Walkingshaw Pass, R. White

**Rutherford Appleton Laboratory, Didcot, United Kingdom**

K.W. Bell, A. Belyaev<sup>85</sup> , C. Brew , R.M. Brown, D.J.A. Cockerill, C. Cooke, K.V. Ellis, K. Harder, S. Harper, M.-L. Holmberg<sup>86</sup>, J. Linacre , K. Manolopoulos, D.M. Newbold , E. Olaiya, D. Petyt, T. Reis , T. Schuh, C.H. Shepherd-Themistocleous, I.R. Tomalin, T. Williams 

**Imperial College, London, United Kingdom**

R. Bainbridge , P. Bloch , S. Bonomally, J. Borg , S. Breeze, O. Buchmuller, V. Cepaitis , G.S. Chahal<sup>87</sup> , D. Colling, P. Dauncey , G. Davies , M. Della Negra , S. Fayer, G. Fedi , G. Hall , M.H. Hassanshahi, G. Iles, J. Langford, L. Lyons, A.-M. Magnan, S. Malik, A. Martelli , D.G. Monk, J. Nash<sup>88</sup> , M. Pesaresi, D.M. Raymond, A. Richards, A. Rose, E. Scott , C. Seez, A. Shtipliyski, A. Tapper , K. Uchida, T. Virdee<sup>21</sup> , M. Vojinovic , N. Wardle , S.N. Webb , D. Winterbottom

**Brunel University, Uxbridge, United Kingdom**

K. Coldham, J.E. Cole , A. Khan, P. Kyberd , I.D. Reid , L. Teodorescu, S. Zahid 

**Baylor University, Waco, Texas, USA**

S. Abdullin , A. Brinkerhoff , B. Caraway , J. Dittmann , K. Hatakeyama , A.R. Kanuganti, B. McMaster , N. Pastika, M. Saunders , S. Sawant, C. Sutantawibul, J. Wilson 

**Catholic University of America, Washington, DC, USA**

R. Bartek , A. Dominguez , R. Uniyal , A.M. Vargas Hernandez

**The University of Alabama, Tuscaloosa, Alabama, USA**

A. Buccilli , S.I. Cooper , D. Di Croce , S.V. Gleyzer , C. Henderson , C.U. Perez , P. Rumerio<sup>89</sup> , C. West 

**Boston University, Boston, Massachusetts, USA**

A. Akpinar , A. Albert , D. Arcaro , C. Cosby , Z. Demiragli , E. Fontanesi, D. Gastler, S. May , J. Rohlf , K. Salyer , D. Sperka, D. Spitzbart , I. Suarez , A. Tsatsos, S. Yuan, D. Zou

**Brown University, Providence, Rhode Island, USA**

G. Benelli , B. Burkle , X. Coubez<sup>22</sup>, D. Cutts , M. Hadley , U. Heintz , J.M. Hogan<sup>90</sup> , T. KWON, G. Landsberg , K.T. Lau , D. Li, M. Lukasik, J. Luo , M. Narain, N. Pervan, S. Sagir<sup>91</sup> , F. Simpson, E. Usai , W.Y. Wong, X. Yan , D. Yu , W. Zhang

#### **University of California, Davis, Davis, California, USA**

J. Bonilla , C. Brainerd , R. Breedon, M. Calderon De La Barca Sanchez, M. Chertok , J. Conway , P.T. Cox, R. Erbacher, G. Haza, F. Jensen , O. Kukral, R. Lander, M. Mulhearn , D. Pellett, B. Regnery , D. Taylor , Y. Yao , F. Zhang 

#### **University of California, Los Angeles, California, USA**

M. Bachtis , R. Cousins , A. Datta , D. Hamilton, J. Hauser , M. Ignatenko, M.A. Iqbal, T. Lam, W.A. Nash, S. Regnard , D. Saltzberg , B. Stone, V. Valuev 

#### **University of California, Riverside, Riverside, California, USA**

K. Burt, Y. Chen, R. Clare , J.W. Gary , M. Gordon, G. Hanson , G. Karapostoli , O.R. Long , N. Manganelli, M. Olmedo Negrete, W. Si , S. Wimpenny, Y. Zhang

#### **University of California, San Diego, La Jolla, California, USA**

J.G. Branson, P. Chang , S. Cittolin, S. Cooperstein , N. Deelen , D. Diaz , J. Duarte , R. Gerosa , L. Giannini , J. Guiang, R. Kansal , V. Krutelyov , R. Lee, J. Letts , M. Masciovecchio , F. Mokhtar, M. Pieri , B.V. Sathia Narayanan , V. Sharma , M. Tadel, A. Vartak , F. Würthwein , Y. Xiang , A. Yagil 

#### **University of California, Santa Barbara - Department of Physics, Santa Barbara, California, USA**

N. Amin, C. Campagnari , M. Citron , A. Dorsett, V. Dutta , J. Incandela , M. Kilpatrick , J. Kim , B. Marsh, H. Mei, M. Oshiro, M. Quinnan , J. Richman, U. Sarica , F. Setti, J. Sheplock, P. Siddireddy, D. Stuart, S. Wang 

#### **California Institute of Technology, Pasadena, California, USA**

A. Bornheim , O. Cerri, I. Dutta , J.M. Lawhorn , N. Lu , J. Mao, H.B. Newman , T.Q. Nguyen , M. Spiropulu , J.R. Vlimant , C. Wang , S. Xie , Z. Zhang , R.Y. Zhu 

#### **Carnegie Mellon University, Pittsburgh, Pennsylvania, USA**

J. Alison , S. An , M.B. Andrews, P. Bryant , T. Ferguson , A. Harilal, C. Liu, T. Mudholkar , M. Paulini , A. Sanchez, W. Terrill

#### **University of Colorado Boulder, Boulder, Colorado, USA**

J.P. Cumalat , W.T. Ford , A. Hassani, E. MacDonald, R. Patel, A. Perloff , C. Savard, K. Stenson , K.A. Ulmer , S.R. Wagner 

#### **Cornell University, Ithaca, New York, USA**

J. Alexander , S. Bright-Thonney , X. Chen , Y. Cheng , D.J. Cranshaw , S. Hogan, J. Monroy , J.R. Patterson , D. Quach , J. Reichert , M. Reid , A. Ryd, W. Sun , J. Thom , P. Wittich , R. Zou 

#### **Fermi National Accelerator Laboratory, Batavia, Illinois, USA**

M. Albrow , M. Alyari , G. Apollinari, A. Apresyan , A. Apyan , S. Banerjee, L.A.T. Bauerick , D. Berry , J. Berryhill , P.C. Bhat, K. Burkett , J.N. Butler, A. Canepa, G.B. Cerati , H.W.K. Cheung , F. Chlebana, K.F. Di Petrillo , V.D. Elvira , Y. Feng, J. Freeman, Z. Gecse, L. Gray, D. Green, S. Grünendahl , O. Gutsche , R.M. Harris , R. Heller, T.C. Herwig , J. Hirschauer , B. Jayatilaka , S. Jindariani, M. Johnson, U. Joshi, T. Klijnsma , B. Klama , K.H.M. Kwok, S. Lammel , D. Lincoln , R. Lipton, T. Liu, C. Madrid, K. Maeshima, C. Mantilla , D. Mason, P. McBride , P. Merkel, S. Mrenna 

S. Nahn [ID](#), J. Ngadiuba [ID](#), V. O'Dell, V. Papadimitriou, K. Pedro [ID](#), C. Pena<sup>60</sup> [ID](#), O. Prokofyev, F. Ravera [ID](#), A. Reinsvold Hall [ID](#), L. Ristori [ID](#), E. Sexton-Kennedy [ID](#), N. Smith [ID](#), A. Soha [ID](#), W.J. Spalding [ID](#), L. Spiegel, S. Stoynev [ID](#), J. Strait [ID](#), L. Taylor [ID](#), S. Tkaczyk, N.V. Tran [ID](#), L. Uplegger [ID](#), E.W. Vaandering [ID](#), H.A. Weber [ID](#)

**University of Florida, Gainesville, Florida, USA**

D. Acosta [ID](#), P. Avery, D. Bourilkov [ID](#), L. Cadamuro [ID](#), V. Cherepanov, F. Errico [ID](#), R.D. Field, D. Guerrero, B.M. Joshi [ID](#), M. Kim, E. Koenig, J. Konigsberg [ID](#), A. Korytov, K.H. Lo, K. Matchev [ID](#), N. Menendez [ID](#), G. Mitselmakher [ID](#), A. Muthirakalayil Madhu, N. Rawal, D. Rosenzweig, S. Rosenzweig, J. Rotter, K. Shi [ID](#), J. Sturdy [ID](#), J. Wang [ID](#), E. Yigitbası [ID](#), X. Zuo

**Florida State University, Tallahassee, Florida, USA**

T. Adams [ID](#), A. Askew [ID](#), R. Habibullah [ID](#), V. Hagopian, K.F. Johnson, R. Khurana, T. Kolberg [ID](#), G. Martinez, H. Prosper [ID](#), C. Schiber, O. Viazlo [ID](#), R. Yohay [ID](#), J. Zhang

**Florida Institute of Technology, Melbourne, Florida, USA**

M.M. Baarmann [ID](#), S. Butalla, T. Elkafrawy<sup>92</sup> [ID](#), M. Hohlmann [ID](#), R. Kumar Verma [ID](#), D. Noonan [ID](#), M. Rahmani, F. Yumiceva [ID](#)

**University of Illinois at Chicago (UIC), Chicago, Illinois, USA**

M.R. Adams, H. Becerril Gonzalez [ID](#), R. Cavanaugh [ID](#), S. Dittmer, O. Evdokimov [ID](#), C.E. Gerber [ID](#), D.A. Hangal [ID](#), D.J. Hofman [ID](#), A.H. Merrit, C. Mills [ID](#), G. Oh [ID](#), T. Roy, S. Rudrabhatla, M.B. Tonjes [ID](#), N. Varelas [ID](#), J. Viinikainen [ID](#), X. Wang, Z. Wu [ID](#), Z. Ye [ID](#)

**The University of Iowa, Iowa City, Iowa, USA**

M. Alhusseini [ID](#), K. Dilsiz<sup>93</sup> [ID](#), L. Emediato, R.P. Gandrajula [ID](#), O.K. Köseyan [ID](#), J.-P. Merlo, A. Mestvirishvili<sup>94</sup>, J. Nachtman, H. Ogul<sup>95</sup> [ID](#), Y. Onel [ID](#), A. Penzo, C. Snyder, E. Tiras<sup>96</sup> [ID](#)

**Johns Hopkins University, Baltimore, Maryland, USA**

O. Amram [ID](#), B. Blumenfeld [ID](#), L. Corcodilos [ID](#), J. Davis, M. Eminizer [ID](#), A.V. Gritsan [ID](#), S. Kyriacou, P. Maksimovic [ID](#), J. Roskes [ID](#), M. Swartz, T.Á. Vámi [ID](#)

**The University of Kansas, Lawrence, Kansas, USA**

A. Abreu, J. Anguiano, C. Baldenegro Barrera [ID](#), P. Baringer [ID](#), A. Bean [ID](#), A. Bylinkin [ID](#), Z. Flowers, T. Isidori, S. Khalil [ID](#), J. King, G. Krintiras [ID](#), A. Kropivnitskaya [ID](#), M. Lazarovits, C. Le Mahieu, C. Lindsey, J. Marquez, N. Minafra [ID](#), M. Murray [ID](#), M. Nickel, C. Rogan [ID](#), C. Royon, R. Salvatico [ID](#), S. Sanders, E. Schmitz, C. Smith [ID](#), J.D. Tapia Takaki [ID](#), Q. Wang [ID](#), Z. Warner, J. Williams [ID](#), G. Wilson [ID](#)

**Kansas State University, Manhattan, Kansas, USA**

S. Duric, A. Ivanov [ID](#), K. Kaadze [ID](#), D. Kim, Y. Maravin [ID](#), T. Mitchell, A. Modak, K. Nam

**Lawrence Livermore National Laboratory, Livermore, California, USA**

F. Rebassoo, D. Wright

**University of Maryland, College Park, Maryland, USA**

E. Adams, A. Baden, O. Baron, A. Belloni [ID](#), S.C. Eno [ID](#), N.J. Hadley [ID](#), S. Jabeen [ID](#), R.G. Kellogg, T. Koeth, S. Lascio, A.C. Mignerey, S. Nabili, C. Palmer [ID](#), M. Seidel [ID](#), A. Skuja [ID](#), L. Wang, K. Wong [ID](#)

**Massachusetts Institute of Technology, Cambridge, Massachusetts, USA**

D. Abercrombie, G. Andreassi, R. Bi, W. Busza [ID](#), I.A. Cali, Y. Chen [ID](#), M. D'Alfonso [ID](#), J. Eysermans, C. Freer [ID](#), G. Gomez Ceballos, M. Goncharov, P. Harris, M. Hu, M. Klute [ID](#), D. Kovalevskyi [ID](#), J. Krupa, Y.-J. Lee [ID](#), C. Mironov [ID](#), C. Paus [ID](#), D. Rankin [ID](#), C. Roland [ID](#), G. Roland, Z. Shi [ID](#), G.S.F. Stephans [ID](#), J. Wang, Z. Wang [ID](#), B. Wyslouch [ID](#)

**University of Minnesota, Minneapolis, Minnesota, USA**

R.M. Chatterjee, A. Evans , J. Hiltbrand, Sh. Jain , M. Krohn, Y. Kubota, J. Mans , M. Revering, R. Rusack , R. Saradhy, N. Schroeder , N. Strobbe , M.A. Wadud

**University of Nebraska-Lincoln, Lincoln, Nebraska, USA**

K. Bloom , M. Bryson, S. Chauhan , D.R. Claes, C. Fangmeier, L. Finco , F. Golf , C. Joo, I. Kravchenko , M. Musich, I. Reed, J.E. Siado, G.R. Snow<sup>†</sup>, W. Tabb, F. Yan, A.G. Zecchinelli

**State University of New York at Buffalo, Buffalo, New York, USA**

G. Agarwal , H. Bandyopadhyay , L. Hay , I. Iashvili , A. Kharchilava, C. McLean , D. Nguyen, J. Pekkanen , S. Rappoccio , A. Williams 

**Northeastern University, Boston, Massachusetts, USA**

G. Alverson , E. Barberis, Y. Haddad , A. Hortiangtham, J. Li , G. Madigan, B. Marzocchi , D.M. Morse , V. Nguyen, T. Orimoto , A. Parker, L. Skinnari , A. Tishelman-Charny, T. Wamorkar, B. Wang , A. Wisecarver, D. Wood 

**Northwestern University, Evanston, Illinois, USA**

S. Bhattacharya , J. Bueghly, Z. Chen , A. Gilbert , T. Gunter , K.A. Hahn, Y. Liu, N. Odell, M.H. Schmitt , M. Velasco

**University of Notre Dame, Notre Dame, Indiana, USA**

R. Band , R. Bucci, M. Cremonesi, A. Das , N. Dev , R. Goldouzian , M. Hildreth, K. Hurtado Anampa , C. Jessop , K. Lannon , J. Lawrence, N. Loukas , D. Lutton, J. Mariano, N. Marinelli, I. Mcalister, T. McCauley , C. Mcgrady, K. Mohrman, C. Moore, Y. Musienko<sup>52</sup>, R. Ruchti, A. Townsend, M. Wayne, A. Wightman, M. Zarucki , L. Zygalas

**The Ohio State University, Columbus, Ohio, USA**

B. Bylsma, B. Cardwell, L.S. Durkin , B. Francis , C. Hill , M. Nunez Ornelas , K. Wei, B.L. Winer, B.R. Yates 

**Princeton University, Princeton, New Jersey, USA**

F.M. Addesa , B. Bonham , P. Das , G. Dezoort, P. Elmer , A. Frankenthal , B. Greenberg , N. Haubrich, S. Higginbotham, A. Kalogeropoulos , G. Kopp, S. Kwan , D. Lange, D. Marlow , K. Mei , I. Ojalvo, J. Olsen , D. Stickland , C. Tully 

**University of Puerto Rico, Mayaguez, Puerto Rico, USA**

S. Malik , S. Norberg

**Purdue University, West Lafayette, Indiana, USA**

A.S. Bakshi, V.E. Barnes , R. Chawla , S. Das , L. Gutay, M. Jones , A.W. Jung , S. Karmarkar, D. Kondratyev , M. Liu, G. Negro, N. Neumeister , G. Paspalaki, S. Piperov , A. Purohit, J.F. Schulte , M. Stojanovic<sup>17</sup>, J. Thieman , F. Wang , R. Xiao , W. Xie 

**Purdue University Northwest, Hammond, Indiana, USA**

J. Dolen , N. Parashar

**Rice University, Houston, Texas, USA**

A. Baty , T. Carnahan, M. Decaro, S. Dildick , K.M. Ecklund , S. Freed, P. Gardner, F.J.M. Geurts , A. Kumar , W. Li, B.P. Padley , R. Redjimi, W. Shi , A.G. Stahl Leiton , S. Yang , L. Zhang<sup>97</sup>, Y. Zhang 

**University of Rochester, Rochester, New York, USA**

A. Bodek , P. de Barbaro, R. Demina , J.L. Dulemba , C. Fallon, T. Ferbel , M. Galanti,

A. Garcia-Bellido , O. Hindrichs , A. Khukhunaishvili, E. Ranken, R. Taus

**Rutgers, The State University of New Jersey, Piscataway, New Jersey, USA**

B. Chiarito, J.P. Chou , A. Gandrakota , Y. Gershtein , E. Halkiadakis , A. Hart, M. Heindl , O. Karacheban<sup>25</sup> , I. Laflotte, A. Lath , R. Montalvo, K. Nash, M. Osherson, S. Salur , S. Schnetzer, S. Somalwar , R. Stone, S.A. Thayil , S. Thomas, H. Wang 

**University of Tennessee, Knoxville, Tennessee, USA**

H. Acharya, A.G. Delannoy , S. Fiorendi , S. Spanier 

**Texas A&M University, College Station, Texas, USA**

O. Bouhali<sup>98</sup> , M. Dalchenko , A. Delgado , R. Eusebi, J. Gilmore, T. Huang, T. Kamon<sup>99</sup>, H. Kim , S. Luo , S. Malhotra, R. Mueller, D. Overton, D. Rathjens , A. Safonov 

**Texas Tech University, Lubbock, Texas, USA**

N. Akchurin, J. Damgov, V. Hegde, S. Kunori, K. Lamichhane, S.W. Lee , T. Mengke, S. Muthumuni , T. Peltola , I. Volobouev, Z. Wang, A. Whitbeck

**Vanderbilt University, Nashville, Tennessee, USA**

E. Appelt , S. Greene, A. Gurrola , W. Johns, A. Melo, H. Ni, K. Padeken , F. Romeo , P. Sheldon , S. Tuo, J. Velkovska 

**University of Virginia, Charlottesville, Virginia, USA**

M.W. Arenton , B. Cox , G. Cummings , J. Hakala , R. Hirosky , M. Joyce , A. Ledovskoy , A. Li, C. Neu , C.E. Perez Lara , B. Tannenwald , S. White 

**Wayne State University, Detroit, Michigan, USA**

N. Poudyal 

**University of Wisconsin - Madison, Madison, WI, Wisconsin, USA**

K. Black , T. Bose , C. Caillol, S. Dasu , I. De Bruyn , P. Everaerts , F. Fienga , C. Galloni, H. He, M. Herndon , A. Hervé, U. Hussain, A. Lanaro, A. Loeliger, R. Loveless, J. Madhusudanan Sreekala , A. Mallampalli, A. Mohammadi, D. Pinna, A. Savin, V. Shang, V. Sharma , W.H. Smith , D. Teague, S. Trembath-Reichert, W. Vetens 

†: Deceased

1: Also at TU Wien, Wien, Austria

2: Also at Institute of Basic and Applied Sciences, Faculty of Engineering, Arab Academy for Science, Technology and Maritime Transport, Alexandria, Egypt

3: Also at Université Libre de Bruxelles, Bruxelles, Belgium

4: Also at Universidade Estadual de Campinas, Campinas, Brazil

5: Also at Federal University of Rio Grande do Sul, Porto Alegre, Brazil

6: Also at The University of the State of Amazonas, Manaus, Brazil

7: Also at University of Chinese Academy of Sciences, Beijing, China

8: Also at Department of Physics, Tsinghua University, Beijing, China

9: Also at UFMS, Nova Andradina, Brazil

10: Also at Nanjing Normal University Department of Physics, Nanjing, China

11: Now at The University of Iowa, Iowa City, Iowa, USA

12: Also at Institute for Theoretical and Experimental Physics named by A.I. Alikhanov of NRC ‘Kurchatov Institute’, Moscow, Russia

13: Also at Joint Institute for Nuclear Research, Dubna, Russia

14: Also at Cairo University, Cairo, Egypt

15: Also at Suez University, Suez, Egypt

16: Now at British University in Egypt, Cairo, Egypt

- 
- 17: Also at Purdue University, West Lafayette, Indiana, USA
  - 18: Also at Université de Haute Alsace, Mulhouse, France
  - 19: Also at Tbilisi State University, Tbilisi, Georgia
  - 20: Also at Erzincan Binali Yildirim University, Erzincan, Turkey
  - 21: Also at CERN, European Organization for Nuclear Research, Geneva, Switzerland
  - 22: Also at RWTH Aachen University, III. Physikalisches Institut A, Aachen, Germany
  - 23: Also at University of Hamburg, Hamburg, Germany
  - 24: Also at Isfahan University of Technology, Isfahan, Iran
  - 25: Also at Brandenburg University of Technology, Cottbus, Germany
  - 26: Also at Forschungszentrum Jülich, Juelich, Germany
  - 27: Also at Physics Department, Faculty of Science, Assiut University, Assiut, Egypt
  - 28: Also at Karoly Robert Campus, MATE Institute of Technology, Gyongyos, Hungary
  - 29: Also at Institute of Physics, University of Debrecen, Debrecen, Hungary
  - 30: Also at Institute of Nuclear Research ATOMKI, Debrecen, Hungary
  - 31: Also at MTA-ELTE Lendület CMS Particle and Nuclear Physics Group, Eötvös Loránd University, Budapest, Hungary
  - 32: Also at Wigner Research Centre for Physics, Budapest, Hungary
  - 33: Also at IIT Bhubaneswar, Bhubaneswar, India
  - 34: Also at Institute of Physics, Bhubaneswar, India
  - 35: Also at Punjab Agricultural University, Ludhiana, India, LUDHIANA, India
  - 36: Also at Shoolini University, Solan, India
  - 37: Also at University of Hyderabad, Hyderabad, India
  - 38: Also at University of Visva-Bharati, Santiniketan, India
  - 39: Also at Indian Institute of Technology (IIT), Mumbai, India
  - 40: Also at Deutsches Elektronen-Synchrotron, Hamburg, Germany
  - 41: Also at Sharif University of Technology, Tehran, Iran
  - 42: Also at Department of Physics, University of Science and Technology of Mazandaran, Behshahr, Iran
  - 43: Now at INFN Sezione di Bari (a), Università di Bari (b), Politecnico di Bari (c), Bari, Italy
  - 44: Also at Italian National Agency for New Technologies, Energy and Sustainable Economic Development, Bologna, Italy
  - 45: Also at Centro Siciliano di Fisica Nucleare e di Struttura Della Materia, Catania, Italy
  - 46: Also at Scuola Superiore Meridionale, Università di Napoli Federico II, Napoli, Italy
  - 47: Also at Università di Napoli 'Federico II', Napoli, Italy
  - 48: Also at Consiglio Nazionale delle Ricerche - Istituto Officina dei Materiali, PERUGIA, Italy
  - 49: Also at Riga Technical University, Riga, Latvia
  - 50: Also at Consejo Nacional de Ciencia y Tecnología, Mexico City, Mexico
  - 51: Also at IRFU, CEA, Université Paris-Saclay, Gif-sur-Yvette, France
  - 52: Also at Institute for Nuclear Research, Moscow, Russia
  - 53: Now at National Research Nuclear University 'Moscow Engineering Physics Institute' (MEPhI), Moscow, Russia
  - 54: Also at Institute of Nuclear Physics of the Uzbekistan Academy of Sciences, Tashkent, Uzbekistan
  - 55: Also at St. Petersburg State Polytechnical University, St. Petersburg, Russia
  - 56: Also at University of Florida, Gainesville, Florida, USA
  - 57: Also at Imperial College, London, United Kingdom
  - 58: Also at P.N. Lebedev Physical Institute, Moscow, Russia
  - 59: Also at Moscow Institute of Physics and Technology, Moscow, Russia
  - 60: Also at California Institute of Technology, Pasadena, California, USA

- 61: Also at Budker Institute of Nuclear Physics, Novosibirsk, Russia  
62: Also at Faculty of Physics, University of Belgrade, Belgrade, Serbia  
63: Also at Trincomalee Campus, Eastern University, Sri Lanka, Nilaveli, Sri Lanka  
64: Also at INFN Sezione di Pavia (a), Università di Pavia (b), Pavia, Italy  
65: Also at National and Kapodistrian University of Athens, Athens, Greece  
66: Also at Ecole Polytechnique Fédérale Lausanne, Lausanne, Switzerland  
67: Also at Universität Zürich, Zurich, Switzerland  
68: Also at Stefan Meyer Institute for Subatomic Physics, Vienna, Austria  
69: Also at Laboratoire d'Annecy-le-Vieux de Physique des Particules, IN2P3-CNRS, Annecy-le-Vieux, France  
70: Also at Şırnak University, Sirnak, Turkey  
71: Also at Near East University, Research Center of Experimental Health Science, Nicosia, Turkey  
72: Also at Konya Technical University, Konya, Turkey  
73: Also at Piri Reis University, Istanbul, Turkey  
74: Also at Adiyaman University, Adiyaman, Turkey  
75: Also at Ozyegin University, Istanbul, Turkey  
76: Also at Necmettin Erbakan University, Konya, Turkey  
77: Also at Bozok Universitetesi Rektörlüğü, Yozgat, Turkey  
78: Also at Marmara University, Istanbul, Turkey  
79: Also at Milli Savunma University, Istanbul, Turkey  
80: Also at Kafkas University, Kars, Turkey  
81: Also at Istanbul Bilgi University, Istanbul, Turkey  
82: Also at Hacettepe University, Ankara, Turkey  
83: Also at Istanbul University - Cerrahpasa, Faculty of Engineering, Istanbul, Turkey  
84: Also at Vrije Universiteit Brussel, Brussel, Belgium  
85: Also at School of Physics and Astronomy, University of Southampton, Southampton, United Kingdom  
86: Also at Rutherford Appleton Laboratory, Didcot, United Kingdom  
87: Also at IPPP Durham University, Durham, United Kingdom  
88: Also at Monash University, Faculty of Science, Clayton, Australia  
89: Also at Università di Torino, TORINO, Italy  
90: Also at Bethel University, St. Paul, Minneapolis, USA  
91: Also at Karamanoğlu Mehmetbey University, Karaman, Turkey  
92: Also at Ain Shams University, Cairo, Egypt  
93: Also at Bingol University, Bingol, Turkey  
94: Also at Georgian Technical University, Tbilisi, Georgia  
95: Also at Sinop University, Sinop, Turkey  
96: Also at Erciyes University, KAYSERI, Turkey  
97: Also at Institute of Modern Physics and Key Laboratory of Nuclear Physics and Ion-beam Application (MOE) - Fudan University, Shanghai, China  
98: Also at Texas A&M University at Qatar, Doha, Qatar  
99: Also at Kyungpook National University, Daegu, Korea